Exploring the effects of classical immune activation on circuit excitability and cell viability in the mouse brain

by

Sasha Tinelli

TNLSAS001

Department of Human Biology

SUBMITTED TO THE UNIVERSITY OF CAPE TOWN

In fulfillment of the requirements for the degree

Master of Medical Sciences in *Neuroscience*

Supervisor:

Dr Joseph Valentino Raimondo

Co-Supervisor:

Dr Anja de Lange

Department of Human Biology
University of Cape Town

July 2021

The David and Elaine Potter Foundation, Ada and Bertie Levenstein Foundation and the University of Cape Town are acknowledged for financial support of this project.

Declaration

I, Sasha Tinelli, hereby declare that the work described in this thesis is my own (except where acknowledgements indicate otherwise) and that neither the whole work nor any part of it has been, is being, or will be submitted for another degree at this or any other educational institute.

I empower the university to reproduce, for the purpose of research, the whole work or any part thereof.

Signed by candidate

06 July 2021

Abstract

Epilepsy directly affects approximately 50 million people globally and is the most common neurological disorder in sub-Saharan Africa, mainly due to high rates of neuroinfections and head trauma experienced by people in the region. A common factor in these causes of acquired epilepsy is their association with significant neuroinflammation, which is thought to drive the epileptogenic process. Although epilepsy exerts a heavy toll on the health, well-being and socio-economic outcomes of Africans, there are still major deficits in our understanding of how infections and inflammatory processes drive seizure development. Using the hippocampal organotypic brain slice culture model in mouse brains, I investigated the effects of classical immune activation on circuit excitability and cell viability. To initiate inflammation, I administered lipopolysaccharide (LPS), an endotoxin derived from gram-negative bacteria, and interferon-gamma (IFNy), a cytokine typically released by lymphocytes, to brain slices on varying time scales. I used enzyme-linked immune-sorbent assays to show that this reliably induced the release of the proinflammatory cytokines TNF-α and IL-6 from the brain slices. I used patch-clamp electrophysiology to assess both the intrinsic electrical characteristics as well as the synaptic strength between pyramidal neurons after immune activation. I found no changes in the basic membrane properties of pyramidal neurons after short term neuroinflammation, but I did observe changes to the function of hippocampal networks at intermediate (24 hours) and lengthy (72 hours) time scales of immune activation in the form of significantly reduced spontaneous excitatory and inhibitory postsynaptic current frequencies and amplitudes. In addition, I developed an assay to determine neuronal survival to monitor the health of neurons in brain slices after immune activation and report that hippocampal organotypic brain slice cultures that were immune-activated for 72 hours do not appear to experience either apoptotic or necrotic cell death. Taken together, these data constitute a valuable contribution towards understanding how inflammatory mechanisms drive changes to neuronal function, which could be relevant for understanding epileptogenesis in infectious and inflammatory causes of epilepsy.

Acknowledgements

Joseph Raimondo – My supervisor – Joe, I am extremely grateful for how much you have taught me – academically, professionally and as a human - in the last few years. Thank you for believing in me when I approached you all those years ago. Thank you for patiently guiding me through my experiments and for your endless, excellent advice in every application I have done. I know with certainty that I would not be the scientist or person that I am today without your help – I will always be grateful.

Anja De Lange – My dear friend, I cannot thank you enough for your support, mentorship, kindness and friendship during the last 2.5 years. Thank you for taking me on all of the adventures!

Helen and Mike – My second parents – thank you for being a home away from home, for supporting me and for believing in me. Helen, thank you for being my biggest supporter, my shoulder to cry on, my best friend and for always being willing to drink champagne with me. Thank you for teaching me how to be a woman.

Ouma and Oupa – My dearest varkie en drakie, thank you for putting me through school and university, for fostering in me a sense of curiosity about the world and for loving me so unconditionally. Thank you for teaching me how to be a human.

Nonno – My nonno, thank you for supporting me, loving me and believing in me. Thank you for our friendship, for all that you have taught me, and for your openness with me.

Ruby – My number one, my sister – Thank you for answering every panicked call and every shaky message with gentleness, calmness and kind words of support. You understand me like no other person and I value our friendship and sisterhood deeply.

Matteo – To my favorite brother – I love you so much! Thank you for always helping me to see the joy in simple adventures and for making me laugh like no one else can.

Sandro – Pops – thank you for believing in me so relentlessly for all of these years (even when my choices made little sense). Thank you for showing me how to be a good person, to persevere relentlessly and to stand up for myself and for what I believe in.

Bronte, Chelene and Alice – To my best friends – thank you for your love, kindness and the endless entertainment you have provided me during our friendship. You lot understand me deeply – something I treasure immensely. Thank you for supporting me in everything I have done and for laughing along the way when things went awry!

Mark Hambrock – My darling sweet potato – Thank you for loving me and making me laugh whenever I was happy or sad. You are home in a person, a true comfort. Thank you for cooking with me, showing me all of your strange music and even stranger youtube comedy sketches. We loves it!

Lee, Kristy, Mayur and Kieron – The science gang – thank you for making me a rigorous scientist and someone who is willing to argue about little details. You all got me through undergrad (including the second year speed wobble!).

Mac – My dear roommate and friend – thank you for giving me a gentle and accepting space when I needed it most. Thank you for letting me figure out what I needed when I needed it. I value our home and friendship dearly!

Sketch – My dear, old friend – This thesis is in so many ways attributable to you. Thank you for letting me live on your couch in first year, thank you for studying all night with me in exam week, thank you for believing in me when I couldn't believe in myself, and most of all for understanding me the way you do. I love you, friend!

Rachael Dangarembizi – Rach – thank you for your guidance and advice on cell staining – I would have been clueless without you!

Hayley Tomes – Darling Hayley, thank you for giving me endless advice, for being the glue that holds the lab together and for giving me a space to stress-organise! Thank you also for your generosity of time and advice about this thesis.

The Raimondo Lab Family – The most precious lab family! Thank you for being such rigorous, excellent scientists and for creating a space where ordinary humans can do incredible science!

Table of contents

List of Figures

Chapter 1: Introduction

Chapter 3: Results

3.1: Application of LPS+IFNγ for 72 hours induces significant pro-inflammatory cytokine release and affects neuronal network function, but not neuronal death.

3.2: Immune activation by LPS+IFNγ for 24 hours causes electrophysiological disturbances.

List of Tables

Chapter 3: Results

3.1: Application of LPS+IFNγ for 72 hours induces significant pro-inflammatory cytokine release and affects neuronal network function, but not neuronal death.

List of Abbreviations

Symbol	Description
4-AP	4-aminopyridine
ABS Max SR	Absolute maximum spike rate
aCSF	Artificial cerebro-spinal fluid
AED	Anti-epileptic drug
AMPA	α-Amino-3-hydroxy-5-methyl-4-isoxazolepropionic acid
AMPAR	α-Amino-3-hydroxy-5-methyl-4-isoxazolepropionic acid receptor
ANOVA	Analysis of variance
APs	Action potentials
ATP	Adenosine triphosphate
BBB	Blood brain barrier
CA1	Cornu Ammonis 1
CA2	Cornu Ammonis 2
Ca^{2+}	Calcium
CA3	Cornu Ammonis 3
Cl^-	Chloride
C_m	Membrane capacitance
CNS	Central nervous system
CTD	Current threshold density
DAMP	Damage-associated molecular pattern
DG	Dentate gyrus
E. coli	*Escherichia coli*
EBSS	Earle's balanced salt solution
GABA	γ-aminobutyric acid
IEI	Inter-event interval
IFNγ	Interferon-γ
IFNγR	Interferon-γ receptor

IL-10	Interleukin-10
IL-1β	Interleukin-1β
IL-6	Interleukin-6
iNOS	Inducible nitric oxide synthase
Inos	The promoter for the gene encoding inducible nitric oxide synthase
JAK-STAT3	Janus activated kinase-signal transducer and activator of transcription-3
K^+	Potassium
LDH	Lactate dehydrogenase
LPS	Lipopolysaccharide
LTP	Long term potentiation
MAP2	Microtubule-associated protein-2
Mg^{2+}	Magnesium
mPSCs	Miniature postsynaptic currents
Na^+	Sodium
NADPH	Reduced nicotinamide adenine dinucleotide phosphate
NCC	Neurocysticercosis
NF-IL-6	Nuclear factor interleukin-6
NF-κβ	Nuclear factor-κβ
NMDA	N-methyl-D-aspartate
NMDAR	N-methyl-D-aspartate receptor
NO	Nitric oxide
OBSCs	Organotypic brain slice cultures
PAMP	Pathogen-associated molecular pattern
PBS	Phosphate buffered saline
Poly I:C	Polyinosinic-polycytidylic acid
PRR	Pattern recognition receptor
R_a	Access resistance
R_m	Membrane resistance
R_T	Total resistance

RMS	Root mean square
SE	Status epilepticus
SEM	Standard error of the mean
sEPSCs	Spontaneous excitatory post-synaptic currents
sIPSCs	Spontaneous inhibitory post-synaptic currents
SLE	Seizure-like event
sPSCs	Spontaneous postsynaptic currents
STAT1	Signal Transducer And Activator Of Transcription 1
T.crass	Tania crassiceps
TLR	Toll-like receptor
TLR-4	Toll-like receptor 4
TNF-α	Tumor necrosis factor-α
V_m	Membrane potential

Chapter 1

Introduction: How does Central Nervous System inflammation affect the propensity for seizure development?

1.1 Epilepsy is especially prevalent in sub-Saharan Africa due to high levels of head trauma and brain infections

Epilepsy is an umbrella term including multiple diseases and syndromes, thus epilepsies can have a multiplicity of unique etiologies including (but not limited to) genetic mutations, neurotrauma, brain malformations and neuroinflammation (Rana & Musto, 2018). The main symptom of epilepsy is the seizure. Thus, according to the World Health Organization, to diagnose a patient with epilepsy at least two unprovoked seizures must occur; and these are usually the consequence of a brain disorder rather than occurring unprovoked by an acute systemic or brain insult. A single seizure is defined as "the manifestation of an abnormal, hyper-synchronous discharge of a population of [cortical] neurons" (EB Bromfield *et al*., 2006), an event that can occur at any point during the lifetime.

Despite the long history of epilepsy research and the effectiveness of many therapies, at least 30% of epilepsy patients do not respond to medical treatment and may suffer numerous debilitating side effects as a result (Bazhanova *et al*., 2021; Rana & Musto, 2018). Epilepsy prevalence is particularly high in the third world; the World Health Organization estimates that roughly 80% of people suffering from epilepsy live in low- or middle-income countries. This is particularly evident in sub-Saharan Africa, where the lifetime prevalence was reported as high as 16 sufferers per 1000 of the population (Owolabi *et al*., 2020) in 2020, compared to the global lifetime prevalence of 7.6 per 1000 (Fiest *et al*., 2016) reported in 2017. The prevalence in Sub-Saharan Africa is considerably higher than the global average due to high levels of head trauma and brain infections including meningitis, malaria and

neurocysticercosis (Preux & Druet-Cabanac, 2005), the downstream damage of which can cause seizures and/or epilepsy. A common factor in these causes of acquired epilepsy is significant neuroinflammation, which in turn is thought to drive the epileptogenic process (Vezzani *et al*., 2011).

1.2 Communication in the nervous system

An understanding of normal neuronal communication and function is necessary prior to understanding how disruptions to the brain's homeostatic state (such as by genetic mutations, neurotrauma, brain malformations or neuroinflammation) can result in seizures and/or epilepsy. Neurons and glia are the two main cell types of the human nervous system. Neurons form a vast, highly interconnected network which allows for rapid communication of information across the body. They typically consist of a cell body (which contains organelles), dendrite (which receives information) and the axon (which sends information to other cells), and these can be in various arrangements. Glia are the regulatory cells of the nervous system, maintaining the necessary homeostasis that facilitates normal neuronal function as well as performing constant immune supervision (Kandel, 2000).

Neurons are capable of communication via both chemical and electric signals (Kandel, 2000). Neurons at rest exhibit an electric potential difference (voltage) across their membranes which is produced largely by two factors; 1) the difference in concentration of Na^+ and K^+ ions as well as electrically charged amino acids and proteins between the inside and outside of the neuron; and 2) the selective permeability of the neuronal membrane to K^+ (Kandel, 2000). The inside of a neuron is typically negatively charged relative to the external environment (resting roughly between -40 and -80mV, depending on the cell type). The specific voltage at which a neuron rests is known as the "resting membrane potential" of that neuron. This voltage potential is both created and maintained by the action of multiple ion-transporting, transmembrane proteins embedded in the membrane of the neuron (Ackermann & Moshé, 2010). Most important among these is the Na^+-K^+ pump, a membrane protein which maintains a very low concentration of Na^+ inside the neuron and a very high concentration of K^+ ions inside the cell (Kandel, 2000). Moreover, the ion channels in the neuronal membrane are highly permeable to K^+ ions but much less permeable to Na^+ ions,

and as such, at rest, K^+ ions leak out of the cell leaving a relatively negatively charged environment inside the neuron. The potential difference across neuronal membranes facilitates the complex and extensive neuronal communication that we observe in the nervous system.

To communicate, neurons form connections with one another known as synapses. At each synapse, the pre-synaptic neuron (the neuron which passes its signal to its neighbour) will release neurotransmitters from its axon terminal into the synaptic cleft (pictured in Figure 1.2.1). This release is the result of chemical signaling which the pre-synaptic cell would have received from another neuron. Released neurotransmitters bind to membrane-bound receptors on the post-synaptic neuron (the neuron receiving the chemical signal), causing conformational changes in the receptors that allow for the flow of charged ions into or out of the post-synaptic neuron, thus causing a shift in its resting membrane potential.

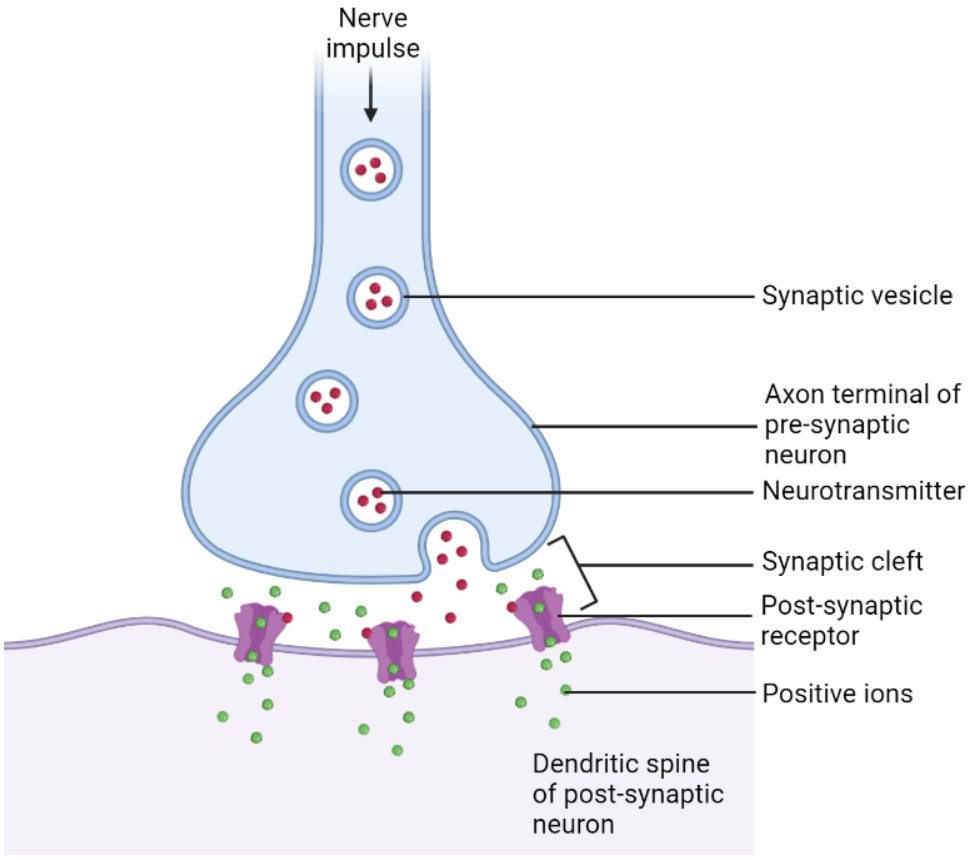

Figure 1.2.1. Anatomy of the synaptic cleft. *Nerve impulses received at the axon terminal of the presynaptic cell cause the release of neurotransmitter into the synaptic cleft. These bind to receptors*

on the dendritic spine on the post-synaptic cell, causing them to open, allowing a flow of ions into the post-synaptic cell, shifting its membrane potential. Created using Biorender.

If the resting membrane potential becomes more negative, known as hyperpolarization, the post-synaptic cell becomes less likely to generate an output and send this signal to other neurons (inhibition). On the contrary, if the resting membrane potential becomes more positive, known as depolarization, an output is more likely to be generated and propagated to other neurons (excitation). Whether a neuron is hyper- or depolarized depends on the charge and the ions that move through the activated post-synaptic receptors (Ackermann & Moshé, 2010).

1.3 The action potential represents the output signal of a neuron

If the neuron receives enough excitatory synaptic input, the membrane potential is shifted to a specific value, known as the "threshold potential" of the neuron (usually around -40mV), causing voltage-gated Na^+ transmembrane protein channels to open, which allow Na^+ ions to flow into the neuron. This shift in membrane potential allows for the opening of neighboring voltage-gated Na^+ channels (and in some neurons, voltage-gated Ca^{2+} channels, too), causing a large influx of positively charged ions which temporarily depolarizes the neuron, lasting about one millisecond. Very soon after this depolarization, the neuron is repolarized (or hyperpolarized) via the voltage-dependent closing and opening of Na^+ and K^+ channels respectively. This chain of events is known as an action potential (AP), the 'all or nothing' output signal of a neuron, sometimes referred to as 'firing' or 'spiking', and is pictured in Figure 1.3.1. This temporary perturbation in ionic concentration across the membrane then travels in all directions away from the initial site ("initial segment"), causing adjacent voltage-sensitive ion channels to open, thus causing the depolarization of the membrane at those adjacent sites. This signal is transferred to other cells that the neuron is connected to by causing a shift in the membrane potential of those cells, and so the signal travels through a network. The maximum firing rate of a neuron is set by the specific expression profile of various voltage-gated ion channels along the surface of the cell. This in turn affects the overall excitability of the cell. Variation in the expression of these different types of ion channels can

therefore produce neurons with different firing properties and levels of excitability. For example some thalamic neurons are able to display different firing modes (ie repetitive vs burst firing) depending on their baseline membrane potential due to the action of specific voltage-gated Ca2+ channels (Llinás & Jahnsen, 1982). Changes in the properties of voltage-gated channels can be pathological and predispose neurons to contribute to seizure development. Indeed, mutations in voltage-gated sodium channels are well known to underlie certain inherited forms of epilepsy (Catterall, 2012).

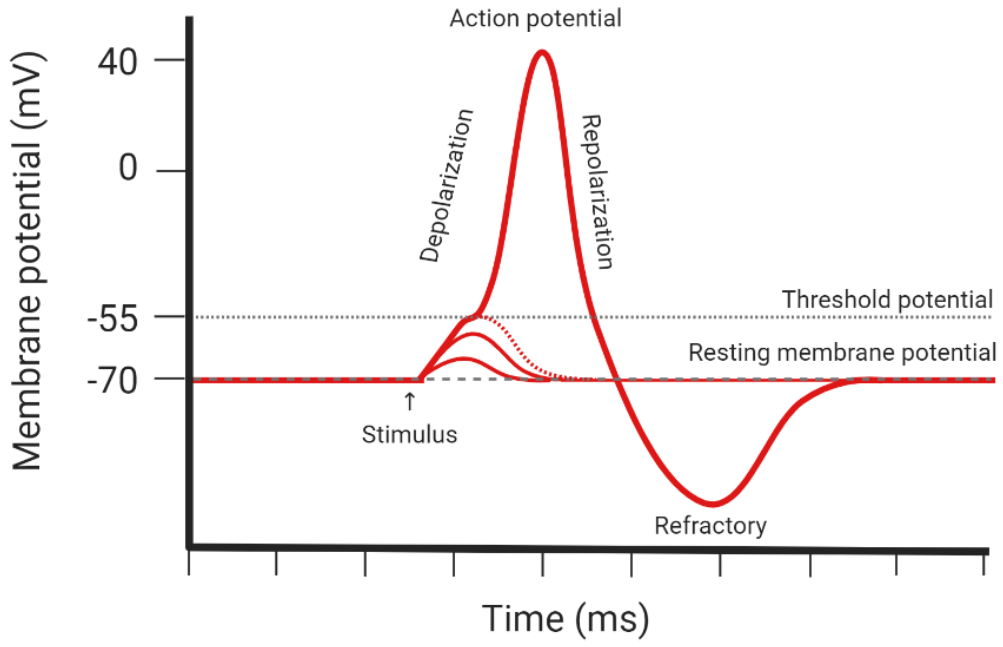

Figure 1.3.1. Phases of an action potential. *Membrane potential recording showing a neuron receiving stimulus. The stimulus shifts the resting potential of the neuron to its threshold potential causing a full depolarization. Thereafter the cell undergoes a repolarization and brief refractory period of hyperpolarization before returning to its resting membrane potential. Created using Biorender.*

1.4 Synaptic excitation and inhibition

If an AP causes the release of neurotransmitters at synaptic contacts, which depolarize the post-synaptic neurons, it is referred to as excitatory. In contrast, if the post-synaptic neuron is hyperpolarized, the message received was inhibitory. Neurons express a range of different receptors which facilitate different types of communication. Typically, excitatory signals are

conveyed by pyramidal neurons which release the neurotransmitter glutamate to produce complex processing and transfer of information across the nervous system; as such, these neurons are known as glutamatergic pyramidal neurons. Released glutamate binds to excitatory receptors, which include N-methyl-D-aspartate (NMDA), α-Amino-3-hydroxy-5-methyl-4-isoxazolepropionic acid (AMPA), kainic acid receptors and metabotropic glutamate receptors, which open and allow ion flow in response to glutamate-binding as well as binding of their respective agonists NMDA, AMPA, kainite and glutamate. Inhibitory messages, sent predominantly by inhibitory interneurons via release of the neurotransmitter gamma-amino-butyric acid (GABA), modulate and fine tune these messages (Mark F. Bear *et al*., 2007), and prevent runaway excitation that could lead to seizures (Ackermann & Moshé, 2010). GABA binds mainly to $GABA_A$ and $GABA_B$ receptors which typically allow the flow of negative ions into the neuron to hyperpolarize it.

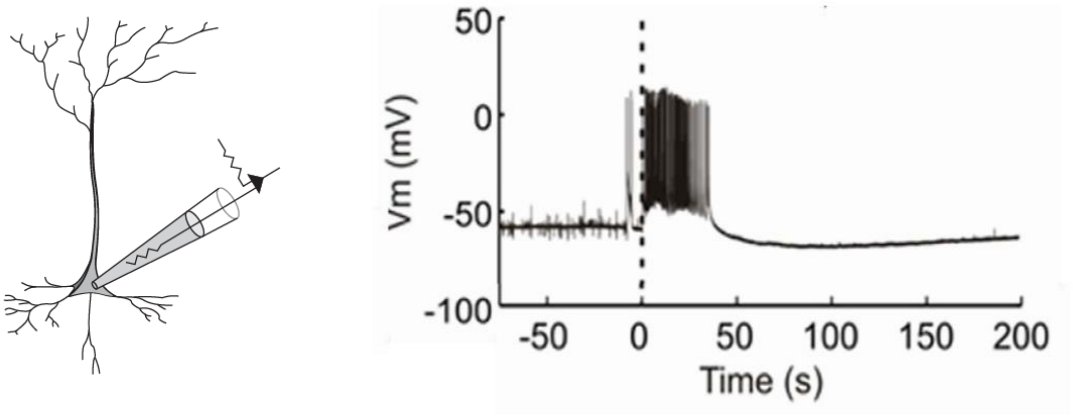

Figure 1.4.1. Whole-cell patch-clamp recording from a pyramidal neuron in a hippocampal organotypic brain slice culture undergoing a seizure-like event. *The seizure (starting after the dashed line) is evidenced by the rapid, repeated firing of the neuron. Adapted from Raimondo et al. (2012).*

Importantly, the balance of excitatory and inhibitory synaptic activity in brain networks directly affects the overall function of the nervous system (Bhatia et al., 2019). An imbalance whereby levels of synaptic excitation are not matched by similar levels of synaptic inhibition can result in unstable neuronal networks and seizures. For example, selective loss of inhibitory interneurons, or other perturbations which reduce the inhibitory efficacy of

GABAergic synaptic signaling can all result in seizures and epilepsy (MacFadden et al., 1987).

1.5 The hippocampus is especially vulnerable to seizure development

The hippocampus is a structure localized deep in the brain involved mainly in aspects of memory storage, learning and emotion (Kandel, 2000). This structure is comprised of highly organized, interconnected layers of pyramidal neurons and is pictured in Figure 1.5.1. It is divided into two key regions, namely CA1 and CA3 (where CA is an abbreviation for Cornu Ammonis). In CA1 and CA3, pyramidal neurons are arranged in a continuous layer called the stratum pyramidale, below which is the layer called the stratum radiatum, where axons from each region stretch and connect to other regions. Between CA3 and CA1 lies the lesser region, CA2. CA3 emanates out of the dentate gyrus, the structure which folds around CA3, together forming a structure that resembles two interlocking “c” shapes. Neurons in CA3 synapse onto other CA3 cells via associated axon collaterals as well as onto CA1 neurons via the Schaffer collaterals (Kandel, 2000) (which are found in the stratum radiatum). This highly interconnected nature of the hippocampus enables its complex function in learning and memory formation (especially by long term potentiation). Unfortunately, the highly recurrently connected nature of the hippocampus also causes it to be very amenable to runaway excitation and excitotoxic damage – the hippocampus is therefore a major focal site for seizure generation (Ang *et al*., 2006). As such, it is a site of great interest to epileptologists.

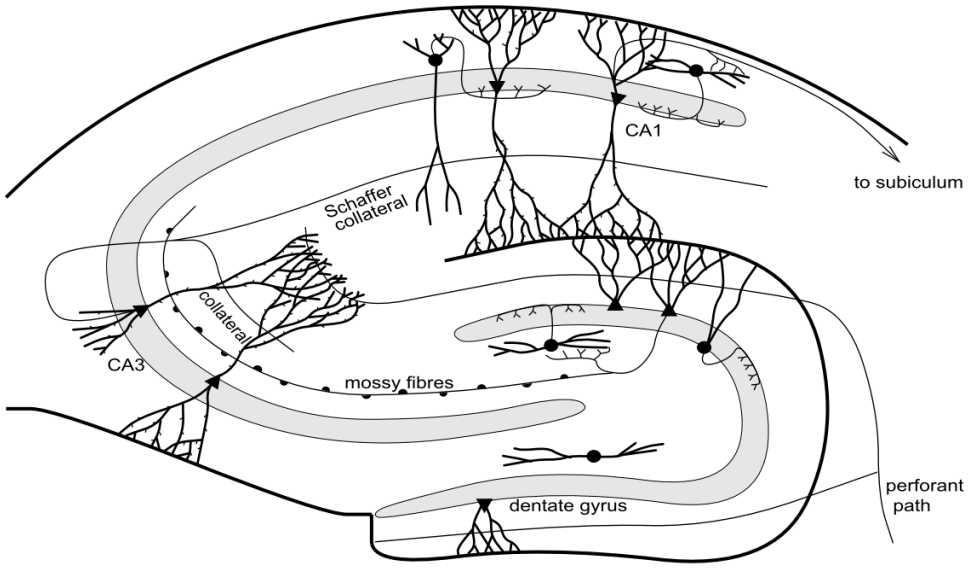

Figure 1.5.1. Anatomy of the hippocampal formation. *The dentate gyrus wraps around the CA3 region. Pyramidal neurons in the CA3 region synapse onto other neurons in CA3 via associated axon collaterals and onto cells in CA1 via the Schaffer collaterals. Adapted from Analogue resolution in a model of the Schaffer collaterals by Schultz et al. (1997).*

1.6 Neuroinflammation and epilepsy – The chicken and the egg

Drug resistant (or refractory) epilepsies – epilepsies which do not respond to any of the typical anti-epileptic drugs (AEDs) - make up about 30% of epilepsy cases (Bazhanova *et al*., 2021). Importantly, these cases have been linked to neuroinflammation, autoimmune and neurodegenerative disorders (Bazhanova *et al*., 2021). For example, it has been found that people experiencing autoimmune disease have a 3.8 times higher risk of developing epilepsy (Kopczynska *et al*., 2018). This is likely due to the fact that unregulated inflammatory processes, be they focal or systemic, promote aberrant neuronal connections and hyperexcitable neuronal networks (Rana & Musto, 2018). Unsurprisingly, anti-inflammatory treatment regimens can assist in the treatment of such refractory cases. Switching to a ketogenic (or modified Atkins diet) (Kossoff & Dorward, 2008; Wells *et al*., 2020), or eating a gluten-free diet (Verrotti *et al*., 2020) (all of which reduce systemic inflammation to some degree (Dupuis *et al*., 2015; Soares *et al*., 2013)), can lead to a positive outcome for patients refractory to AEDs. When epilepsy patients experience systemic inflammation, such as arises

from fever, immunization, trivial infection, or flare ups of autoimmune disorders, they are likely to experience seizures (Rana & Musto, 2018). Moreover, the severity and number of seizures patients experience are both reduced by application of drugs that specifically target inflammation in the brain (Ravizza *et al*., 2011), such as steroids, cytokine antagonists, monoclonal antibodies and intravenous immunoglobulins (Vezzani & Granata, 2005).

1.7 Central Nervous System Immunity is facilitated by microglia and astrocytes

For many years (since the 1920s, at least) the brain was considered an "immune privileged site" – i.e. a site where adaptive immunity and inflammation are extremely well regulated. This idea has however been challenged with research demonstrating immune cell presence post-inflammation and/or trauma, transport of adaptive immune cells across the blood-brain barrier, proliferation of innate immune cells following injury/infection as well as the release of potent cytokines and chemokines (Hubbard & Binder, 2016) after brain infection/trauma. This has given way to a more nuanced understanding of the unique immune function of the nervous system.

1.7.1 Microglia constantly monitor the brain immune landscape

The major executors of immunology in the central nervous system are the glial cells; these include microglia, astrocytes, oligodendrocytes, and ependymal cells (von Bartheld *et al*., 2016). Microglia, the tissue-resident macrophages of the brain, comprise the major innate immune cells of the central nervous system (Papageorgiou *et al*., 2016), recognizing potential infection and detecting and removing cellular debris from dying brain cells (Mark F. Bear *et al*., 2007). Further, they play the important role of pruning synapses, both during development in order to shape neuronal connections and in the adult brain when neurons are damaged (Bar & Barak, 2019). Under normal conditions, these highly dynamic cells constantly scan the brain (Davalos *et al*., 2005; Nimmerjahn *et al*., 2005) by extending their motile projections and making contact with neurons (Baalman *et al*., 2015; Y. Li *et al*., 2012; Tremblay *et al*., 2010; Wake *et al*., 2009), thereby modulating neuronal transmission (Hoshiko *et al*., 2012; Ji *et al*., 2013; Y. Li *et al*., 2012; Paolicelli *et al*., 2011; Paolicelli &

Gross, 2011; Pascual *et al*., 2012; Zhang *et al*., 2014) and keeping watch for infection or damage (Wu *et al*., 2015). When they encounter a threat they rapidly (Davalos *et al*., 2005) change morphology from a ramified shape to a more motile, ameboid shape (Zhao *et al*., 2018) allowing for migration to the site of damage, they release cytokines and chemokines, they change their receptor expression and antigen presentation, engage in phagocytosis and can release nitric oxide (Biber *et al*., 2014; Hanisch & Kettenmann, 2007; Ransohoff & Perry, 2009), a group of characteristics marking the cells as "activated" (Eyo *et al*., 2017). The activated phenotypes can range from pro-inflammatory (and possibly neurotoxic) to anti-inflammatory and neuroprotective, depending on the types and duration of stimuli they receive (Papageorgiou *et al*., 2016).

1.7.2 Multifaceted and multifunctional astrocytes regulate more than just immunity

Astrocytes are the largest group of glial cells. They contribute critically to normal CNS development, provide structural and metabolic support to neurons, assist in the creation of the blood brain barrier, assist in maintaining homeostasis, regulate synaptic transmission and blood flow, provide immune protection to neurons and respond to injury (Hubbard & Binder, 2016). Furthermore, astrocytes have been shown to regulate water homeostasis, balance acidity in the brain and control extracellular ion concentration. They likely play an essential role in preventing off target neurotransmitter effects by wrapping themselves around synapses (Nagelhus *et al*., 2013), forming what is known as the "tripartite synapse" (Hubbard & Binder, 2016) (the other two components of which are the pre- and post-synaptic neurons). By associating so closely with neurons, they are also able to modulate neuronal communication by releasing both neuro- and glio-transmitters (Nagelhus *et al*., 2013) and by controlling the availability of neurotransmitters in the synapse (Diaz Verdugo *et al*., 2019). They play an essential role in regulating potassium availability (Diaz Verdugo *et al*., 2019; Papageorgiou *et al*., 2016) at the synapse and form a "functional syncytium" via their extensive gap junction connections, which allows for the rapid redistribution of ions across long distances in the brain (Diaz Verdugo *et al*., 2019; Scemes & Spray, 2003; Volman *et al*., 2012). Crucially, astrocytes control the uptake, degradation and resupply of glutamate at synapses, thus enabling normal neuronal communication (Coulter & Eid, 2012), but also

poising themselves as critical players in runaway excitotoxicity when this regulation goes awry. Indeed, changes to astrocytic coupling and clearances of potassium have been linked with temporal lobe epilepsy in both rodents and humans (Bedner *et al*., 2015; Schröder *et al*., 2000; Wallraff, 2006). Furthermore, spontaneous seizures are observed in transgenic mice deficient in astrocytic gap junction coupling (Diaz Verdugo *et al*., 2019; Wallraff, 2006).

1.7.3 The Blood-Brain Barrier and infiltrating peripheral immune cells

A description of nervous system immunology would not be complete without mention of the blood-brain barrier (BBB), a complex structure which protects the brain from blood-borne pathogens and foreign substances, thus enabling a stable environment for normal neuronal function (Kandel, 2000). The existence of this structure contributed to early ideas of the brain as an 'immune-privileged' site, since it was believed to prevent the movement of immune cells into the brain at all times. The BBB is formed primarily by the endothelial cells of unfenestrated brain micro-vessels. Wrapped around these are pericytes, and around these lie the processes of astrocytes (seen in Figure 1.7.3.1), creating a multi-layered sheath which is highly selective in what it allows into the blood supply entering the brain (Kandel, 2000; van Vliet *et al*., 2015). Unfortunately this specialized organ is not always fully functional. When inflammatory events such as infections or trauma occur, activated microglia and astrocytes cause the upregulation of adhesion molecules, cytokine and chemokine production and chemokine receptor expression in the endo- and epithelial cells of the BBB. Adhesion molecules interact with integrins on circulating leukocytes (including T lymphocytes), monocytes and platelets, allowing for their extravasation through the BBB and into the brain, which in turn enhances the immune response (Rana & Musto, 2018) when these peripheral cells are stimulated by antigen presenting cells or antigenic proteins in the brain. For example, activated peripheral T lymphocytes express and release interferon-gamma (IFNγ), a potent pro-inflammatory cytokine that can bolster the immune response (Papageorgiou *et al*., 2016; Ta *et al*., 2019; Zhang *et al*., 2020) and contribute to immune-related damage. Additionally, activation of metalloproteinases and catabolism of arachidonic acid (which can produce pro-inflammatory eicosanoids) occurs in the brain microvasculature in response to activated microglia and astrocytes (Bosetti, 2007). All of these events increase the overall

permeability of the BBB, yet further enhancing the infiltration of serum proteins (such as albumin) and peripheral immune cells, and thus a vicious sequence of runaway inflammatory events which can lead to the development of seizures and/or epilepsy (Marchi *et al*., 2007, 2010; Rana & Musto, 2018; Seiffert *et al*., 2004; van Vliet *et al*., 2007).

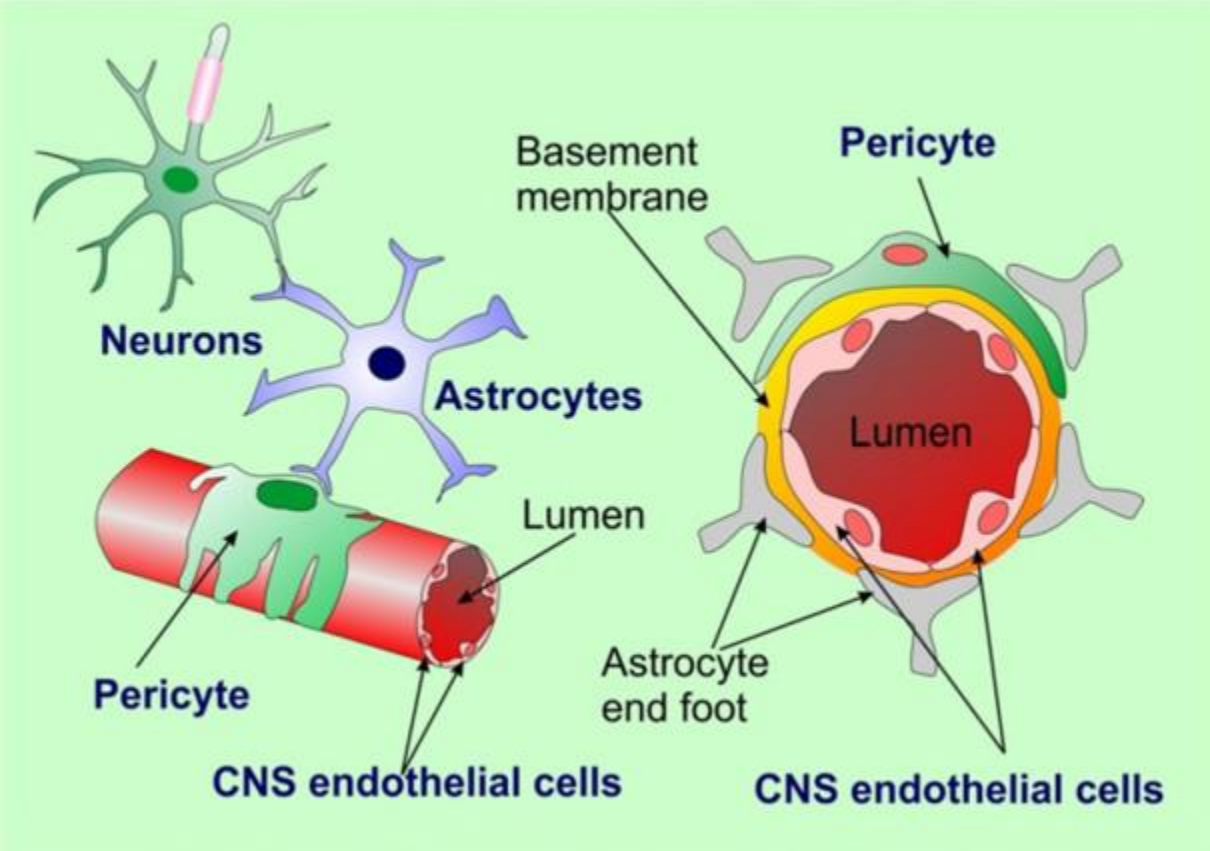

Figure 1.7.3.1. Anatomy of the blood-brain barrier. *The BBB is formed by CNS blood vessel endothelial cells which are surrounded by pericytes and astrocytic end-feet. Adapted from Gupta, Dhanda and Sandhir (2019).*

1.8 LPS and IFNγ elicit powerful CNS immune activation

Like peripheral immune cells, microglia and astrocytes express pattern recognition receptors (PRRs) in order to sense damage and/or infection (via recognition of pathogen-associated molecular patterns, PAMPs) and to induce their activation (Bowman *et al*., 2003). Among these PRRs are the Toll-Like Receptors (TLRs), of which there are multiple sub-types in mice and humans (Facci *et al*., 2015), each recognizing a specific set of PAMPs. Of particular

interest is TLR-4, a PRR that recognizes the bacterial cell wall component lipopolysaccharide (LPS) from gram-negative bacteria, as well as danger-associated molecular patterns (DAMPs) that are released by injured tissue (Bianchi & Manfredi, 2009; Vogl *et al*., 2007); it can thus sense both non-sterile and sterile danger.

LPS (typically sourced from *E.coli* in scientific studies) has become central to studying immune activation in the nervous system because it so reliably produces detectable immune responses (Kwon *et al*., 2010; Maroso *et al*., 2010; Papageorgiou *et al*., 2016; Pascual *et al*., 2012) by potently activating TLR-4. Indeed, systemic pre-administration of LPS to mice heightened their susceptibility to seizures, an effect which could be blocked by treatment with anti-inflammatory drugs (Sayyah *et al*., 2003). Once recognized by TLR-4 and LPS-binding protein, the transcription factor NF-κβ is activated, causing the activation of multiple pro-inflammatory genes, including those coding for cytokines and chemokines, as well as participating in inflammasome formation (T. Liu *et al*., 2017; Maroso *et al*., 2010). Curiously, previous work has shown (in rat glial cells and human glioma cells) that some AEDs decrease LPS-induced activation of NF-κβ and production of nitric oxide (NO) and pro-inflammatory prostaglandins, contributing to the inflammatory hypothesis of seizure generation (Ichiyama *et al*., 2000; Matoth *et al*., 2000). LPS can also induce the production and release of the free radical NO from microglia (Papageorgiou *et al*., 2016). In sustained or high concentrations, NO is typically toxic to neurons and has been among the proposed culprits of neuronal dysfunction in neuroinflammatory studies (Papageorgiou *et al*., 2016).

Some studies have attempted to bolster the effect of LPS by addition (or by priming, where the immune system is pre-exposed to immune stimulants) of various other inflammatory molecules such as polyinosinic-polycytidylic acid (poly I:C) (Combrinck *et al*., 2002; Cunningham *et al*., 2005, 2009; Field *et al*., 2010) and IFNγ (Papageorgiou *et al*., 2016; Ta *et al*., 2019; Zhang *et al*., 2020). IFNγ is a soluble, dimerized cytokine and the only member of the type 2 class of IFNs. It is released predominantly by leukocyte subtypes such as natural killer cells, T helper type 1 lymphocytes and cytotoxic T lymphocytes (Ta *et al*., 2019) and causes activation of the transcription factor STAT1 (Papageorgiou *et al*., 2016). Interestingly, these cells also express TLR-4 and respond to LPS, thus heightening any already-present

immune activation (Papageorgiou *et al*., 2016). Thus, addition of IFNγ to cultured cells is a way to mimic the adaptive immune response. IFNγ receptors (IFNγR) are expressed on microglia, astrocytes and neurons (Carpentier *et al*., 2005; Mizuno *et al*., 2008; Monteiro *et al*., 2016). Once released, it can also stimulate other infiltrating peripheral immune cells. IFNγ is recognized by microglia and can potently activate them, causing the release of pro-inflammatory cytokines like TNF-α (Ta *et al*., 2019). Under normal conditions, this release usually happens later in the disease progression once peripheral immune cells are recruited to the brain, and could be what sustains a pro-inflammatory milieu.

Combinations of immune stimulants typically produce immune responses stronger than that which individual types of molecules can evoke (Papageorgiou *et al*., 2016; Ta *et al*., 2019), such as those observed when LPS and IFNγ were co-applied to rat hippocampal OBSCs by Papageorgiou *et al*. (2016).

1.9 Cytokines link inflammation to electrical changes by modulating glutamate regulation and receptor trafficking

As mentioned above, activated brain immune cells release cytokines and chemokines which can have major downstream effects because the receptors for these are found on neurons, glia and endothelial cells (Vezzani, 2014). Cytokines are mainly released by activated microglia and astrocytes after they recognize a PAMP or DAMP, but interestingly, cytokines can also be released by neurons in the acute phase of brain insult. Importantly, the over-production and/or prolonged presence of cytokines in brain tissue is associated with notable brain dysfunction such as neuropathic pain, psychiatric disorders, neurodegenerative diseases and epilepsy (Vezzani, 2014). Whether inflammation is protective or deleterious depends on the concentration of cytokines released, the length of time that the tissue is exposed to inflammatory agents and the balance between neurotrophic and cytotoxic factors produced by immune cells (Vezzani & Granata, 2005). There seems to be a chicken-egg scenario (Laxer *et al*., 2014) when it comes to seizures and cytokines – studies report raised levels of cytokines very soon after status epilepticus (Borges *et al*., 2003; Rojas *et al*., 2014; Varvel *et al*., 2016; Vezzani *et al*., 2015), and others report that raised cytokine levels (as a result of trauma or infection) can predispose the brain to seizure-like events (SLEs),

lengthening and worsening these at later time points (Laxer *et al*., 2014; Musto *et al*., 2011, 2016; Rana & Musto, 2018).

1.9.1 IL-1β

A trove of recent inquiry into the role of cytokines in the development of seizures has highlighted a few key players, namely: TNF-α, IL-6, IL-1β, IL-10 and IFNγ. The pro-inflammatory cytokines TNF-α, IL-6 and IL-1β have been shown to be increased in both experimental and clinical epilepsy studies (M. G. De Simoni *et al*., 2000; Rana & Musto, 2018). IL-1β, expressed by activated microglia has been found to be upregulated as late as 60 days after status epilepticus in rats with spontaneous seizures (M. G. De Simoni *et al*., 2000) and is known to be increased in the brain (Alyu & Dikmen, 2017) and cerebrospinal fluid (Ichiyama *et al*., 1998) of humans after seizures. Excitatory pyramidal neurons express receptors for cytokines; when bound by TNF-α and/or IL-1β the result is a change in the expression of glutamate (increased) and GABA (decreased) receptors that makes the neuron more excitable (Rana & Musto, 2018). Furthermore, IL-1β causes increased glutamate release from astrocytes as well as reduces glutamate re-uptake by astrocytes, resulting in an external milieu with increased glutamate (Rana & Musto, 2018). Interestingly, IL-1 and TNF- α receptors are swiftly upregulated in neurons during seizures (Balosso *et al*., 2005; Ravizza & Vezzani, 2006), adding to the idea that these are key players in inflammation-induced damage during status epilepticus/SLEs/seizures. This, combined with changes to receptor expression on neurons can predispose neuronal networks to severe excitotoxicity and possibly seizures.

1.9.2 TNF-α

In addition to the action of IL-1β, TNF-α has multiple, complementary mechanisms by which it enhances glutamate-mediated cytotoxicity. First it affects glial cells: glutamate release from astrocytes is strongly stimulated by TNF-α and glutamate transporters on astrocytes are inhibited (Olmos & Lladó, 2014) thereby limiting the ability of the astrocytes to mop up the extra glutamate. In microglia, TNF-α stimulates its own release (Stellwagen & Malenka, 2006). It also stimulates glutamate release, and this glutamate acts on microglial metabotropic glutamate receptors stimulating those very microglia to release yet more TNF-

α (Olmos & Lladó, 2014; Rana & Musto, 2018). Second, TNF-α swiftly induces the expression of Ca^{2+}-permeable AMPA receptors (Papageorgiou *et al*., 2016) and NMDA receptors on the neuronal membrane surface and simultaneously causes $GABA_A$ receptor endocytosis from the neuron (Stellwagen *et al*., 2005). The overall effect of these changes tips the balance of excitation and inhibition in the neuron, resulting in a higher excitation:inhibition ratio, and thus a more excitable (and therefore more likely to participate in seizure behavior) neuron (Olmos & Lladó, 2014). This excessive excitation:inhibiton ratio allows Ca^{2+} to flood into neurons, causing them to undergo excitotoxic death and to release their internal contents, which act as DAMPs. These DAMPs keep the glia in activated states, releasing yet more TNF-α (and other cytokines). Interestingly, when cultured neurons were exposed to TNF-α-containing media from activated microglia, caspase-3 was activated in the neurons and they died specifically by apoptosis (Taylor *et al*., 2005; Zhu *et al*., 2010).

1.9.3 IL-6

The role of IL-6 pre- and post SLEs is slightly more nuanced. It is upregulated in response to other cytokines such as TNF-α and IL-1β (Erta *et al*., 2012), and has been shown to increase gliosis, contributing to a pro-epileptogenic environment, as new glial cells can release more pro-inflammatory cytokines. Interestingly, this cytokine is release by microglia, astrocytes, endothelial cells and neurons (Erta *et al*., 2012). Other work has shown that treatment with IL-6 or overexpression of the cytokine are pro-convulsant (Kalueff *et al*., 2004; Samland *et al*., 2003). Furthermore, upregulation of IL-6 can reduce LTP and neurogenesis in the hippocampus while simultaneously enhancing gliosis – a dangerous environment that could facilitate seizure development (Erta *et al*., 2012; Levin & Godukhin, 2017). Nevertheless, it seems that IL-6 is also necessary for survival and is normally released following injury or damage (Erta *et al*., 2012). In line with the protective hypothesis, IL-6 knock-out mice are more susceptible to convulsant stimuli, showing clear hippocampal damage as a response (De Sarro *et al*., 2004; Luca *et al*., 2004; Penkowa *et al*., 2001). It is clear that IL-6 is an important factor in CNS immunity, but its role may be more complex than current understanding supports.

1.9.4 IL-10

IL-10 is an anti-inflammatory cytokine that has neuroprotective and anti-convulsive effects (Y. Youn *et al*., 2013) and microglia are the primary producers of IL-10 in the CNS (Lobo-Silva *et al*., 2016). Evidence exists that IL-10 acts to dampen the activated immune system after inflammatory insults via a negative feedback loop (Y. Youn *et al*., 2013), suppressing pro-inflammatory cytokine production (G. Li *et al*., 2011). IL-10 spikes in plasma 48-72 hours after seizures in neonates and seems to play an anti-convulsant role in doing so (Y. A. Youn *et al*., 2012).

1.10 Hippocampal Organotypic Brain Slice Cultures are an ideal model to study the electrical effects of LPS+IFNγ-induced neuroinflammation

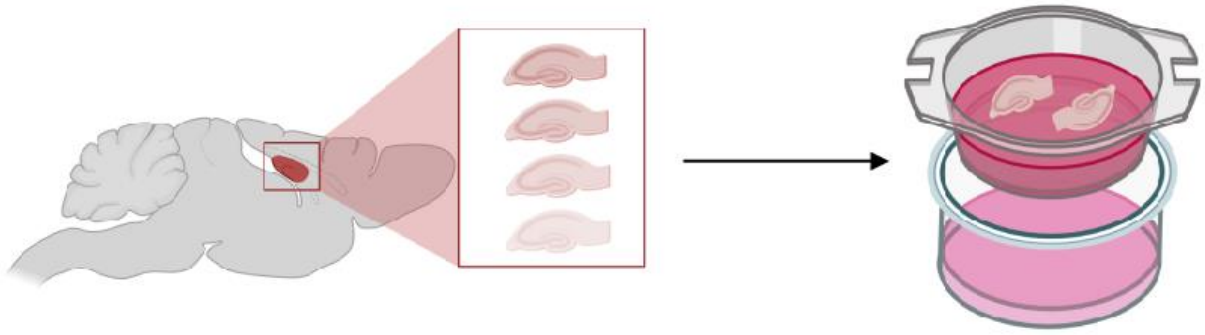

Figure 1.10.1. Preparation of hippocampal organotypic brain slice cultures. *The hippocampus is removed from the brain, sliced and then cultured on interface membranes for use in various experimental paradigms. Created using Biorender.*

Hippocampal organotypic brain slice cultures (OBSCs) constitute an *in situ* model (pictured in Figure 1.10.1) that is ideal for studying neuroinflammation. OBSCs retain all normal brain cell types as well as the finely preserved, complex cytoarchitecture of the hippocampus (Coleman *et al*., 2020; Sheppard *et al*., 2019). The cultures survive for prolonged periods (Stoppini *et al*., 1991) (up to 3 weeks), have functional neuronal networks (Ta *et al*., 2019) and display functional maturation of synapses (Bonhoeffer & Yuste, 2002; Hasegawa *et al*., 2015; Nägerl *et al*., 2008; Verkuyl & Matus, 2006). OBSCs from rodents have been

extensively used to study inflammation using various pro-inflammatory agents (Papageorgiou *et al*., 2016; Pascual *et al*., 2012; Ta *et al*., 2019) as well as for the extensive study of microglial behavior under different circumstances (Coleman *et al*., 2020; Ji *et al*., 2013; Masuch *et al*., 2016; Montero *et al*., 2009; Vinet *et al*., 2012; Weinhard *et al*., 2018). These cultures critically lack access to the circulatory system during experimentation, and thus lack adaptive immunity/infiltration of leukocytes (Ajmone-Cat *et al*., 2013; Daria *et al*., 2017; Kann *et al*., 2011; Vinet *et al*., 2012), allowing for purely experimental control in modelling the effect of infiltrating leukocytes by addition of the cytokine IFNγ. Crucially, OBSCs allow very good experimental access to tissue – this allows for the electrophysiological investigations following immune activation treatments. Beyond this, OBSCs culture media can be used to detect released cytokines and various staining and/or immunohistochemical analyses can be performed using the same slices. This maximizes experimental output while drastically reducing the number of animals needed to perform such analyses.

1.11 Addressing the lack of understanding of the electrical effects of "bolstered" immune activation

Clearly, there exist an extensive array of mechanisms by which neuro-immune activation can alter normal neuronal function. As described above, CNS immune cells and cytokines can tip the brain into a more excitable state. To the contrary, others have found that bolstered immune activation can cause the death of brain cells (Papageorgiou *et al*., 2016) and the slowing (Ta *et al*., 2019) or abolishment (Papageorgiou *et al*., 2016) of gamma oscillations which are indicative of normal network function. A study by Hellstrom *et al*. (2005) examining the effects of chronic immune activation showed that long-term LPS exposure causes decreased membrane resistance, increased AP threshold, less frequent APs and increased IL-1β-dependent GABAergic transmission. Taken together, their results suggest that chronic immune activation reduces intrinsic neuronal excitability and increases inhibitory tone. These particular studies suggest that neuroinflammation can also increase inhibition and reduce the ability of networks to generate and sustain seizures, casting doubt on the pro-convulsant effects of neuroinflammation mentioned previously.

As such, there still lacks a clear overall picture of the effects of immune activation on the network function (Aims 3&4) and basic membrane properties (Aim 5) of hippocampal neurons. This thesis sought to address the current lack of understanding of the electrical effects of "bolstered" immune activation through co-application of LPS and IFNγ and subsequent electrophysiological studies. This data is further coupled with measurement of cytokine release (Aim 1) and cell death studies (Aim 2) to provide an overarching description of neuroinflammation in the hippocampal OBSCs model.

1.12 Aims

Aim 1: Characterize the production of cytokines following immune activation over multiple days.

Aim 2: Explore and characterize cell death outcomes of hippocampal organotypic brain slice cultures following chronic immune activation.

Aim 3: Explore the effect of chronic immune activation on network synaptic function.

Aim 4: Investigate the effect of medium-term immune activation on network synaptic function.

Aim 5: Explore the effect of acute immune activation on the basic membrane properties of pyramidal neurons.

1.13 Objectives

Aim 1: Characterize the production of cytokines following immune activation over multiple days.

Objective 1.1: Use enzyme-linked immunosorbent assays (ELISAs) to quantify the presence of the cytokines TNF-α, IL-6, IL-1β and IL-10 in the culture media of OBSCs following immune activation.

Aim 2: Explore and characterize cell death outcomes of hippocampal organotypic brain slice cultures following chronic immune activation.

Objective 2.1: Develop an assay to determine apoptotic and necrotic cell death in OBSCs.

Objective 2.2: Use a developed cell-death assay to explore cell death after chronic immune activation in OBSCs.

Aim 3: Explore the effect of chronic immune activation on network synaptic function.

Objective 3.1: Set up a model of "bolstered" immune activation in hippocampal organotypic brain slices using co-application of LPS and IFNγ in culture media for 72 hours. Compare this to control slices, slices treated with LPS only and slices treated with NMDA+4-AP (positive excitotoxic control).

Objective 3.2: Record both excitatory and inhibitory spontaneous post synaptic currents from immune activated hippocampal OBSCs, as well as basic cell properties.

Aim 4: Investigate the effect of medium-term immune activation on network synaptic function.

Objective 4.1: Set up a model of "bolstered" immune activation in hippocampal organotypic brain slices using co-application of LPS and IFNγ in culture media for 24 hours.

Objective 4.2: Record both excitatory and inhibitory spontaneous post synaptic currents from immune activated hippocampal OBSCs, as well as basic cell properties. Compare this to control slices and slices treated with NMDA+4-AP (positive excitotoxic control).

Aim 5: Explore the effect of acute immune activation on the basic membrane properties of pyramidal neurons.

Objective 5.1: Set up a model of acute immune activation during whole-cell patch-clamping.

Objective 5.2: Use whole-cell patch-clamping to record basic membrane properties of pyramidal neurons before and during acute exposure to LPS and IFNγ.

Chapter 2

Methodology

2.1 Animals

All animal handling, care and procedures were carried out in accordance with South African national guidelines (South African National Standard: The Care and Use of Animals for Scientific Purposes 2008) and with approval from the University of Cape Town Animal Ethics Committee (Protocol No: AEC 018/018). All animal rooms were maintained between 22-24°C, with a lux of 100-300, relative humidity between 50-70% and food and water available ad libitum.

2.2 Organotypic Hippocampal Brain Slice Culture

Hippocampal OBSCs were prepared using 6-9 day old male/female C57BL/6 mice based on the protocol originally described by Stoppini *et al*. (1991). Mice were transported from the UCT Animal Unit to the tissue culture laboratory and allowed to acclimate before the procedure. The brains were extracted and quickly placed in ice-cold (4 °C) dissection media (EBSS, supplemented with 6.1 g/L HEPES, 6.6 g/L D-glucose and 200 µL saturated sodium hydroxide (all from Sigma-Aldrich)). The hemispheres were separated and the hippocampi removed. These were immediately cut into 350 µm thick slices using a McIlwain tissue chopper (Brinkmann, Mickle). Slices were then rinsed and swirled in cold dissection media to separate them from one another. The slices with the best architectural integrity were selected and placed onto 6-well-plate MilliCell-CM membrane inserts (Merck) in warmed (37 ºC) culture medium (1.2 mL per well in 6-well plates) consisting of (vol/vol); 23 % EBSS, 50 % MEM with glutamax, 25 % heat-inactivated horse serum (Biochrom), 2 % B27 and 6.5 g/L glucose (all from Sigma-Aldrich unless otherwise specified). Slices were kept in a humidified incubator at between 35-37 °C, 5 % carbon dioxide (CO_2) and culture medium was replaced every 2-3 days. For some experiments LPS (10 µg/mL), IFNγ (100 ng/mL), NMDA (5 µM) or 4-AP (100 µM) were added to the culture medium for 24 or 72 hours. Slices were used for electrophysiological recordings or analyses of cell death after 6-14 days in culture, since this

is the optimal time for slice recovery after slicing procedures (i.e. cell debris is removed and major inflammatory events have passed) but the slice is not yet old enough for recurrent connections to be common (which usually results in excessive excitability). Slices used for electrophysiological recordings were plated 2 or 3 slices per well, and those used for cell death staining were plated 6 per well. Hippocampal slices were chosen for this project for two main reasons; first, the hippocampus is frequently involved in the development of seizures (A. De Simoni & MY Yu, 2006) and second, the high reliability of the hippocampal organotypic slice culture method.

2.3 Electrophysiology

2.3.1 In vitro patch-clamp recordings

After 6-14 days in culture and relevant treatment application, brain slices were transferred to a submerged recording chamber on a patch-clamp rig and continuously superfused with standard artificial cerebrospinal fluid (aCSF) (NaCl (102 mM); KCl (3 mM); $MgCl_2$ (2 mM); $CaCl_2$ (2 mM); NaH_2PO_4 (1.2 mM); $NaHCO_3$ (23 mM) and D-glucose (11 mM) in deionized water with pH adjusted to between 7.35-7.40 using 0.1 mM NaOH (Sigma-Aldrich)). The aCSF was maintained at a temperature between 28-33 °C and constantly bubbled with carbogen gas (95 % O_2:5 % CO_2) using peristaltic pumps (102R, Watson-Marlow Fluid Technology Group). Pyramidal neurons in the CA3 and CA1 regions of the hippocampus were located using a Olympus BX51WI upright microscope using the 10x and 40x air and water immersion objectives, respectively, and selected for recording. Borosilicate glass capillaries (outer diameter 1.2 mm, inner diameter 0.69 mm, Harvard Apparatus Ltd) were used to prepare glass micropipettes with a tip resistance between 3 and 8 MΩ using a horizontal pipette puller (Sutter). Patch-clamp recordings were made using Axopatch 200B amplifiers (Axon Instruments) and mains noise was reduced using a Humbug noise eliminator. Data was acquired using WinWCP (University of Strathclyde). Recordings where access resistance was higher than 30 MΩ were discarded. Traces from all patch-clamp recordings were analyzed using custom Matlab (R2015b, Mathworks) scripts written by Dr Joseph Raimondo (University of Cape Town). Depending on the experiment, data were acquired in either current- or voltage-clamp mode. Two pipette-internal solutions were used:

1. A standard internal solution (K-gluconate (126 mM), KCl (4 mM), HEPES (10 mM), Na_2ATP (4 mM), NaGTP (0.3 mM) and Na_2-phosphocreatine (10 mM); all from Sigma-Aldrich);

2. A cesium internal solution (CsOH (120 mM), Gluconic acid (120 mM), HEPES (40 mM), Na_2ATP (2 mM), NaGTP (0.3 mM) and NaCl (10 mM), (all from Sigma-Aldrich).

2.3.2 Basic membrane properties

To study the effect of acute immune activation on the intrinsic properties of pyramidal neurons, whole-cell voltage- and current-clamp recordings were made from CA3/CA1 pyramidal neurons in organotypic hippocampal culture slices. There recordings were made using the standard internal solution (1) and standard aCSF. A baseline recording was established for 15 minutes. Following this, and whilst recording the electrical activity from single neurons, LPS (10 µg/mL) + IFNγ (100 ng/mL) (mixed into circulating standard aCSF) were washed over the slice using the perfusion system at a pump rate of 15 rpm. Every five minutes for 60 minutes, voltage and current steps were applied to the cell, and a voltage output was recorded from the cell whilst in current-clamp mode for 1 minute. These recordings were made using pipette-internal solution (1) above. Traces were analyzed using custom Matlab scripts written by Dr Joseph Raimondo (University of Cape Town) to extract the following data:

Resting membrane potential, action potential threshold, access resistance, total resistance, membrane resistance, membrane capacitance, current threshold density, absolute maximum spike rate and maximum sodium current.

2.3.3 Spontaneous Post-Synaptic Currents

To understand the effect of LPS- and IFNγ-induced neuroinflammation on synaptic function, spontaneous Post-Synaptic Currents (sPSCs) of both an excitatory and inhibitory nature were recorded. This was achieved in voltage-clamp mode using the cesium internal solution described above (2). In voltage-clamp mode, cultured pyramidal neurons from the CA3 or CA1 area were held at -70 mV (to record excitatory sPSCs, sEPSCs) or +15 mV (to record inhibitory sPSCs, sIPSCs). After a giga-seal was achieved and a patch established, cells were allowed to stabilize for two minutes, following which voltage steps were applied to the

neuron. The cell was then shifted slowly to -70 mV and allowed to stabilize for two minutes, following which a five minute recording of sEPSC was initiated. The cell was then very slowly shifted to +15 mV and allowed to stabilize for two minutes, following which another five minute recording of sIPSCs was initiated. Voltage step recordings were analyzed using custom MATLAB scripts written by Dr Joseph Raimondo (University of Cape Town) to extract total resistance, access resistance, membrane resistance and membrane capacitance for each patched cell. Post-synaptic currents were analyzed using custom MATLAB scripts written by Dr Thijs Verhoog (University of Cape Town), as well as Synaptosoft MiniAnalysis software (Justin Lee, Columbia University, 1997) and pClamp Clampfit 10.2 (Molecular Devices). A reading of Root Mean Square (RMS) noise was detected using Synaptosoft MiniAnalysis. Based on this value, a current threshold was set at a minimum of 1.5 times the value of the measured RMS noise. IF the programme failed to run an analysis, the threshold was adjusted accordingly. All events were recorded with a threshold between +/-15pA and +/-40pA based on the measured noise in each recording.

2.4 Cell death studies

Propidium Iodide (PI) is a fluorescent, intercalating molecule which binds to DNA between bases with low sequence preference. Unbound, propidium iodide displays an excitation maximum near 500 nm and an emission maximum near 625 nm. When bound to DNA, there is a red shift of the excitation maximum to 540nm and the emission maximum to 640 nm, with a two- to threefold increase in fluorescence intensity from baseline (Chacon *et al*., 1997). Due to its fairly large size, PI cannot enter cells unless their membranes are compromised. As such, PI is commonly used to study cell viability, or more specifically to stain dead/dying cells with a compromised membrane – i.e. cells dying by necrosis.

Caspases are a family of protease enzymes which play essential roles in both inflammatory and cell death pathways (including apoptosis and necrosis). The activation of different members in this family can secure the fate of a cell – as well as indicate which type of cell death it is undergoing. Caspase-3, for example, is a key effector in the apoptosis pathway, where it amplifies signals from initiator caspases (such as caspase-8); its activation commits the cell to full cellular disassembly (*Caspase-3 Activation: An Indicator of Apoptosis in Image-*

Based Assays, 2012). Activation of these enzymes can be detected using caspase-cleavage detectors such as CellEvent Caspase3/7 Green detection reagent (ThermoFisher). This cell-permeant molecule consists of a four-amino acid peptide (aspartate-glutamate-valine-aspartate; DEVD); this contains a recognition site for caspases 3 and 7. This sequence is additionally conjugated to a nucleic acid-binding dye. The DEVD peptide inhibits the ability of the dye to bind to DNA, and as such the molecule is not fluorescent until activated caspases 3 or 7 cleave the DEVD peptide. This cleavage allows the dye to bind DNA and as such to fluoresce (a bright green signal is produced, with absorption/emission maxima at approx. 502/530 nm), indicative of apoptosis.

The following method was adapted and modified from Welsch *et al*. (2017) and developed for my specific experimental needs. The entire assay was performed in the darkest possible conditions, since all dyes used are light-sensitive. Hippocampal OBSCs were prepared (6 slices per well) and cultured for 5 days as described above. On DIV05, the culture medium was replaced with culture medium supplemented with LPS (10 µg/mL), LPS (10 µg/mL) + IFNγ (100 ng/mL) or NMDA (5 µM) + 4-AP (100 µM). Control slices received fresh culture medium only. This treatment was applied for either 24 or 72 hours. After treatment, the interface membrane around each slice was cut such that each slice was free floating on a piece of membrane with roughly 1 cm diameter. Each slice+membrane was transferred to a well within a 24-well-plate containing 500 µL solution of culture medium supplemented with 5mM CellEvent Green Caspase 3/7 Detection agent (Thermofisher). The well-plate was wrapped in foil and allowed to incubate at 37 ºC and 5 % CO_2 for 1 hour. Slices were removed from each well and dipped and swirled in 1 mL sterile PBS (pH 7.40) to rinse. Each slice was then placed into a well in a 24-well plate containing 800 µL culture medium supplemented with 5 µg/mL PI (Thermofisher). The well-plate was covered in foil and allowed to incubate for 30 minutes at 37 °C and 5 % CO_2. Slices were then removed and dipped/swirled in 1 mL sterile PBS (pH 7.40) in a well of a fresh, foil-covered 12-well plate to rinse. Slices were then transferred into a well in another 12-well plate containing 1 mL sterile 4 % paraformaldehyde (PFA) for 25-30 minutes at room temperature to fix. Slices were removed from PFA and immediately placed into a well of a 12-well plate containing 1mL sterile PBS (pH 7.40)

containing 1:1000 Hoechst to stain nuclei for 15 minutes at room temperature, also covered in foil to protect from light bleaching. Finally, slices were removed and placed into another foil-covered 12-well plate containing 1 mL sterile PBS (pH 7.40). The plate was placed on a belly dancer and allowed to wash gently for 10 minutes. After washing, slices were carefully removed from the culture membrane using a paintbrush and mounted individually with 20 µL mowiol mounting medium containing antifade (Sima-Aldrich) and cover-slipped (B&M Scientific). Mounted slices were allowed to dry horizontally at 4 °C overnight. Slices were imaged using a LSM 880 airyscan confocal microscope (Carl Zeiss, ZEN SP 2 Software) with a 20x objective (Zeiss). A tiled, 3-layer z-stack was acquired of each whole slice. Images were background adjusted and the fluorescence and area of each slice were analyzed using ZenBlue software.

2.5 Cytokine release studies: Enzyme-linked immunosorbent assays

Hippocampal OBSCs were prepared and cultured as described above. Slices were cultured (2 or 6 slices per well, depending on whether slices would be used for patch-clamping or cell death staining after ELISA) for 5 days. On DIV05, the culture medium was replaced with culture medium supplemented with LPS (10 µg/mL), LPS (10 µg/mL) + IFNγ (100 ng/mL) or NMDA (5 µM) + 4-AP (100 µM). Control slices received fresh culture medium only. This treatment was applied for 72 hours. At 24, 48 and 72 hours, 150 µL culture medium was collected from each culture well and stored at -80 ºC. ELISAs were performed to detect the cytokines IL-6, TNFα, IL-10 and IL-1β according to the protocol developed by Dr Anja De Lange, a detailed version of which is available online at https://dx.doi.org/10.17504/protocols.io.bh2fj8bn.

2.6 Data analysis and statistics

All data were recorded, graphed and analyzed using WinWCP, Synaptosoft MiniAnalysis software (Justin Lee, Columbia University, 1997) and pClamp Clampfit 10.2 (Molecular Devices), Microsoft Excel 14, GraphPad Prism 8, and Matlab R2015b. Adobe Illustrator CS6 was used to create all figures herein. A Shapiro-Wilk test was applied to all data sets to determine normality/Gaussian distributions. Data sets with Gaussian distributions were

subject to parametric statistical tests and those without Gaussian distributions were tested with non-parametric statistical tests. Parametric tests used included unpaired t-tests with Welch's correction and Brown-Forsythe ANOVAs with Games-Howell's multiple comparison post-hoc test. Non-parametric tests used included unpaired Mann-Whitney U tests and Kruskal-Wallis one-way ANOVAs with post-hoc Dunn's Multiple Comparison tests. Parametric data are reported with mean ± SEM. Nonparametric data are reported with median ± IQR. All statistical tests were performed with confidence interval set at 95 %; as such differences were only considered significant if p</=0.05.

Chapter 3

Results

3.1 Application of LPS+IFNγ for 72 hours induces significant pro-inflammatory cytokine release and affects neuronal network function, but not neuronal death.

Recent work has demonstrated that co-application of LPS and IFNγ in the culture medium of hippocampal organotypic brain slice cultures (OBSCs) has a profound effect on slice health and normal electric properties of pyramidal neurons (Papageorgiou *et al*., 2016; Pascual *et al*., 2012; Ta *et al*., 2019). To establish whether treatment with LPS+IFNγ produces an immune response in my context, hippocampal OBSCs were treated with vehicle (culture medium), LPS-only (10 µg/mL), LPS (10 µg/mL) + IFNγ (100 ng/mL) or NMDA (5 µM) + 4-AP (100 µM) in culture medium for 72 hours. NMDA+4-AP is a positive control treatment which aims to model excitotoxicity. At 24, 48 and 72 hours of treatment, culture media was collected from each well. Enzyme-linked immunosorbent assays (ELISAs) were performed using collected media to detect release of the cytokines IL-6, TNF-α, IL-10 and IL-1β (Figure 3.1.1A).

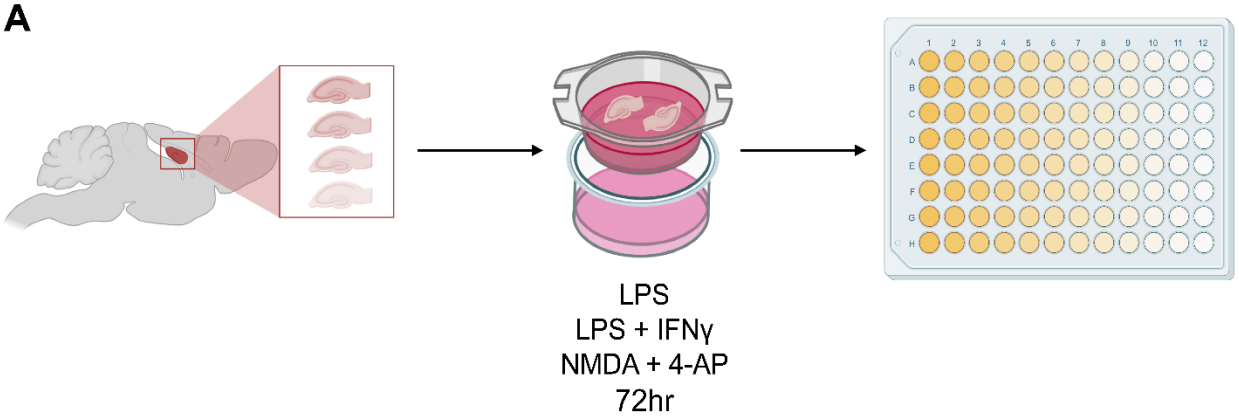
A
LPS
LPS + IFNγ
NMDA + 4-AP
72hr

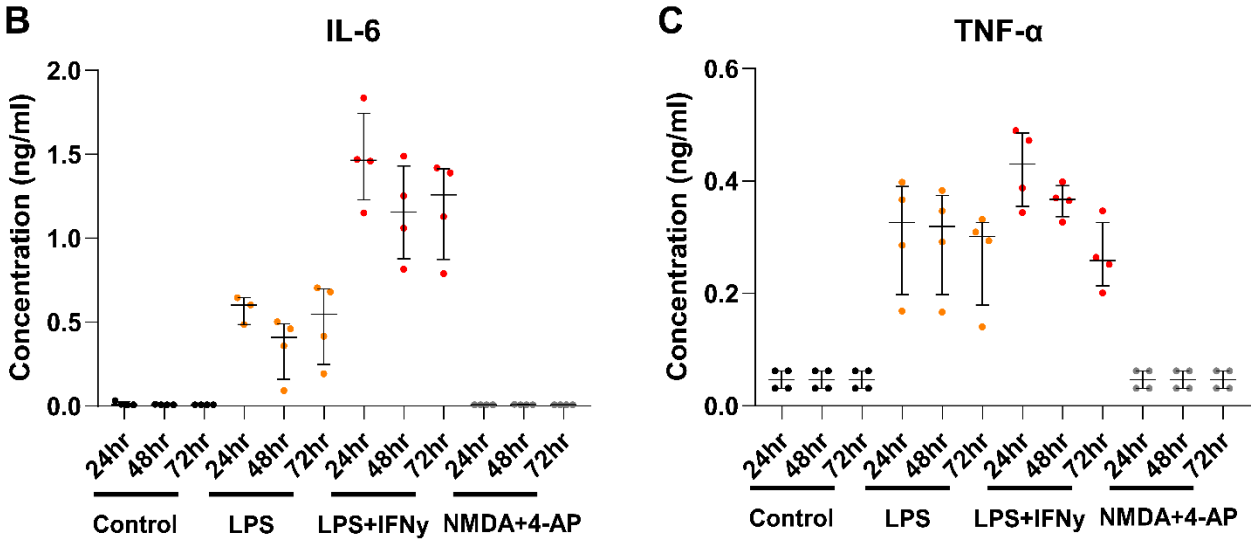
B
IL-6
Concentration (ng/ml)
2.0
1.5
1.0
0.5
0.0
24hr
48hr
72hr
Control
LPS
LPS+IFNγ
NMDA+4-AP

C
TNF-α
Concentration (ng/ml)
0.6
0.4
0.2
0.0
24hr
48hr
72hr
Control
LPS
LPS+IFNγ
NMDA+4-AP

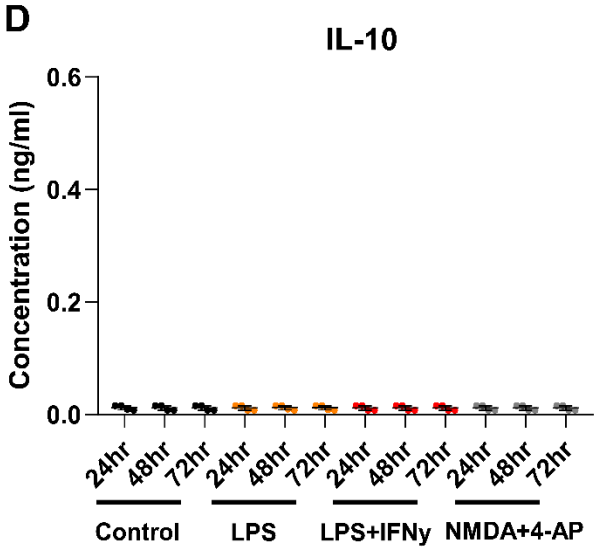
D
IL-10
Concentration (ng/ml)
0.6
0.4
0.2
0.0
24hr
48hr
72hr
Control
LPS
LPS+IFNγ
NMDA+4-AP

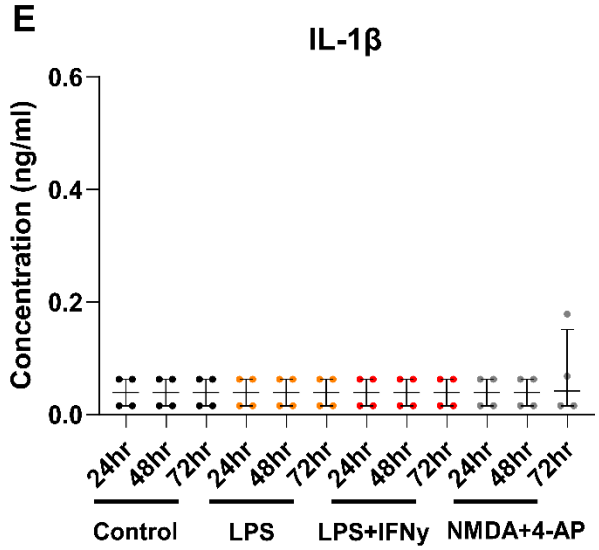
E
IL-1β
Concentration (ng/ml)
0.6
0.4
0.2
0.0
24hr
48hr
72hr
Control
LPS
LPS+IFNγ
NMDA+4-AP

Figure 3.1.1. LPS+IFNγ treatment causes pro-inflammatory cytokine release at 24, 48 and 72 hours. *(A) Schematic diagram showing experimental protocol (created using Biorender). Hippocampal OBSCs (2 per well) were treated with vehicle, LPS-only (10 µg/mL), LPS (10 µg/mL) + IFNγ (100 ng/mL) or NMDA (5 µM) + 4-AP (100 µM) in the culture medium for* ***72 hours****. At 24, 48 and 72 hours of treatment, culture media was collected from each well. ELISAs were performed using collected media to detect release of the cytokines IL-6, TNF-α, IL-10 and IL-1β. LPS treatment alone (N=4) as well as LPS+IFNγ (N=4) induced significant IL-6 (B) and TNF-α (C) release as compared to control slices (N=4) or NMDA+4-AP (N=4) treated slices. Combination treatment with LPS+IFNγ induced higher IL-6 release than LPS alone (B). IL-10 (D) and IL-1β (E) were undetectable in all treatment conditions. All groups were tested for Gaussian distributions using the Shapiro-Wilk normality test. If any group was found to not have a Gaussian distribution or was too small to test for normality (nonparametric), the data were compared using an unpaired Mann-Whitney U test. If all groups were found to have Gaussian distributions (parametric), an unpaired t-test with Welch's correction was performed. Values with mean ± SEM (parametric) or median ± IQR (nonparametric); * p ≤ 0.05; ** p ≤ 0.01; *** p ≤ 0.001. Each data point represents cytokine data from a single culture well.*

I found that LPS treatment alone or a combination treatment of LPS+IFNγ induced significant release of IL-6 at 48 and 72 hours (Figure 3.1.1B) and of TNF-α at 24, 48 and 72 hours (Figure 3.1.1C) as compared to that detected in control media (statistical data available in Tables 3.1.1 and 3.1.2 below), confirming what has been reported by others (Papageorgiou *et al*., 2016). Furthermore, combination treatment of LPS+IFNγ induced higher IL-6 release than LPS treatment alone at all three time points (Figure 3.1.1B, Tables 3.1.1 & 3.1.2). There is a similar trend for higher release of TNF-α in slices treated with combined LPS+IFNγ than from those treated with LPS alone, but this difference is not significant (Figure 3.1.1C, Tables 3.1.1 & 3.1.2). I did not find any detectable release of IL-10 (Figure 3.1.1D) or of IL-1β (Figure 3.1.1E) in any treatment group.

Table 3.1.5. Median and IQR values for ELISA performed on culture media from hippocampal OBSCs used for spontaneous post-synaptic current studies as represented in Figure 3.1.1.

C=Control; L=LPS-only; I=LPS+IFNγ; N=NMDA+4-AP.

		24hr				48hr				72hr			
		C	L	I	N	C	L	I	N	C	L	I	N
IL-6	Median	0.009086	0.6030	1.465	0.007815	0.007815	0.4093	1.156	0.007815	0.007815	0.5482	1.260	0.007815
	IQR	0.007810-0.02728	0.4862-0.6450	1.228-1.744	0.007810-0.007820	0.007810 - 0.009601	0.1586-0.4915	0.8773-1.431	0.007810-0.009611	0.007810-0.007820	0.2491-0.6988	0.8741-1.412	0.007810-0.007820
TNF-α	Median	0.04688	0.3263	0.4301	0.04688	0.04688	0.3195	0.3674	0.04688	0.04688	0.3015	0.2581	0.04688
	IQR	0.03125-0.06250	0.1981-0.3901	0.3550-0.4853	0.03125-0.06250	0.03125-0.06250	0.1982-0.3741	0.3365-0.3917	0.03125-0.06250	0.03125-0.06250	0.1792-0.3263	0.2137-0.3264	0.03125-0.06250
IL-10	Median	0.012422	0.01172	0.01172	0.01172	0.011722	0.01271	0.01172	0.01172	0.01172	0.01230	0.01172	0.01172
	IQR	0.008163-0.01563	0.007813-0.01563	0.007813-0.01563	0.007813-0.01563	0.007813-0.01563	0.008310-0.01563	0.007813-0.01563	0.007813-0.01563	0.007813-0.01563	0.008105-0.01563	0.007813-0.01563	0.007813-0.01563
IL-1β	Median	0.03906	0.03906	0.03906	0.03906	0.03906	0.03906	0.03906	0.03906	0.03906	0.03906	0.03906	0.04206
	IQR	0.01563-0.06250	0.01563-0.06250	0.01563-0.06250	0.01563-0.06250	0.01563-0.06250	0.01563-0.06250	0.01563-0.06250	0.01563-0.06250	0.01563-0.06250	0.01563-0.06250	0.01563-0.06250	0.01563-0.1512

Table 3.1.6. Results of statistic tests performed on ELISA data from Figure 3.1.1.

	Test condition	Test performed	24hr	Test performed	48hr	Test performed	72hr
IL-6	Control vs LPS	Mann Whitney-U	ns p > 0.05	Mann Whitney-U	*p = 0.0286	Mann Whitney-U	*p = 0.0286
	Control vs LPS+IFNγ	Mann Whitney-U	*p = 0.0286	Mann Whitney-U	*p = 0.0286	Mann Whitney-U	*p = 0.0286
	Control vs NMDA+4-AP	Mann Whitney-U	ns p > 0.05	Mann Whitney-U	ns p > 0.05	Mann Whitney-U	ns p > 0.05
	LPS vs LPS+IFNγ	Welch's t-test	**p = 0.0049	Welch's t-test	**p = 0.0050	Welch's t-test	*p = 0.0121
	LPS vs NMDA+4-AP	Mann Whitney-U	*p = 0.0286	Mann Whitney-U	*p = 0.0286	Mann Whitney-U	*p = 0.0286
	LPS+IFNγ vs NMDA+4-AP	Mann Whitney-U	*p = 0.0286	Mann Whitney-U	*p = 0.0286	Mann Whitney-U	*p = 0.0286
TNF-α	Control vs LPS	Mann Whitney-U	*p = 0.0286	Mann Whitney-U	*p = 0.0286	Mann Whitney-U	*p = 0.0286
	Control vs LPS+IFNγ	Mann Whitney-U	*p = 0.0286	Mann Whitney-U	*p = 0.0286	Mann Whitney-U	*p = 0.0286
	Control vs NMDA+4-AP	Mann Whitney-U	ns p > 0.05	Mann Whitney-U	ns p > 0.05	Mann Whitney-U	ns p > 0.05
	LPS vs LPS+IFNγ	Welch's t-test	ns p > 0.05	Welch's t-test	ns p > 0.05	Welch's t-test	ns p > 0.05
	LPS vs NMDA+4-AP	Mann Whitney-U	*p = 0.0286	Mann Whitney-U	*p = 0.0286	Mann Whitney-U	*p = 0.0286
	LPS+IFNγ vs NMDA+4-AP	Mann Whitney-U	*p = 0.0286	Mann Whitney-U	*p = 0.0286	Mann Whitney-U	*p = 0.0286
IL-10	Control vs LPS	Mann Whitney-U	ns p > 0.05	Mann Whitney-U	ns p > 0.05	Mann Whitney-U	ns p > 0.05
	Control vs LPS+IFNγ	Mann Whitney-U	ns p > 0.05	Mann Whitney-U	ns p > 0.05	Mann Whitney-U	ns p > 0.05
	Control vs NMDA+4-AP	Mann Whitney-U	ns p > 0.05	Mann Whitney-U	ns p > 0.05	Mann Whitney-U	ns p > 0.05

	LPS vs LPS+IFNγ	Mann Whitney-U	ns p > 0.05	Mann Whitney-U	ns p > 0.05	Mann Whitney-U	ns p > 0.05
	LPS vs NMDA+4-AP	Mann Whitney-U	ns p > 0.05	Mann Whitney-U	ns p > 0.05	Mann Whitney-U	ns p > 0.05
	LPS+IFNγ vs NMDA+4-AP	Mann Whitney-U	ns p > 0.05	Mann Whitney-U	ns p > 0.05	Mann Whitney-U	ns p > 0.05
IL-1β	Control vs LPS	Mann Whitney-U	ns p > 0.05	Mann Whitney-U	ns p > 0.05	Mann Whitney-U	ns p > 0.05
	Control vs LPS+IFNγ	Mann Whitney-U	ns p > 0.05	Mann Whitney-U	ns p > 0.05	Mann Whitney-U	ns p > 0.05
	Control vs NMDA+4-AP	Mann Whitney-U	ns p > 0.05	Mann Whitney-U	ns p > 0.05	Mann Whitney-U	ns p > 0.05
	LPS vs LPS+IFNγ	Mann Whitney-U	ns p > 0.05	Mann Whitney-U	ns p > 0.05	Mann Whitney-U	ns p > 0.05
	LPS vs NMDA+4-AP	Mann Whitney-U	ns p > 0.05	Mann Whitney-U	ns p > 0.05	Mann Whitney-U	ns p > 0.05
	LPS+IFNγ vs NMDA+4-AP	Mann Whitney-U	ns p > 0.05	Mann Whitney-U	ns p > 0.05	Mann Whitney-U	ns p > 0.05

These experiments demonstrated that I could reliably induce a pro-inflammatory immune response in OBSCs using LPS alone or LPS+IFNγ. It has been reported that neuroinflammation can predispose the brain to seizures by induction of rapid post-translational changes to neuronal ion channels and transporters as well as by affecting neurotransmitter release and reuptake (Terrone *et al*., 2019). These types of changes can affect normal neuronal network function. A proxy for measuring such network function is the measurement of postsynaptic currents (PSC). There are two types of PSCs, namely spontaneous PSCs (sPSCs) and miniature PSCs (mPSCs). The former are produced by action-potential-dependent and -independent release of neurotransmitter without experimental stimulation and reveal information about the network (Ke *et al*., 2010; Pascual *et al*., 2012). The latter are currents recorded in the absence of presynaptic action potentials and as such are recorded in the presence of tetrodotoxin to block voltage-gated Na^+ channels. mPSCs are believed to represent the response elicited from the release of a single vesicle of neurotransmitter (Pinheiro & Mulle, 2008). Hence, sPSCs comprise both mPSCs and AP-evoked release of neurotransmitter. I recorded sPSCs in this work since I was interested in the overall function of the network rather than focusing more closely on individual vesicle release (and thus the isolated functions of various postsynaptic receptors). Despite their differences, the characteristics (such as frequency and amplitude) of both types of PSCs represent similar concepts (Malkin *et al*., 2014).

Data derived from the recording of sPSCs can shed light on the function of a neuronal network since these currents constitute spontaneous neurotransmitter release at synapses (Ke *et al*., 2010). For example, the frequency of such currents provides information about the number of functional synapses in the network and the probability of presynaptic neurotransmitter release (Ke *et al*., 2010). The amplitude of these currents is a reflection of the conductance of post-synaptic receptors at individual synapses (Duan *et al*., 2018). Moreover, the frequency and amplitude of these events contribute to the overall synaptic strength of neurons (Duan *et al*., 2018). Interestingly, Pascual *et al*. (2012) showed that acute wash-in of LPS can cause a rapid, brief, transient rise in the frequency of spontaneous

and miniature PSCs. Further, the balance of excitatory and inhibitory post-synaptic events can provide information about the excitability of a network.

Using the same treated hippocampal OBSCs from which the culture media was used to probe cytokine release, I also investigated the effect of chronic immune activation on neuronal network function (*i.e.* on cells exposed to immune-activating factors for 72 hours). I made whole-cell patch-clamp recordings from cultured hippocampal CA3/CA1 pyramidal neurons using a cesium-based internal solution. Recordings were performed in voltage-clamp mode to record sPSCs. Once patched, neurons were held at -60 mV while current pulses were applied to acquire data about the membrane properties of the neuron. Neurons were then held at -70 mV to record excitatory PSCs and at +15 mV to record inhibitory PSCs (Figure 3.1.2A). The frequency and amplitude of excitatory and inhibitory events could then be quantified in downstream analysis.

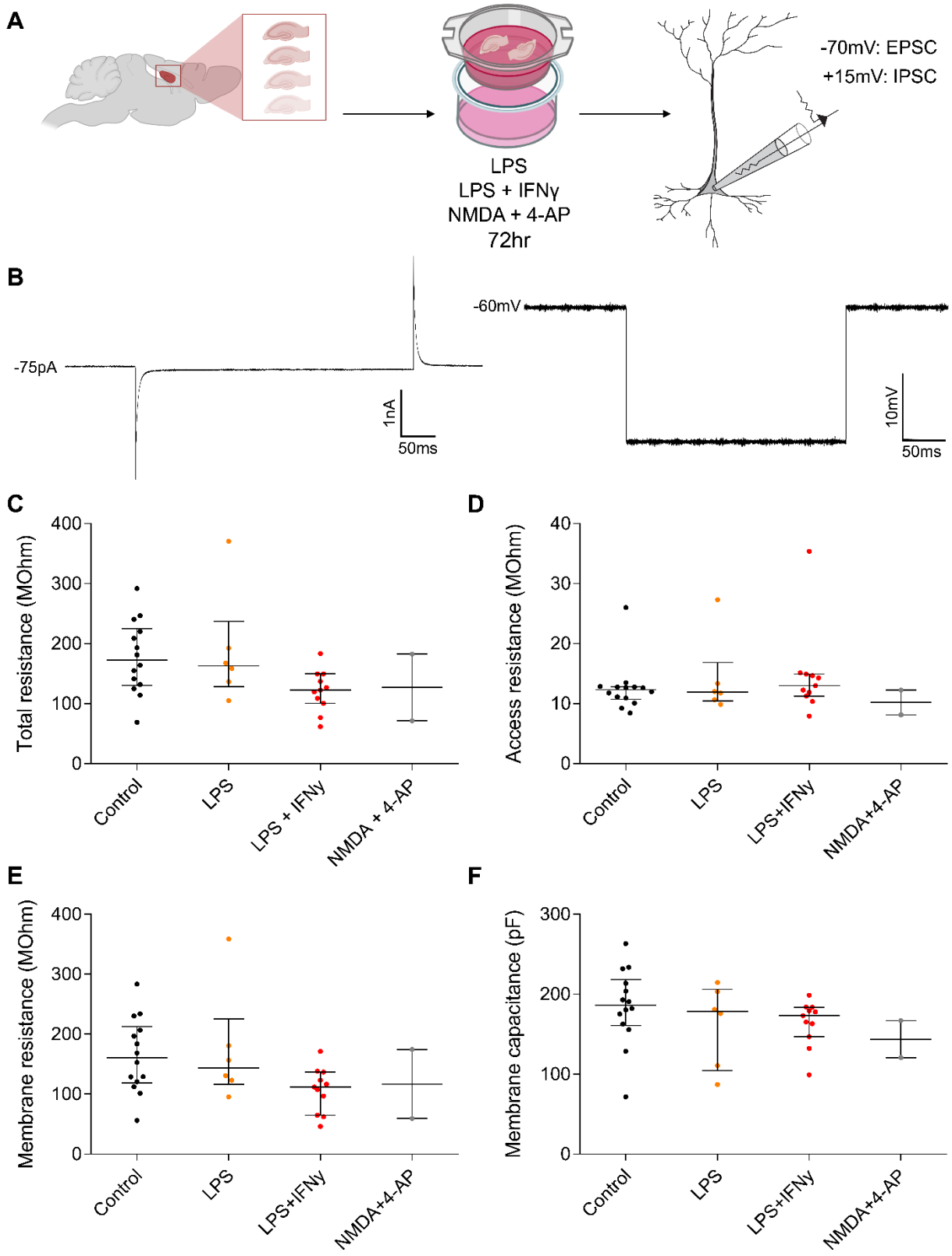
A
-70mV: EPSC
+15mV: IPSC
LPS
LPS + IFNγ
NMDA + 4-AP
72hr
B
-75pA
1nA
50ms
-60mV
10mV
50ms
C
Total resistance (MOhm)
400
300
200
100
0
Control
LPS
LPS + IFNγ
NMDA + 4-AP
D
Access resistance (MOhm)
40
30
20
10
0
Control
LPS
LPS+IFNγ
NMDA+4-AP
E
Membrane resistance (MOhm)
400
300
200
100
0
Control
LPS
LPS+IFNγ
NMDA+4-AP
F
Membrane capacitance (pF)
300
200
100
0
Control
LPS
LPS+IFNγ
NMDA+4-AP

Figure 3.1.2. Immune activation by combined LPS+IFNγ or LPS alone for 72 hours does not change the membrane properties of cultured hippocampal CA3/CA1 pyramidal neurons. *(A) Schematic diagram of experimental set-up. Hippocampal OBSCs (2 per well) were treated with vehicle, LPS-only (10 µg/mL), LPS (10 µg/mL) + IFNγ (100 ng/mL) or NMDA (5 µM) + 4-AP (100 µM) in the culture medium for* ***72 hours****. Whole-cell patch-clamp recordings were then made from cultured hippocampal CA3/CA1 pyramidal neurons using a cesium-based internal solution. Recordings were performed in voltage-clamp mode to record spontaneous post-synaptic currents (sPSCs). Neurons were held at -70 mV to record sEPSCs and at +15 mV to record sIPSCs. (B) Example voltage-clamp mode recording (left panel) from a pyramidal neuron while voltage pulses were applied (right panel). Neuronal membrane properties are analyzed from these recordings. Population data (with median ± IQR or mean ± SEM) demonstrating no change across control (N=14), LPS-only (N=6), LPS+IFNγ (N=11) or NMDA+4-AP (N=2) treatment conditions in total resistance (C), access resistance (D), membrane resistance (E) or membrane capacitance (F) of patched cells. All groups were tested for Gaussian distributions using the Shapiro-Wilk normality test. If any group was found to not have a Gaussian distribution (nonparametric) or was too small to test for normality, the data were compared using a Kruskal-Wallis ANOVA test with Dunn's multiple comparison post-hoc test. If all groups were found to have Gaussian distributions (parametric), a Brown-Forsyth and Welch ANOVA test with Games-Howell's multiple comparison post-test was performed. Values with median ± IQR (nonparametric) or mean ± SEM (parametric); * $p \leq 0.05$; ** $p \leq 0.01$; *** $p \leq 0.001$. Each data point represents a neuron.*

Neuronal membrane properties (Figure 3.1.2C-F) were deduced from voltage steps (Figure 3.1.2B) applied to each neuron. The quality of each patch was assessed by calculating the access resistance (R_a) which governs how efficient the electrical access (or conductance) is to the cell. Cells with R_a above 30 MΩ were excluded from analyses to ensure high quality of recorded data. The median Ra's for the control, LPS-only, LPS+IFNγ and NMDA+4-AP groups were 12.30 MΩ (IQR 10.71-12.80 MΩ, N=14), 11.90 MΩ (IQR 10.45-16.85 MΩ, N=6), 12.98 MΩ (IQR 11.26-14.93 MΩ, N=11) and 10.18 MΩ (IQR 8.112-12.24 MΩ, N=2), respectively and these were not significantly different from one another ($p>0.05$, Kruskal-Wallis ANOVA with Dunn's multiple comparison post-hoc test, data not shown on figure) (Figure 3.1.2D).

Next, I quantified the total resistance, membrane resistance and membrane capacitance which comprise the basic membrane properties of neurons and are the most fundamental modulators of neuronal signaling. The membrane resistance is a proxy for how easily ions can flow through the neuronal membrane and is therefore an indicator of the number of ion channels, especially K^+ leak channels in the membrane. Total resistance is the sum of membrane resistance and access resistance. The median total resistances for the control,

LPS-only, LPS+IFNγ and NMDA+4-AP were 172.4 MΩ (IQR 130.1-225.3 MΩ, N=14), 162.9 MΩ (IQR 128.7-236.9 MΩ, N=6), 122.6 MΩ (IQR 100.4-149.5 MΩ, N=11) and 127.1 MΩ (IQR 71.66-182.6 MΩ, N=2), respectively and these were not significantly different from one another ($p>0.05$, Kruskal-Wallis ANOVA with Dunn's multiple comparison post-hoc test) (Figure 3.1.2C). The median membrane resistance of the control, LPS-only, LPS+IFNγ and NMDA+4-AP groups were 160.6 MΩ (IQR 118.7-212.6 MΩ, N=14), 143.7 MΩ (IQR 116.4-225.2 MΩ, N=6), 111.7 MΩ (IQR 64.68-136.7 MΩ, N=11) and 116.9 MΩ (IQR 59.41-174.5 MΩ, N=2), respectively, and these were not significantly different from one another ($p>0.05$, Kruskal-Wallis ANOVA with Dunn's multiple comparison post-hoc test) (Figure 3.1.2E).

The membrane capacitance of a neuron is representative of the size of the lipid membrane and thus the charge it is able to store across it as a capacitor. Further, it defines how fast a cell's membrane potential can respond to a change in current. The median membrane capacitance for the control, LPS-only, LPS+IFNγ and NMDA+4-AP groups were 186.4 MΩ (IQR 160.8-218.2 MΩ, N=14), 178.4 MΩ (IQR 104.7-206.1 MΩ, N=6), 173.2 MΩ (IQR 147-183.5 MΩ, N=11) and 143.7 MΩ (IQR 120.6-166.9 MΩ, N=2), respectively, and these were again not significantly different from one another ($p>0.05$, Kruskal-Wallis ANOVA with Dunn's multiple comparison post-hoc test) (Figure 3.1.2F).

Combined, the membrane resistance and membrane capacitance govern the membrane time constant, which in turn determines the integrative properties of a neuron. This set of data shows that treatment with either LPS alone or LPS+IFNγ did not have any significant effect on the basic membrane properties of cultured hippocampal CA3/CA1 pyramidal neurons.

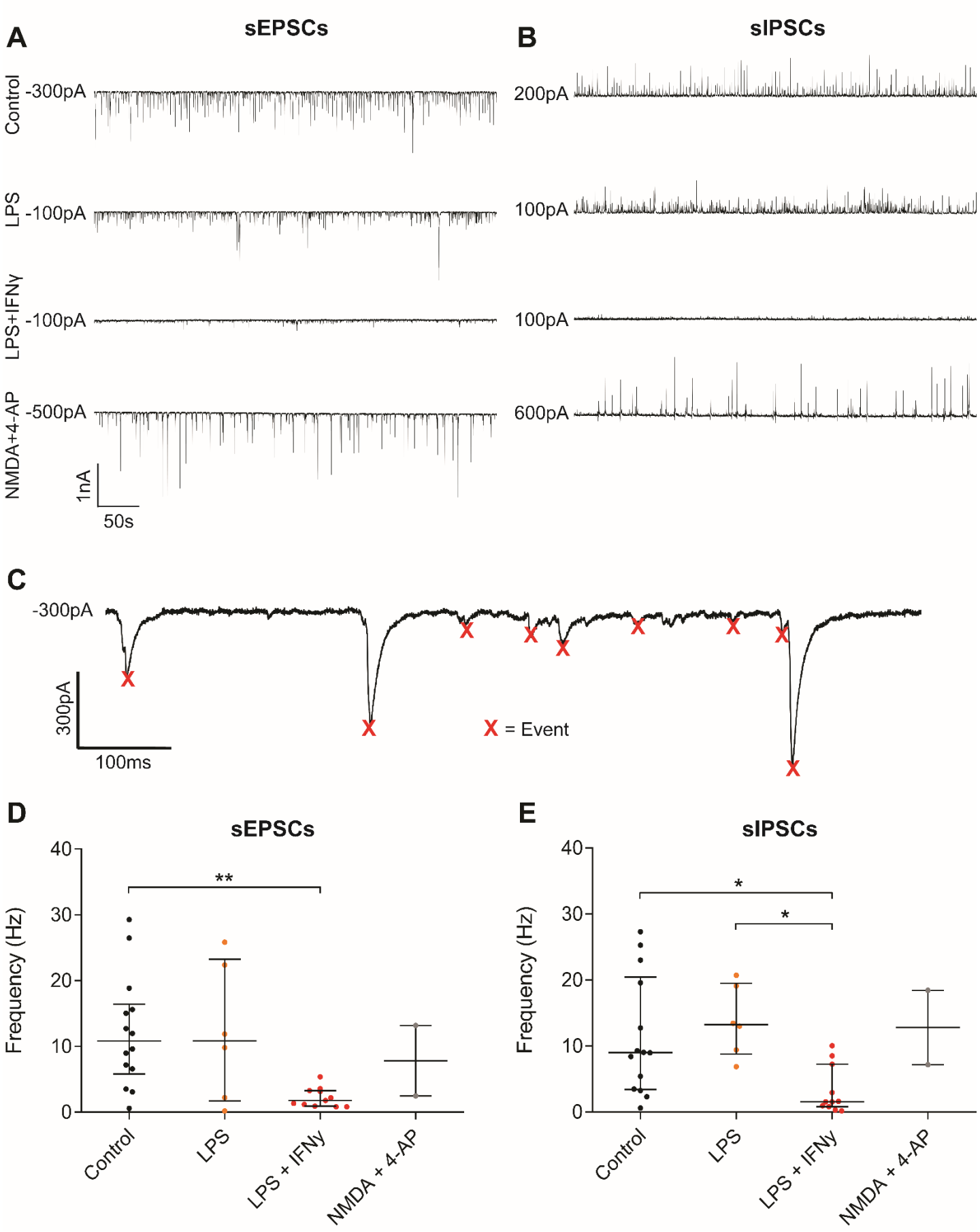
A
sEPSCs
Control
-300pA
LPS
-100pA
LPS+IFNγ
-100pA
NMDA+4-AP
-500pA
1nA
50s
B
sIPSCs
200pA
100pA
100pA
600pA
C
-300pA
300pA
100ms
X = Event
D
sEPSCs
Frequency (Hz)
40
30
20
10
0
**
Control
LPS
LPS + IFNγ
NMDA + 4-AP
E
sIPSCs
Frequency (Hz)
40
30
20
10
0
*
*
Control
LPS
LPS + IFNγ
NMDA + 4-AP

Figure 3.1.3. Immune activation via LPS+IFNγ for 72 hours reduces both sEPSC and sIPSC event frequency in cultured hippocampal CA3/CA1 pyramidal neurons but LPS treatment alone does not. *Example sEPSC (A) and sIPSC (B) traces from each treatment group. Hippocampal OBSCs (2 per well) were treated with vehicle, LPS-only (10 µg/mL), LPS (10 µg/mL) + IFNγ (100 ng/mL) or NMDA (5 µM) + 4-AP (100 µM) in the culture medium for* ***72 hours****. Whole-cell patch-clamp recordings were then made from cultured hippocampal CA3/CA1 pyramidal neurons using a cesium-based internal solution. Recordings were performed in voltage clamp to record spontaneous post-synaptic currents. Neurons were held at -70 mV to record sEPSCs and at +15 mV to record sIPSCs. (C) Example trace illustrating event detection in post-synaptic current recordings. Population data (with median ± IQR or mean ± SEM) demonstrating frequency of sEPSCs (D) and sIPSCs (E) in control (N=14), LPS-only (10 µg/mL) (N=6), LPS (10 µg/mL)+ IFNγ (100 ng/mL) (N=11) or NMDA (5 µM) + 4-AP (100 µM) (N=2) treatment conditions. Frequency of sEPSCs (D) and sIPSCs (E) in LPS+IFNγ-treated neurons was significantly lower than that observed in control neurons. All groups were tested for Gaussian distributions using the Shapiro-Wilk normality test. If any group was found to not have a Gaussian distribution or was too small to test for normality, the data were compared using a Kruskal-Wallis ANOVA test with Dunn's multiple comparison post-hoc test. If all groups were found to have Gaussian distributions, a Brown-Forsythe ANOVA with Games-Howell's multiple comparison post-hoc test was performed. Values with median ± IQR (nonparametric) or mean ± SEM (parametric); * $p \leq 0.05$; ** $p \leq 0.01$; *** $p \leq 0.001$. Each data point represents a neuron.*

The frequency of sPSCs provides insight into the overall synaptic function of a network (Duan *et al*., 2018; Ke *et al*., 2010). Using a cesium-based internal solution, I performed whole-cell patch clamping on CA3/CA1 pyramidal neurons in cultured hippocampal organotypic slices. Holding the cells in voltage clamp at -70 mV and +15 mV allowed the recording of spontaneous excitatory and inhibitory PSCs, respectively (Figure 3.1.3A-C).

After 72 hours of combined LPS+IFNγ treatment, the median frequency of sEPSCs (1.780 Hz, IQR 0.9300-3.273 Hz, N=11) (Kruskal-Wallis ANOVA with Dunn's multiple comparison post-hoc test, p=0.0079) and of sIPSCs (1.553 Hz, IQR 0.8333-7.240 Hz, N=11) (Kruskal-Wallis ANOVA with Dunn's multiple comparison post-hoc test, p=0.0429) had decreased considerably compared to that of control slices (sEPSCs: 10.81 Hz, IQR 5.818-16.42 Hz, N=14; sIPSCs: 9.020 Hz, IQR 3.424-20.45 Hz, N=14) (Figure 3.1.3D&E). This effect was not observed in the median sEPSC frequency (10.86 Hz, IQR 1.708-23.25 Hz, N=6) or median sIPSC frequency (13.24 Hz, IQR 8.772-19.51 Hz, N=6) of slices treated with LPS alone (Kruskal-Wallis ANOVA with Dunn's multiple comparison post-hoc test, p>0.05 for sEPSCs and sIPSCs) (Figure 3D&E). The positive excitotoxic control treatment of NMDA+4-AP did not cause the median sEPSC frequency (7.833 Hz, IQR 2.473-13.19 Hz, N=2) to differ significantly from control sEPSC frequency (Kruskal-Wallis ANOVA with Dunn's multiple

comparison post-hoc test, $p>0.05$) (Figure 3.1.3D). There was also no change in the median sIPSC frequency of NMDA+4-AP treated slices (12.81 Hz, IQR 7.183-18.44 Hz, N=2) from control values (Kruskal-Wallis ANOVA with Dunn's multiple comparison post-hoc test, $p>0.05$) (Figure 3.1.3E). There was no significant difference between the median sEPSC frequency of the LPS-only and LPS+IFNγ treated groups, though there was a strong trend for the LPS+IFNγ treated group to have a much lower median sEPSC frequency than the LPS-only group (Figure 3.1.3D) (Kruskal-Wallis ANOVA with Dunn's multiple comparison post-hoc test, $p>0.05$). The median sIPSC frequency of cells in the LPS+IFNγ group was however significantly lower than that of the group treated with LPS only (Kruskal-Wallis ANOVA with Dunn's multiple comparison post-hoc test, $p=0.0128$) (Figure 3.1.3E). There was no significant difference in median sEPSC or sIPSC frequency between groups treated with LPS-only and NMDA+4-AP (Kruskal-Wallis ANOVA with Dunn's multiple comparison post-hoc test, sEPSCs: $p>0.05$;sIPSCs: $p>0.05$) or between groups treated with LPS+IFNγ and NMDA+4-AP (Kruskal-Wallis ANOVA with Dunn's multiple comparison post-hoc test, sEPSCs: $p>0.05$; sIPSCs: $p>0.05$). These results are evident in the example traces shown in Figure 3.1.3A and 3.1.3B.

Inter-event interval (IEI) is a measure of the latency between post-synaptic currents and is another measure of the overall function of the neuronal network, similar to the frequency of these currents. My findings here were similar to those regarding event frequency. Control neurons had a median sEPSC IEI of 93.65 ms (IQR 61.37-184.6 ms, N=14) and neurons treated with LPS only had a median sEPSC IEI of 92.96 ms (IQR 43.74-1525 ms, N=6), as such their medians were not significantly different (Kruskal-Wallis ANOVA with Dunn's multiple comparison post-hoc test, $p>0.05$) (Figure 3.1.4A). This result could however have been skewed by the outliers in both the control and LPS-only treated groups. In contrast, neurons treated with LPS and IFNγ had a median sEPSC IEI of 555.1 ms (IQR 293.9-1063 ms, N=11), which was significantly longer than that recorded for control neurons (Kruskal-Wallis ANOVA with Dunn's multiple comparison post-hoc test, $p=0.0079$) (Figure 3.1.4A). Interestingly, the sEPSC IEI median of the LPS-only group did not differ significantly from that of the LPS+IFNγ group (Kruskal-Wallis ANOVA with Dunn's multiple comparison post-hoc

test, p>0.05) (Figure 3.1.4A). The median sEPSC IEI of the positive excitotoxic control group treated with NMDA and 4-AP (median 238.7 ms, IQR 75.91-401.6 ms, N=2) did not differ significantly from control (Kruskal-Wallis ANOVA with Dunn's multiple comparison post-hoc test, p>0.05) (Figure 4A). Furthermore, LPS-only and LPS+IFNγ treated groups did not have sEPSC IEI medians that were significantly different from that of the NMDA+4-AP treated group (Kruskal-Wallis ANOVA with Dunn's multiple comparison post-hoc tests, p>0.05 and p>0.05, respectively) (Figure 3.1.4A). This is represented by the example traces shown in Figure 3.1.3A and by the cumulative frequency plots of sEPSC IEIs in each patched neuron where red traces (representing LPS+IFNγ) are right-shifted compared to black (control) and orange (LPS alone), indicating larger inter-event intervals, and thus less frequent events (Figure 3.1.4C). NMDA+4-AP treated neurons are represented by grey traces.

I found similar results when examining the IEIs of sIPSCs. Control neurons had a sIPSC IEI median of 110.8 ms (IQR 49.27-292.2 ms, N=14) and LPS-only treated neurons were not significantly different from this value, with median 75.58 ms (IQR 51.48-116 ms, N=6) (Kruskal-Wallis ANOVA with Dunn's multiple comparison post-hoc test, p>0.05) (Figure 3.1.4B). On the contrary, the median sIPSC IEI of neurons treated with LPS+IFNγ had a median sIPSC IEI of 643.2 ms (IQR 138-1181 ms, N=11) which was indeed significantly larger than both control neurons (Kruskal-Wallis ANOVA with Dunn's multiple comparison post-hoc test, p=0.0429) and from LPS-only treated neurons (Kruskal-Wallis ANOVA with Dunn's multiple comparison post-hoc test, p=0.0128) (Figure 3.1.4B). It must, however, be noted that both the control and the LPS+IFNγ treated these groups contain outliers which may have cast a skewing influence over the results presented here. Echoing the sEPSCs results, the sIPSC IEI of the NMDA+4-AP treated group of 96.77 ms (IQR 54.31-139.2 ms, N=2) was not significantly different from that of control neurons (Kruskal-Wallis ANOVA with Dunn's multiple comparison post-hoc test, p>0.05) or from that of the LPS-only treated group (Kruskal-Wallis ANOVA with Dunn's multiple comparison post-hoc test, p>0.05) or that of the group treated with LPS+IFNγ (Kruskal-Wallis ANOVA with Dunn's multiple comparison post-hoc test, p>0.05) (Figure 3.1.4B). Again, this is apparent in the example traces in Figure 3.1.3B and in the cumulative frequency plot in Figure 3.1.4D where red traces (representing

LPS+IFNγ) are right-shifted compared to black (control) and orange (LPS alone), indicating larger IEIs, and thus less frequent events. NMDA+4-AP treated neurons are represented by grey traces.

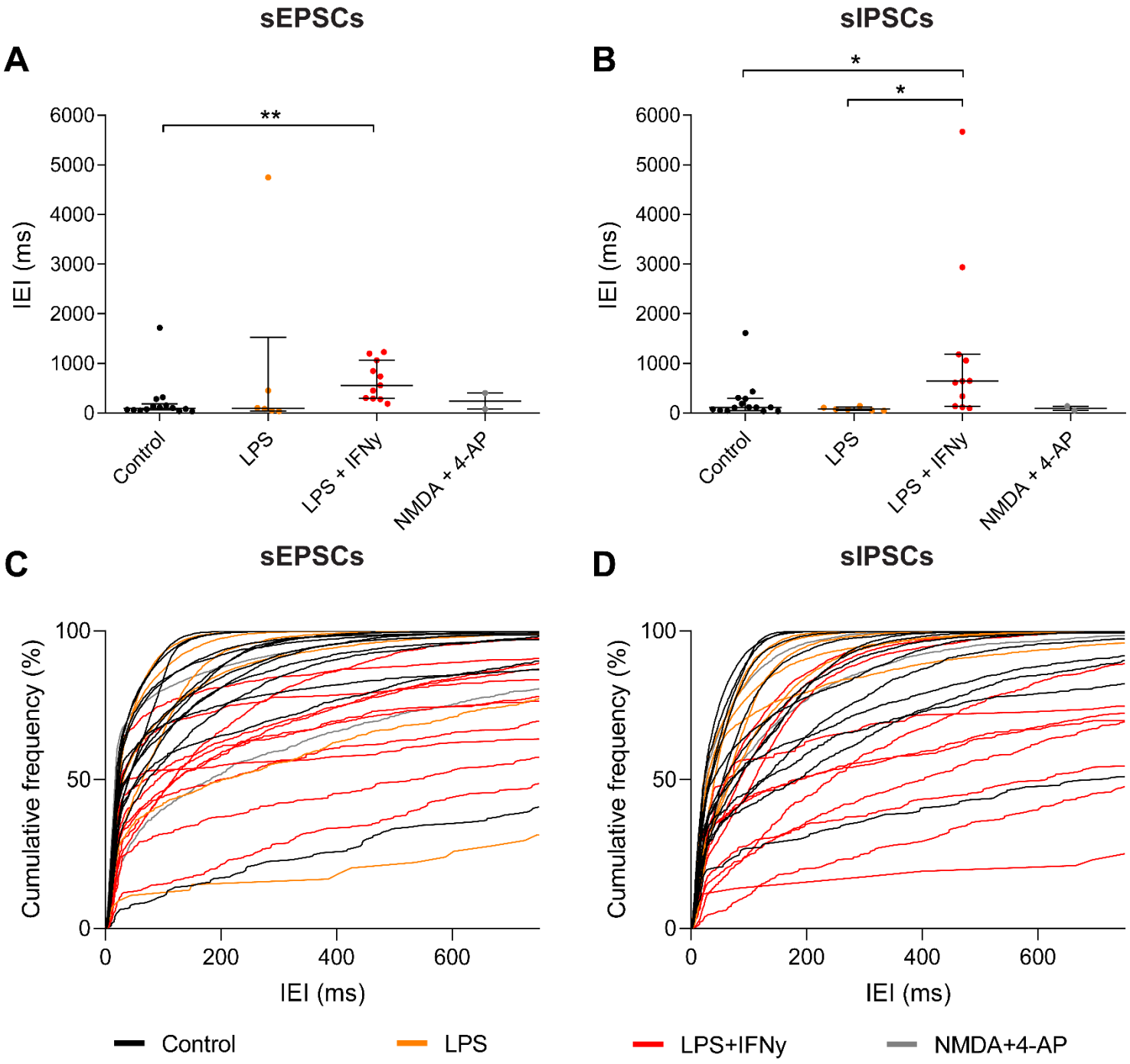

Figure 3.1.4. Immune activation via LPS+IFNγ for 72 hours increases both sEPSC and sIPSC inter-event intervals in cultured hippocampal CA3/CA1 pyramidal neurons but LPS treatment alone does not. *Hippocampal OBSCs (2 per well) were treated with vehicle, LPS-only (10 µg/mL), LPS (10 µg/mL) + IFNγ (100 ng/mL) or NMDA (5 µM) + 4-AP (100 µM) in the culture medium for* ***72 hours****. Whole-cell patch-clamp recordings were then made from cultured hippocampal CA3/CA1 pyramidal neurons using a cesium-based internal solution. Recordings were performed in voltage clamp to record sPSCs. Neurons were held at -70 mV to record sEPSCs and at +15 mV to record sIPSCs. Population data (with median ± IQR or mean ± SEM) demonstrating inter-event interval of sEPSCs (A) and sIPSCs (B) in control (N=14), LPS-only (N=6), LPS+IFNγ (N=11) or NMDA+4-AP (N=2) treatment conditions. IEIs of sEPSCs (A) and sIPSCs (B) in neurons treated with LPS+IFNγ are significantly increased as compared to controls. In slices treated with LPS alone, both sEPSCs and sIPSCs are not significantly different from control-treated groups. Cumulative frequency plots of IEIs of sEPSCs (C) and sIPSCs (D) in each patched neuron indicate that red traces (representing LPS+IFNγ) are right-shifted compared to black (control) and orange (LPS alone), indicating larger IEIs, and thus less frequent events. All groups were tested for Gaussian distributions using the Shapiro-Wilk normality test. If any group was found to not have a Gaussian distribution or was too small to test for normality, the data were compared using a Kruskal-Wallis ANOVA test with Dunn's multiple comparison post-hoc test. If all groups were found to have Gaussian distributions, a Brown-Forsythe ANOVA with Games-Howell's multiple comparison post-hoc test was performed. Values with median ± IQR (nonparametric) or mean ± SEM (parametric); * $p \leq 0.05$; ** $p \leq 0.01$; *** $p \leq 0.001$. Each data point represents a neuron.*

The amplitude of post-synaptic currents is a proxy for the strength of individual synapses and the conductance of postsynaptic receptors in a network (Duan *et al*., 2018). Neurons in the control group had a median sEPSC amplitude of 104 pA (IQR 73.04-154.4 pA, N=14). Neither the LPS-only treated group (median 118.1 pA, IQR 82.31-135.6 pA, N=6) nor the NMDA+4-AP treated (median 164.3 pA, IQR 149.2-179.4 pA, N=2) group had a median amplitude significantly different from control (Kruskal-Wallis ANOVA with Dunn's multiple comparison post-hoc test, $p>0.05$ for both) (Figure 3.1.5D). There was however a trend for the LPS+IFNγ treated group to have a smaller median amplitude (median 71.61 pA, IQR 47.54-93.90 pA, N=11) than controls, though this was not significant (Kruskal-Wallis ANOVA with Dunn's multiple comparison post-hoc test, $p>0.05$) (Figure 3.1.5D). The median sEPSC amplitude of LPS-only treated neurons did not differ significantly from that of neurons treated with LPS+IFNγ (Kruskal-Wallis ANOVA with Dunn's multiple comparison post-hoc test, $p>0.05$) or from that of neurons treated with NMDA+4-AP (Kruskal-Wallis ANOVA with Dunn's multiple comparison post-hoc test, $p>0.05$) (Figure 3.1.5D). The median sEPSC amplitude of LPS+IFNγ treated neurons was also not significantly different from that of neurons treated with NMDA+4-AP (Kruskal-Wallis ANOVA with Dunn's multiple comparison

post-hoc test, p>0.05) (Figure 3.1.5D). These results are represented in the example traces (Figure 3.1.5A) and cumulative frequency plots of sEPSC (Figure 3.1.5F) event amplitude, where red traces (LPS+IFNγ) are left-shifted compared to black (control) and orange (LPS alone) traces. NMDA+4-AP treated neurons are represented by grey traces.

The median sIPSC amplitude of neurons treated with LPS+IFNγ (median 58.07 pA, IQR 35.56-80.71 pA, N=11), however, was significantly smaller (Kruskal-Wallis ANOVA with Dunn's multiple comparison post-hoc test, p=0.0006) than that of control neurons (median 181.4 pA, IQR 125.4-289.5 pA, N=14) (Figure 3.1.5E). However, the wide spread of values in the control group could have skewed this result. The median sIPSC amplitude of LPS-only treated neurons at 129.3 pA (IQR 95-188.9 pA, N=6) was however not significantly different from control neurons (Kruskal-Wallis ANOVA with Dunn's multiple comparison post-hoc test, p>0.05), and neither was the median sIPSC amplitude of NMDA-4-AP treated neurons, at 87.05 pA (IQR 69.36-104.7 pA, N=2) (Kruskal-Wallis ANOVA with Dunn's multiple comparison post-hoc test, p=0.7644) (Figure 3.1.5E). Neurons treated with LPS only did not have a median sIPSC amplitude significantly different from that of neurons treated with both LPS and IFNγ (Kruskal-Wallis ANOVA with Dunn's multiple comparison post-hoc test, p>0.05) (Figure 3.1.5E). It should also be mentioned that the LPS-only treated group contained upper and lower outliers which could have skewed these results. The median sIPSC amplitude of neurons in the NMDA+4-AP treated group was not significantly different from either that of LPS-only (Kruskal-Wallis ANOVA with Dunn's multiple comparison post-hoc test, p>0.05) or LPS+IFNγ treated (Kruskal-Wallis ANOVA with Dunn's multiple comparison post-hoc test, p>0.05) neurons (Figure 3.1.5E). These results are evident in both the example traces (Figure 3.1.5B) and the cumulative frequency plots of sIPSC (Figure 3.1.5G) event amplitude, where red traces (LPS+IFNγ) are left-shifted compared to black (control) and orange (LPS alone) traces. NMDA+4-AP treated neurons are represented by grey traces.

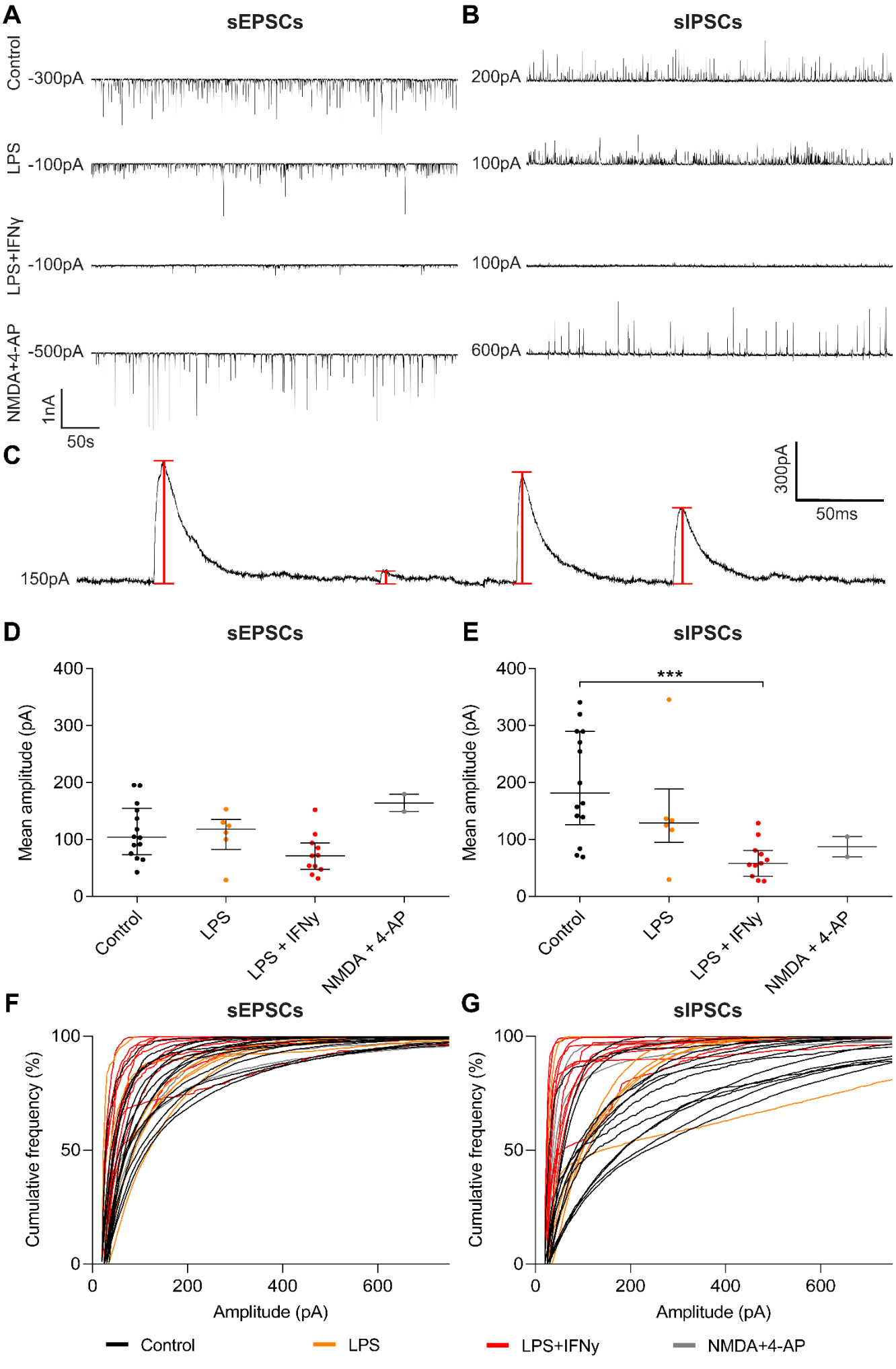
A
sEPSCs
Control
-300pA
LPS
-100pA
LPS+IFNy
-100pA
NMDA+4-AP
-500pA
1nA
50s
B
sIPSCs
200pA
100pA
100pA
600pA
C
300pA
50ms
150pA
D
sEPSCs
Mean amplitude (pA)
400
300
200
100
0
Control
LPS
LPS + IFNy
NMDA + 4-AP
E
sIPSCs
***
Mean amplitude (pA)
400
300
200
100
0
Control
LPS
LPS + IFNy
NMDA + 4-AP
F
sEPSCs
Cumulative frequency (%)
100
50
0
0
200
400
600
Amplitude (pA)
G
sIPSCs
Cumulative frequency (%)
100
50
0
0
200
400
600
Amplitude (pA)
Control
LPS
LPS+IFNy
NMDA+4-AP

Figure 3.1.5. Immune activation via combined LPS+IFNγ treatment for 72 hours reduces the amplitude of sIPSCs in cultured hippocampal CA3/CA1 pyramidal neurons. *Hippocampal OBSCs (2 per well) were treated with vehicle, LPS-only (10 µg/mL), LPS (10 µg/mL) + IFNγ (100 ng/mL) or NMDA (5 µM) + 4-AP (100 µM) in the culture medium for* ***72 hours****. Whole-cell patch-clamp recordings were then made from cultured hippocampal CA3/CA1 pyramidal neurons using a cesium-based internal solution. Recordings were performed in voltage clamp to record sPSCs. Neurons were held at -70 mV to record sEPSCs and at +15 mV to record sIPSCs. Example sEPSC (A) and sIPSC (B) traces from each treatment group. (C) Example sIPSC trace showing detection of event amplitude. Population data (with median ± IQR or mean ± SEM) demonstrating median amplitude of sEPSCs (D) and sIPSCs (E) in control (N=14), LPS-only (N=6), LPS+IFNγ (N=11) or NMDA+4-AP (N=2) treatment conditions. The median amplitude of sIPSCs in neurons treated with LPS+IFNγ is significantly smaller than that of control neurons. There is no significant difference in median amplitude of either sEPSCs or sIPSCs in neurons treated with LPS alone. Cumulative frequency plots of mean event amplitudes of sEPSCs (F) and sIPSCs (G) in each patched cell show that red traces (representing LPS+IFNγ-treated neurons) are left-shifted compared to black (control) and orange (LPS alone) traces, indicating smaller mean amplitudes. All groups were tested for Gaussian distributions using the Shapiro-Wilk normality test. If any group was found to not have a Gaussian distribution or was too small to test for normality, the data were compared using a Kruskal-Wallis ANOVA test with Dunn's multiple comparison post-hoc test. If all groups were found to have Gaussian distributions, a Brown-Forsythe ANOVA with Games-Howell's multiple comparison pot-hoc test was performed. Values with median ± IQR (nonparametric) or mean ± SEM (parametric); * $p \leq 0.05$; ** $p \leq 0.01$; *** $p \leq 0.001$. Each data point represents a neuron.*

Given the observed disruption to neuronal networks after immune activation with LPS+IFNγ, I now wanted to determine if cells in organotypic slices were also dying as a result of chronic immune activation, since significant cell death has been reported by others (Papageorgiou *et al*., 2016). To do this, I developed an assay for determining both apoptotic and necrotic cell death using a combination of Hoechst (Figure 3.1.6A), caspase 3/7 (Figure 3.1.6C) and propidium iodide (Figure 3.1.6E) staining. Caspase 3/7 are proteins active only when the cell has irreversibly entered an apoptotic cascade (*Caspase-3 Activation: An Indicator of Apoptosis in Image-Based Assays*, 2012). Propidium iodide (PI) can only enter a cell when the membrane is disrupted (such as observed when a cell undergoes necrotic cell death). Once inside the nucleus of the cell, PI binds to DNA and its fluorescence properties undergo a red-shift, causing a two- to three-fold increase in fluorescence intensity which is signifies necrotic cell death (Chacon *et al*., 1997; Hezel *et al*., 2012).

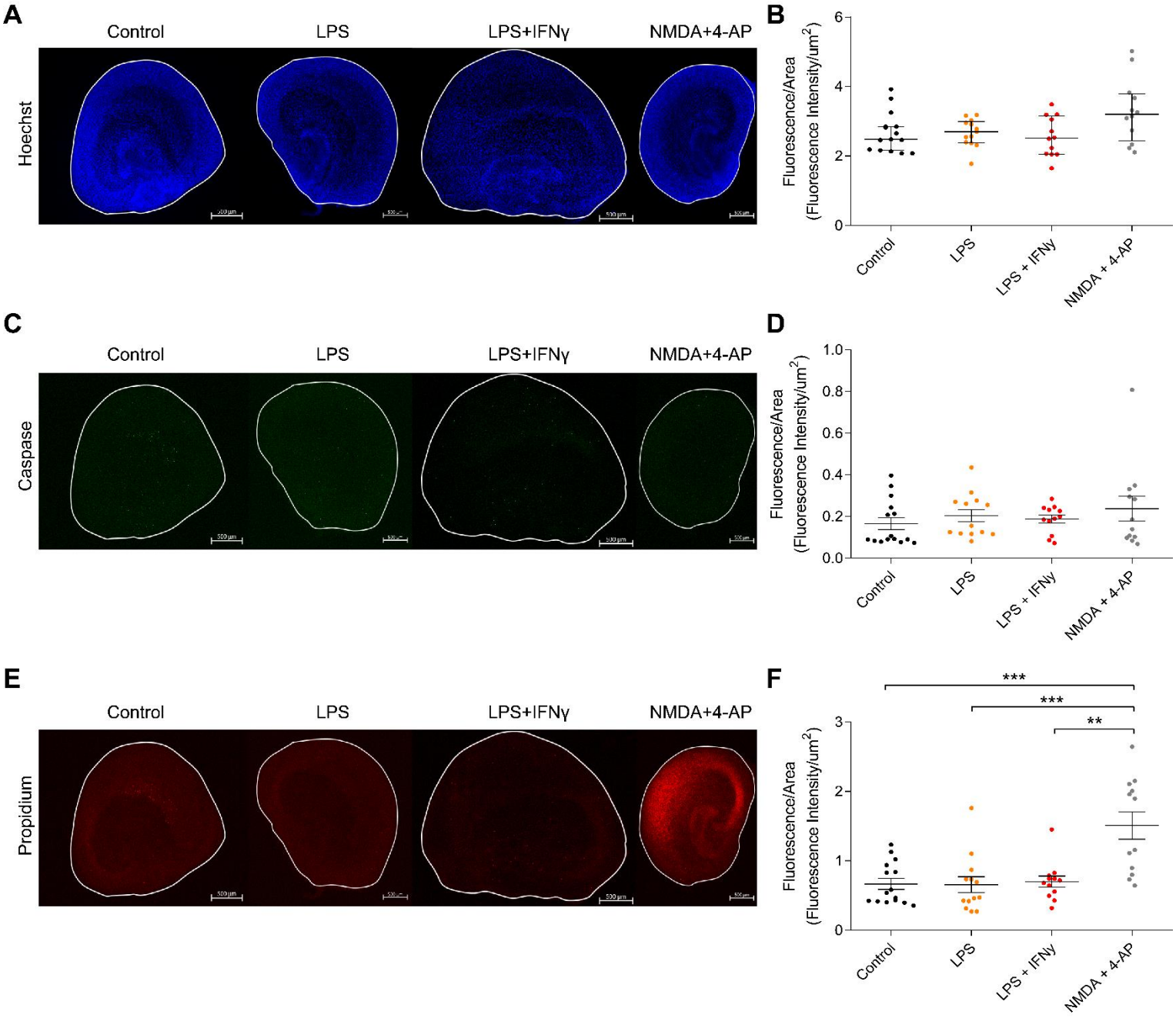

Figure 3.1.6. Immune activation via LPS alone or combined LPS+IFNγ treatment for 72 hours does not cause enhanced cell death by apoptosis or necrosis. *Hippocampal OBSCs (6 per well) were treated with vehicle, LPS-only (10 µg/mL), LPS (10 µg/mL) + IFNγ (100 ng/mL) or NMDA (5 µM) + 4-AP (100 µM) in the culture medium for **72 hours**. Slices were then stained for various types of cell death and imaged using a confocal microscope. Representative images of slices stained with Hoechst (A) to show nuclei, caspase 3/7 markers (C) to indicate apoptotic cell death and propidium iodide (E) to indicate necrotic cell death across treatment groups. Population data (median ± IQR or mean ± SEM) showing quantified fluorescence per area (with background fluorescence adjustment) of Hoechst (B), caspase 3/7 (D) and propidium iodide (F) staining for control (N=15), LPS alone (N=13), LPS+IFNγ (N=12) and NMDA+4-AP (N=12). There is no significant difference in apoptotic (D) or necrotic (F) cell death between groups treated with LPS alone or LPS+IFNγ compared to control slices. Propidium iodide staining in slices treated with NMDA+4-AP (positive control for*

*excitotoxicity) is significantly higher than all other groups. All groups were tested for Gaussian distributions using the Shapiro-Wilk normality test. If any group was found to not have a Gaussian distribution or was too small to test for normality (nonparametric), the data were compared using a Kruskal-Wallis ANOVA test with Dunn's multiple comparison post-hoc test. If all groups were found to have Gaussian distributions (parametric), a Brown-Forsyth and Welch ANOVA test with Games-Howell's multiple comparison post-test was performed. Values with median ± IQR (nonparametric) or mean ± SEM (parametric); * p ≤ 0.05; ** p ≤ 0.01; *** p ≤ 0.001. Each data point represents a stained OBSC.*

Organotypic hippocampal slices (DIV05-07) were treated with vehicle, LPS-only (10 µg/mL), LPS (10 µg/mL) + IFNγ (100 ng/mL) or NMDA (5 µM) + 4-AP (100 µM) in the culture medium for 72 hours and then stained, mounted and imaged using a confocal microscope. Background adjustment was also performed for each image using ZenBlue software. As expected, I found that the mean fluorescence intensity/area for Hoechst staining of control OBSCs, at 2.669 intensity/µm^2 (SEM ±0.1474 intensity/µm^2, N=15) was not significantly different from OBSCs treated with LPS (mean 2.668 intensity/µm^2, SEM ±0.1104 intensity/µm^2, N=13, p>0.05), with LPS+IFNγ (mean 2.558 intensity/µm^2, SEM ±0.1663 intensity/µm^2, N=12, p>0.05) or with NMDA+4-AP (mean 3.294 intensity/µm^2, SEM ±0.2678 intensity/µm^2, N=12, p=0.05) (Brown-Forsyth and Welch ANOVA test with Games-Howell's multiple comparison post-test for all) (Figure 3.1.6B). LPS-treated slices did not have median intensity/area significantly different from LPS+IFNγ-treated slices (Brown-Forsyth and Welch ANOVA test with Games-Howell's multiple comparison post-test, p>0.05) or from that of slices treated with NMDA+4-AP (Brown-Forsyth and Welch ANOVA test with Games-Howell's multiple comparison post-test, p>0.05) (Figure 3.1.6B). Furthermore, the median intensity/area for slices treated with LPS+IFNγ was not different from that of slices treated with NMDA+4-AP (Brown-Forsyth and Welch ANOVA test with Games-Howell's multiple comparison post-test, p>0.05) (Figure 3.1.6B). These data ensured that slices from each treatment group had similar numbers of total cells in each slice, such that no treatment group was biased in other staining conditions.

I now investigated apoptotic cell death outcomes (Figure 3.1.6D). Surprisingly, there was no difference in median intensity/area between control (median 0.09202 intensity/µm^2, IQR 0.08356-0.2433 intensity/µm^2, N=15) and LPS-treated (median 0.1551 intensity/µm^2, IQR 0.1176-0.2734 intensity/µm^2, N=13, p=0.8394) OBSCs or between control and LPS+IFNγ

treated (median 0.1946 intensity/μm^2, IQR 0.1243-0.2390 intensity/μm^2, N=12, p>0.05) OBSCs (Kruskal-Wallis ANOVA with Dunn's multiple comparison post-hoc test for both). Furthermore, slices treated with NMDA+4-AP (median 0.1624 intensity/μm^2, IQR 0.09852-0.3221 intensity/μm^2, N=12) also did not exhibit a different median intensity/area apoptotic stain as compared to controls (Kruskal-Wallis ANOVA with Dunn's multiple comparison post-hoc test, p>0.05). LPS-treated slices did not differ from either LPS+IFNγ treated slices (p>0.05) or from NMDA+4-AP treated slices (p>0.05), and LPS+IFNγ treated slices did not differ from NMDA+4-AP treated slices (p>0.05) either (Kruskal-Wallis ANOVA with Dunn's multiple comparison post-hoc test for all). These data were contrary to what I had expected, since multiple lines of evidence point to apoptotic cell death via nitric oxide toxicity following chronic immune activation (Z. Liu *et al*., 2017; Rumbaugh & Nath, 2009; Wang *et al*., 2017).

Given the lack of difference in apoptotic cell death across treatment groups, I expected to see necrotic cell death, similar to what was observed by Papageorgiou *et al*. (2016) in their lactate dehydrogenase (LDH) assays of cell death. Once again I was surprised by my findings. The median PI fluorescence intensity/area for control slices was 0.5402 intensity/μm^2 (IQR 0.4165-0.9392 intensity/μm^2, N=15) (Figure 3.1.6F). For LPS treated slices, the median intensity/area was 0.4745 intensity/μm^2 (IQR 0.3663-0.8044 intensity/μm^2, N=13), which was not significantly different from controls (Kruskal-Wallis ANOVA with Dunn's multiple comparison post-hoc test, p>0.05) (Figure 3.1.6F). LPS+IFNγ treated slices had a median intensity/area of 0.7009 intensity/μm^2 (IQR 0.5119-0.7765 intensity/μm^2, N=12) which was also not significantly different from controls (Kruskal-Wallis ANOVA with Dunn's multiple comparison post-hoc test, p>0.05) (Figure 3.1.6F). LPS treated and LPS+IFNγ treated slices did not differ from one another in necrotic cell death staining either (Kruskal-Wallis ANOVA with Dunn's multiple comparison post-hoc test, p>0.05) (Figure 6F). On the contrary, slices treated with the positive excitotoxic treatment of NMDA+4-AP had a median intensity/area of 1.527 intensity/μm^2 (IQR 0.8229-2.082 intensity/μm^2, N=12) which was significantly higher than that of controls (p=0.0066), of LPS treated slices (p=0.0022) and of LPS+IFNγ treated slices (p=0.0318) (Kruskal-Wallis ANOVA with Dunn's multiple comparison post-hoc test for all) (Figure 3.1.6F).

I was surprised at not observing any apoptotic or necrotic cell death in slices that had been treated with LPS or LPS+IFNγ, given that other groups have found convincing evidence of cell death (Papageorgiou *et al*., 2016). To confirm that the immune treatments were inducing an immune response, I collected culture media every 24 hours for 72 hours from each of the culture wells in the above staining experiment across treatment conditions. I then used this media to detect release of the cytokines IL-6, TNF-α, IL-10 and IL-1β (Figure 3.1.7A) via ELISAs.

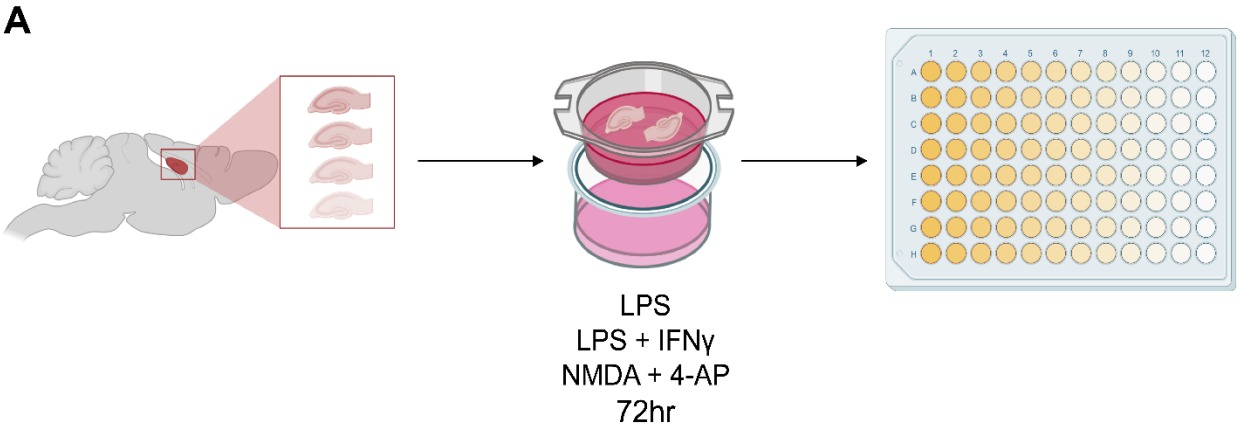
A
LPS
LPS + IFNγ
NMDA + 4-AP
72hr

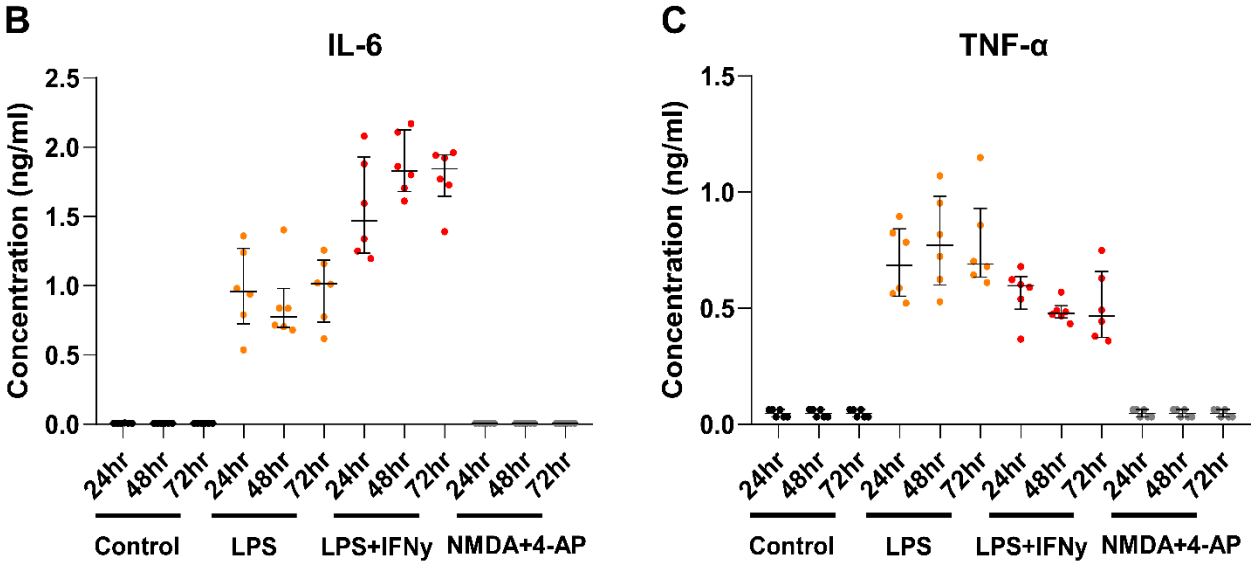
B
IL-6
Concentration (ng/ml)
2.5
2.0
1.5
1.0
0.5
0.0
24hr
48hr
72hr
Control
LPS
LPS+IFNy
NMDA+4-AP

C
TNF-α
Concentration (ng/ml)
1.5
1.0
0.5
0.0
24hr
48hr
72hr
Control
LPS
LPS+IFNy
NMDA+4-AP

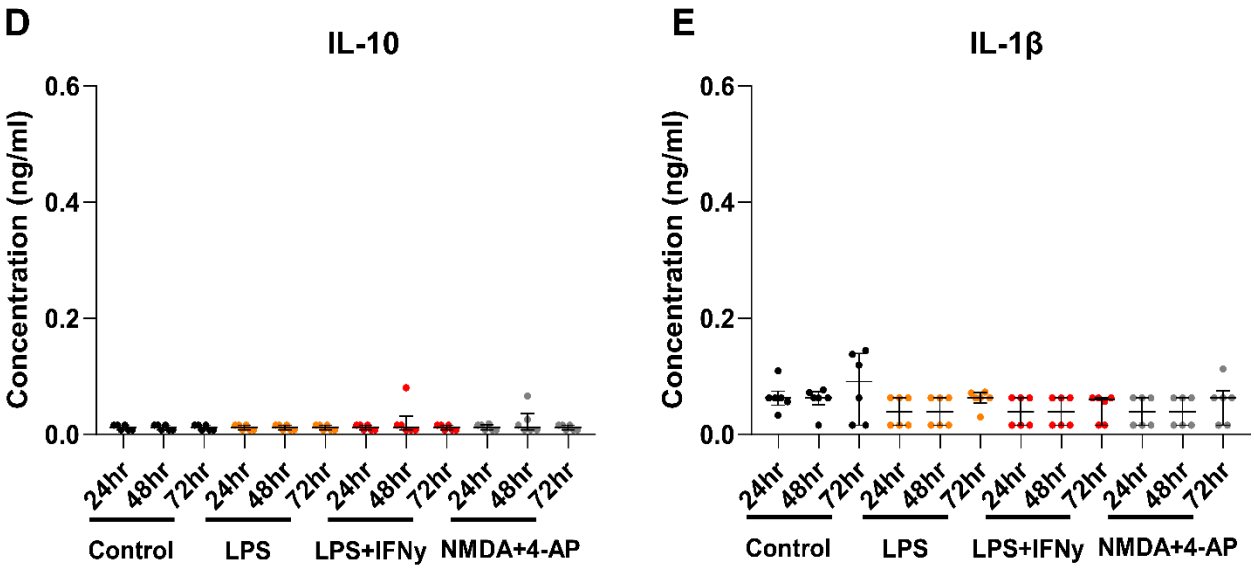
D
IL-10
Concentration (ng/ml)
0.6
0.4
0.2
0.0
24hr
48hr
72hr
Control
LPS
LPS+IFNy
NMDA+4-AP

E
IL-1β
Concentration (ng/ml)
0.6
0.4
0.2
0.0
24hr
48hr
72hr
Control
LPS
LPS+IFNy
NMDA+4-AP

Figure 3.1.7. LPS+IFNγ treatment causes pro-inflammatory cytokine release at 24, 48 and 72 hours in OBSCs that did not experience cell death. *(A) Schematic diagram showing experimental set-up. Hippocampal OBSCs (6 per well) were treated with vehicle, LPS-only (10 µg/mL), LPS (10 µg/mL) + IFNγ (100 ng/mL) or NMDA (5 µM) + 4-AP (100 µM) in the culture medium for* ***72 hours****. At 24, 48 and 72 hours of treatment, culture media was collected from each well. ELISAs were performed using collected media to detect release of the cytokines IL-6, TNF-α, IL-10 and IL-1β. LPS treatment alone (N=6) as well as LPS+IFNγ (N=6) induced significant IL-6 (B) and TNF-α (C) release as compared to control slices (N=6) or NMDA+4-AP (N=6) treated slices. Combination treatment with LPS+IFNγ induced higher IL-6 release than LPS alone (B), but LPS alone caused higher TNF-α release than combined LPS+IFNγ (C). IL-10 (D) and IL-1β (E) were undetectable in all treatment conditions. All groups were tested for Gaussian distributions using the Shapiro-Wilk normality test. If any group was found to not have a Gaussian distribution or was too small to test for normality (nonparametric), the data were compared using an unpaired t-test with Welch's correction. If all groups were found to have Gaussian distributions (parametric), an unpaired Mann-Whitney U test was performed. Values with median ± IQR (nonparametric) or mean ± SEM (parametric); * $p \leq 0.05$; ** $p \leq 0.01$; *** $p \leq 0.001$. Each data point represents cytokine data from a single culture well.*

These data show that both LPS and a combination of LPS and IFNγ induced a significant release of the pro-inflammatory cytokines IL-6 and TNF-α into the culture media of OBSCs at 24, 48 and 72 hours (Figure 3.1.7B&C) (Statistical data available in tables 3.1.3 & 3.1.4) as compared to undetectable levels in control slices. Interestingly, a combination of LPS+IFNγ induced greater release of IL-6 (Figure 3.1.7B) than LPS alone at all three time points, but LPS induced greater release of TNF-α (Figure 3.1.7C) at 48 and 72 hours than LPS+IFNγ, which is in contrast to the data presented in Figure 3.1.1 (derived from culture media of slices used for patch-clamping), where TNF-α was more prominently released by slices treated with LPS+IFNγ. There was no detectable release of IL-6 or TNF-α in slices treated with NMDA+4-AP (Figures 3.1.7B&C, statistical data available in Tables 3.1.3 & 3.1.4). I was unable to detect the release of IL-10 (Figure 3.1.7D) or IL-1β (Figure 3.1.7E) from OBSCs in any treatment group, most likely owing to an insufficient sensitivity of the ELISA cytokines used (Statistical data available in Tables 3.1.3 & 3.1.4).

Table 3.1.3. Median and IQR values for ELISA performed on culture media from hippocampal OBSCs used for cell death studies as represented in Figure 3.1.7. C=Control; L=LPS-only; I=LPS+IFNγ; N=NMDA+4-AP.

		24hr				48hr				72hr			
		C	L	I	N	C	L	I	N	C	L	I	N
IL-6	Median	0.007816	0.9595	1.467	0.007816	0.007816	0.07756	1.831	0.007816	0.007816	1.016	1.846	0.007816
	IQR	0.007813-0.008415	0.07269-1.270	1.237-1.930	0.007813-0.	0.007813-0.007820	0.6988-0.9794	1.681-2.125	0.007813-0.007820	0.007813-0.007903	0.7372-1.184	1.644-1.945	0.007813-0.007820
TNF-α	Median	0.04688	0.6857	0.5965	0.04688	0.04688	0.7705	0.4784	0.04688	0.04688	0.6905	0.4675	0.04688
	IQR	0.03125-0.06250	0.5524-0.8422	0.4959-0.6371	0.03125-0.06250	0.03125-0.06250	0.6001-0.9826	0.4585-0.5107	0.03125-0.06250	0.03125-0.06250	0.6348-0.9309	0.3740-0.6595	0.03125-0.06250
IL-10	Median	0.01172	0.01172	0.01172	0.01171	0.01172	0.01172	0.01171	0.01172	0.01172	0.01172	0.01171	0.01172
	IQR	0.007813-0.01563	0.007813-0.01563	0.007813-0.01563	0.007813-0.01627	0.007813-0.01563	0.007813-0.01563	0.007813-0.03177	0.007813-0.03575	0.007813-0.01563	0.007813-0.01563	0.007813-0.01561	0.007813-0.01563
IL-1β	Median	0.06250	0.03906	0.03906	0.03906	0.06250	0.03906	0.03906	0.03906	0.09082	0.06250	0.05971	0.06250
	IQR	0.05030-0.07421	0.01563-0.06250	0.01563-0.06250	0.01563-0.06250	0.05078-0.07317	0.01563-0.06250	0.01563-0.06250	0.01563-0.06250	0.01563-0.1394	0.05435-0.07182	0.01563-0.06250	0.01563-0.07503

Table 3.1.4. Outcome of statistic tests performed on ELISA data presented in Figure 3.1.7.

	Test conditions	Test performed	24hr	Test performed	48hr	Test performed	72hr
IL-6	Control vs LPS	Mann Whitney-U	**p = 0.0022	Mann Whitney-U	**p = 0.0022	Mann Whitney-U	** p = 0.0022
	Control vs LPS+IFNγ	Mann Whitney-U	** p = 0.0022	Mann Whitney-U	** p = 0.0022	Mann Whitney-U	** p = 0.0022
	Control vs NMDA+4-AP	Mann Whitney-U	ns p > 0.05	Mann Whitney-U	ns p > 0.05	Mann Whitney-U	ns p > 0.05
	LPS vs LPS+IFNγ	Welch's t-test	* p = 0.0128	Mann Whitney-U	** p = 0.0022	Welch's t-test	*** p = 0.0001
	LPS vs NMDA+4-AP	Mann Whitney-U	** p = 0.0022	Mann Whitney-U	** p = 0.0022	Mann Whitney-U	** p = 0.0022
	LPS+IFNγ vs NMDA+4-AP	Mann Whitney-U	** p = 0.0022	Mann Whitney-U	** p = 0.0022	Mann Whitney-U	** p = 0.0022
TNF-α	Control vs LPS	Mann Whitney-U	** p = 0.0022	Mann Whitney-U	** p = 0.0022	Mann Whitney-U	** p = 0.0022
	Control vs LPS+IFNγ	Mann Whitney-U	** p = 0.0022	Mann Whitney-U	** p = 0.0022	Mann Whitney-U	** p = 0.0022
	Control vs NMDA+4-AP	Mann Whitney-U	ns p > 0.05	Mann Whitney-U	ns p > 0.05	Mann Whitney-U	ns p > 0.05
	LPS vs LPS+IFNγ	Welch's t-test	ns p > 0.05	Welch's t-test	* p = 0.0143	Welch's t-test	* p = 0.0303
	LPS vs NMDA+4-AP	Mann Whitney-U	** p = 0.0022	Mann Whitney-U	** p = 0.0022	Mann Whitney-U	** p = 0.0022
	LPS+IFNγ vs NMDA+4-AP	Mann Whitney-U	** p = 0.0022	Mann Whitney-U	** p = 0.0022	Mann Whitney-U	** p = 0.0022
IL-10	Control vs LPS	Mann Whitney-U	ns p > 0.05	Mann Whitney-U	ns p > 0.05	Mann Whitney-U	ns p > 0.05
	Control vs LPS+IFNγ	Mann Whitney-U	ns p > 0.05	Mann Whitney-U	ns p > 0.05	Mann Whitney-U	ns p > 0.05
	Control vs NMDA+4-AP	Mann Whitney-U	ns p > 0.05	Mann Whitney-U	ns p > 0.05	Mann Whitney-U	ns p > 0.05

	LPS vs LPS+IFNγ	Mann Whitney-U	ns p > 0.05	Mann Whitney-U	ns p > 0.05	Mann Whitney-U	ns p > 0.05
	LPS vs NMDA+4-AP	Mann Whitney-U	ns p > 0.05	Mann Whitney-U	ns p > 0.05	Mann Whitney-U	ns p > 0.05
	LPS+IFNγ vs NMDA+4-AP	Mann Whitney-U	ns p > 0.05	Mann Whitney-U	ns p > 0.05	Mann Whitney-U	ns p > 0.05
IL-1β	Control vs LPS	Mann Whitney-U	ns p > 0.05	Mann Whitney-U	ns p > 0.05	Mann Whitney-U	ns p > 0.05
	Control vs LPS+IFNγ	Mann Whitney-U	ns p > 0.05	Mann Whitney-U	ns p > 0.05	Mann Whitney-U	ns p > 0.05
	Control vs NMDA+4-AP	Mann Whitney-U	ns p > 0.05	Mann Whitney-U	ns p > 0.05	Welch's t-test	ns p > 0.05
	LPS vs LPS+IFNγ	Mann Whitney-U	ns p > 0.05	Mann Whitney-U	ns p > 0.05	Mann Whitney-U	ns p > 0.05
	LPS vs NMDA+4-AP	Mann Whitney-U	ns p > 0.05	Mann Whitney-U	ns p > 0.05	Mann Whitney-U	ns p > 0.05
	LPS+IFNγ vs NMDA+4-AP	Mann Whitney-U	ns p > 0.05	Mann Whitney-U	ns p > 0.05	Mann Whitney-U	ns p > 0.05

3.2. Immune activation by LPS+IFNγ for 24 hours causes electrophysiological disturbances.

Given the profound effect of chronic immune activation on the cytokine release and network function of pyramidal neurons, I now wanted to investigate the effect of shorter time scales of "bolstered" immune activation. To achieve this, I repeated the experiment performed in figures 3.1.2-3.1.5, treating hippocampal OBSCs with vehicle (culture medium), LPS (10 µg/mL) + IFNγ (100 ng/mL) or NMDA (5 µM) + 4-AP (100 µM) in the culture medium for **24 hours** (Figure 3.2.1A). I did not include a group treated with LPS-only given that this treatment did not produce profoundly different effects (compared to controls) on network function after 72 hours of treatment. After treatment, I again made whole-cell patch-clamp recordings from cultured hippocampal CA3/CA1 pyramidal neurons using the cesium-based internal solution. Once again, these recordings were performed in voltage-clamp mode to record sPSCs. Holding neurons at -70 mV allowed me to record sEPSCs and holding at +15 mV allowed me to record sIPSCs.

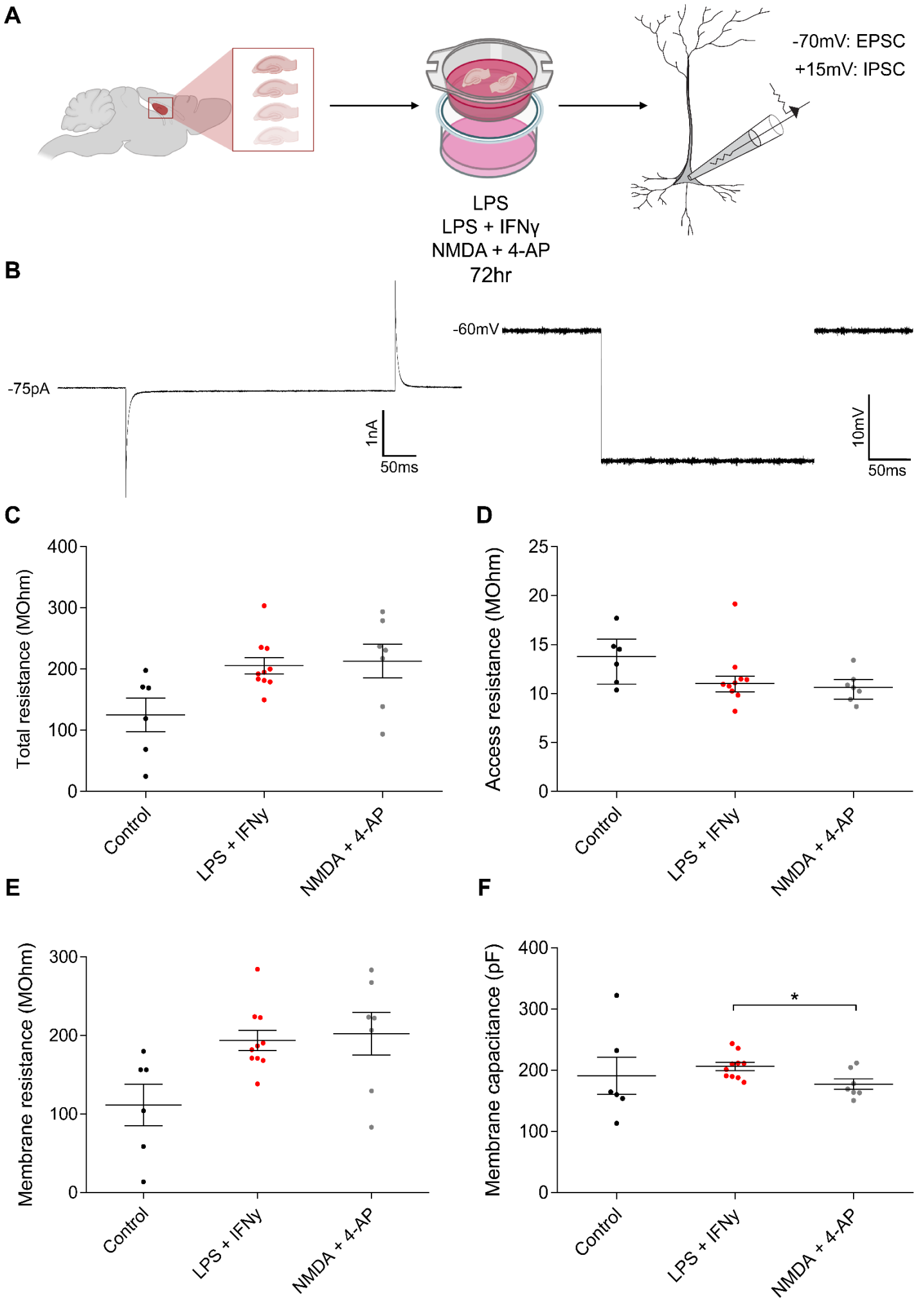
A
-70mV: EPSC
+15mV: IPSC
LPS
LPS + IFNγ
NMDA + 4-AP
72hr
B
-75pA
1nA
50ms
-60mV
10mV
50ms
C
Total resistance (MOhm)
400
300
200
100
0
Control
LPS + IFNγ
NMDA + 4-AP
D
Access resistance (MOhm)
25
20
15
10
5
0
Control
LPS + IFNγ
NMDA + 4-AP
E
Membrane resistance (MOhm)
300
200
100
0
Control
LPS + IFNγ
NMDA + 4-AP
F
Membrane capacitance (pF)
400
300
200
100
0
*
Control
LPS + IFNγ
NMDA + 4-AP

Figure 3.2.1. Immune activation via LPS+IFNγ treatment for 24 hours does not change the membrane properties of cultured hippocampal CA3/CA1 pyramidal neurons. *(A) Schematic diagram of experimental set-up. Hippocampal OBSCs were treated with Control (vehicle), LPS (10 µg/mL) + IFNγ (100 ng/mL) or NMDA (5 µM) + 4-AP (100 µM) in the culture medium for* ***24 hours****. Whole-cell patch-clamp recordings were made from cultured hippocampal CA3/CA1 pyramidal neurons using a cesium-based internal solution (A). Recordings were performed in voltage-clamp mode to record sPSCs, but before this, voltage pulses were applied to the neuron to assess membrane properties. (B) Example voltage-clamp mode recording (left panel) from a pyramidal neuron while voltage pulses (right panel) were applied to the neuron. Neuronal membrane properties were analyzed from these recordings. Population data (with median ± IQR) demonstrating control (N=6), LPS+IFNγ (N=10) or NMDA+4-AP (N=7) treatment conditions. (D) Access resistance, and thus patch quality was stable across treatment conditions. (C) Total resistance is not significantly different across treatment conditions. Membrane resistance (E) is significantly higher in neurons treated with NMDA+4-AP than in control neurons. Access resistance (D) is not significantly different across treatment conditions. Membrane capacitance of LPS+IFNγ treated neurons was significantly different from that of NMDA+4-AP treated neurons (F). All groups were tested for Gaussian distributions using the Shapiro-Wilk normality test. If any group was found to not have a Gaussian distribution or was too small to test for normality (nonparametric), the data were compared using a Kruskal-Wallis ANOVA test with Dunn's multiple comparison post-hoc test. If all groups were found to have Gaussian distributions (parametric), a Brown-Forsyth and Welch ANOVA test with Games-Howell's multiple comparison post-test was performed. Values with median ± IQR for nonparametric data sets or mean ± SEM for parametric data sets; * $p \leq 0.05$; ** $p \leq 0.01$; *** $p \leq 0.001$. Each data point represents a neuron.*

Neuronal membrane properties (Figure 3.2.1C-F) were deduced from voltage steps (Figure 3.2.1B) applied to each neuron. As before, R_a was used to assess the quality of each patch, and cells with R_a above 30 MΩ were once again discarded to maintain data quality. The median R_a was 13.77 MΩ (IQR 10.95-15.54 MΩ, N=6) for control neurons, 11.02 MΩ (IQR 10.16-11.79 MΩ, N=10) for neurons treated with LPS+IFNγ and 10.62 MΩ (IQR 9.396-11.45 MΩ, N=7) for neurons treated with NMDA+4-AP. Neither the LPS+IFNγ or NMDA+4-AP treated groups had medians which differed significantly from that of control neurons (Kruskal-Wallis ANOVA test with Dunn's multiple comparison post-hoc test, $p>0.05$ and $p>0.05$ respectively) (Figure 3.2.1D). The outlier present in the LPS+IFNγ treated group could however have skewed results in these tests. Further, there was no difference between the medians of the LPS+IFNγ and NMDA+4-AP treated groups (Kruskal-Wallis ANOVA test with Dunn's multiple comparison post-hoc test, $p>0.05$) (Figure 3.2.1D).

Knowing that patch quality was stable across all treatment conditions, I now examined the total resistance, membrane resistance and membrane capacitance of patched neurons. The mean total resistance was 125.1 MΩ (SEM ± 27.42 MΩ, N=6) for control neurons, 205.4

MΩ (SEM ±13.53 MΩ, N=10) for LPS+IFNγ treated neurons and 213 MΩ (SEM ±27.38 MΩ, N=7) and none of these were significantly different from one another ($p>0.05$, Brown-Forsythe and Welch ANOVA with Games-Howell's multiple comparison post-hoc test) (Figure 3.2.1C). Each of these groups contained outlier data points, which may in turn have caused skewing in statistical tests I performed. The mean membrane resistance was 111.5 MΩ (SEM ±26.53 MΩ) for control neurons, 193.8 MΩ (SEM ±12.87 MΩ) for neurons treated with LPS+IFNγ and 202.3 MΩ (SEM ±27.25 MΩ) for neurons treated with the positive excitotoxic control NMDA+4-AP and none of these differed significantly from each other ($p>0.05$, Brown-Forsythe and Welch ANOVA with Games-Howell's multiple comparison post-hoc test) (Figure 3.2.1E). Importantly, each of these groups contained outlier data points which may have biased the results.

Finally, I examined the membrane capacitance of the neurons. The mean membrane capacitance for the control, LPS+IFNγ and NMDA+4-AP groups were 191 MΩ (SEM ±30.52 MΩ), 206.2 MΩ (SEM ±6.574 MΩ) and 177.3 MΩ (SEM ±8.577 MΩ), respectively. Neither the LPS+IFNγ nor the NMDA+4-AP treated groups differed significantly from the controls ($p>0.05$, Brown-Forsythe and Welch ANOVA with Games-Howell's multiple comparison post-hoc test), but these groups did differ significantly from one another, with the NMDA+4-AP treated group having lower membrane capacitance than that of the LPS+IFNγ treated group ($p=0.0485$, Brown-Forsythe and Welch ANOVA with Games-Howell's multiple comparison post-hoc test) (Figure 3.2.1F). Vitally, the control group was widely spread and contained outliers which may have skewed these results.

This batch of data shows that treatment with either LPS+IFNγ or NMDA+4-AP did not have any significant effect on the basic membrane or integrative properties of cultured hippocampal CA3/CA1 pyramidal neurons. I now performed the same sEPSC and sIPSC recordings as I had in Figures 3.1.2-3.1.5, but in this instance on neurons from OBSCs that had been immune activated for only 24 hours.

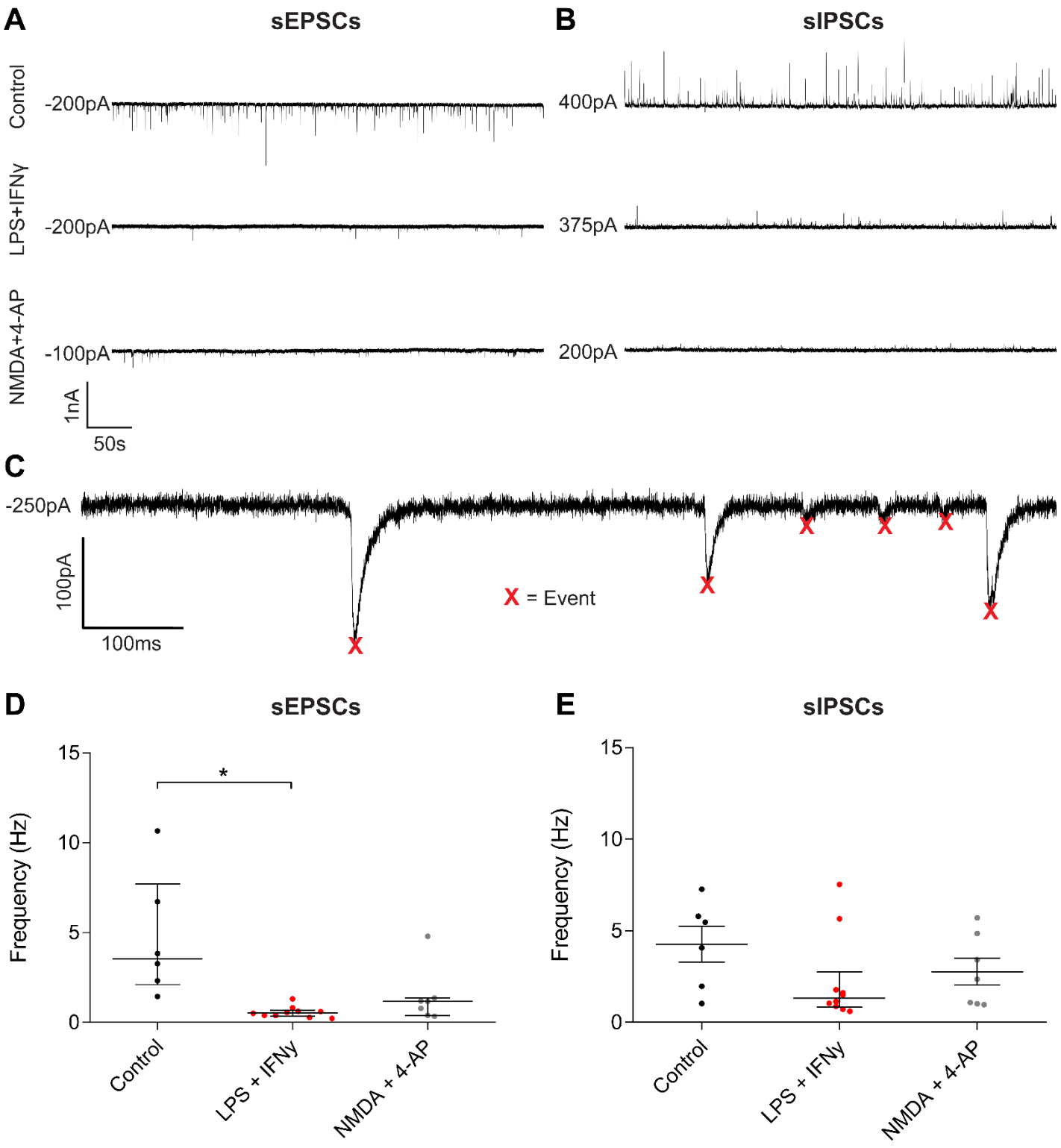

Figure 3.2.2. Immune activation via combined LPS+IFNγ for 24 hours causes a reduction in sEPSC event frequency in cultured hippocampal CA3/CA1 pyramidal neurons. *Example sEPSC (A) and sIPSC (B) traces from each treatment group. Hippocampal OBSCs were treated with vehicle,LPS (10 µg/mL) + IFNγ (100 ng/mL) or NMDA (5 µM) + 4-AP (100 µM) in the culture medium for* ***24 hours****.*

*Whole-cell patch-clamp recordings were made from CA3/CA1 pyramidal neurons using a cesium-based internal solution. Recordings were performed in voltage-clamp to record sPSCs. Neurons were held at -70 mV to record sEPSCs and at +15 mV to record sIPSCs. (C) Example trace illustrating event detection in PSCs. Population data (with median ± IQR) demonstrating frequency of sEPSCs (D) and sIPSCs (E) in control (N=6), LPS+IFNγ (N=10) or NMDA+4-AP (N=7) treatment conditions. Frequency of sEPSCs (D) in LPS+IFNγ treated neurons was significantly lower than that observed in control neurons. All groups were tested for Gaussian distributions using the Shapiro-Wilk normality test. If any group was found to not have a Gaussian distribution or was too small to test for normality (nonparametric), the data were compared using a Kruskal-Wallis ANOVA test with Dunn's multiple comparison post-hoc test. If all groups were found to have Gaussian distributions, a Brown-Forsyth and Welch ANOVA test with Games-Howell's multiple comparison post-test was performed. Values with median ± IQR (nonparametric) or mean ± SEM (parametric); * $p \leq 0.05$; ** $p \leq 0.01$; *** $p \leq 0.001$. Each data point represents a neuron.*

After patching, cells were gently shifted to -70 mV, allowing for the recording of sEPSCs (Figure 3.2.2A&D). The median frequency of sEPSC in control, LPS+IFNγ and NMDA+4-AP treated groups were 3.548 Hz (IQR 2.104-7.703 Hz, N=6), 0.5333 Hz (IQR 0.3608-0.6633 Hz, N=10) and 1.163 Hz (IQR 0.3933-1.357 Hz, N=7) respectively (Figure 3.2.2D). Only the LPS+IFNγ ($p=0.0011$) and not the NMDA+4-AP ($p>0.05$) treated group was significantly lower than the control group, as is evident from the example traces in Figure 3.2.2A (Kruskal-Wallis ANOVA with Dunn's multiple comparison post-hoc test). There was no significant difference between the LPS+IFNγ and NMDA+4-AP treated groups (Kruskal-Wallis ANOVA with Dunn's multiple comparison post-hoc test, $p>0.05$).

Once the cells were shifted to and stabilized at +15 mV, I recorded sIPSCs (Figure 3.2.2B&E). The differences in sIPSC observed between treatments groups were not quite as prominent as in the sEPSC recordings. The median frequency of sIPSC was 4.765 Hz (IQR1.735-6.165 Hz, N=6) in control cells, 1.322 Hz (IQR 0.8383-2.755 Hz, N=10) in cells treated with LPS+IFNγ and 2.350 Hz (IQR 1.020-4.857 Hz, N=7) in NMDA+4-AP treated cells. None of these groups were significantly different from one another ($p>0.05$, Kruskal-Wallis ANOVA with Dunn's multiple comparison post-hoc test) (Figure 3.2.2E) despite the trend for lower event frequency in both the LPS+IFNγ and NMDA+4-AP treated groups seen in the example traces of Figure 3.2.2B.

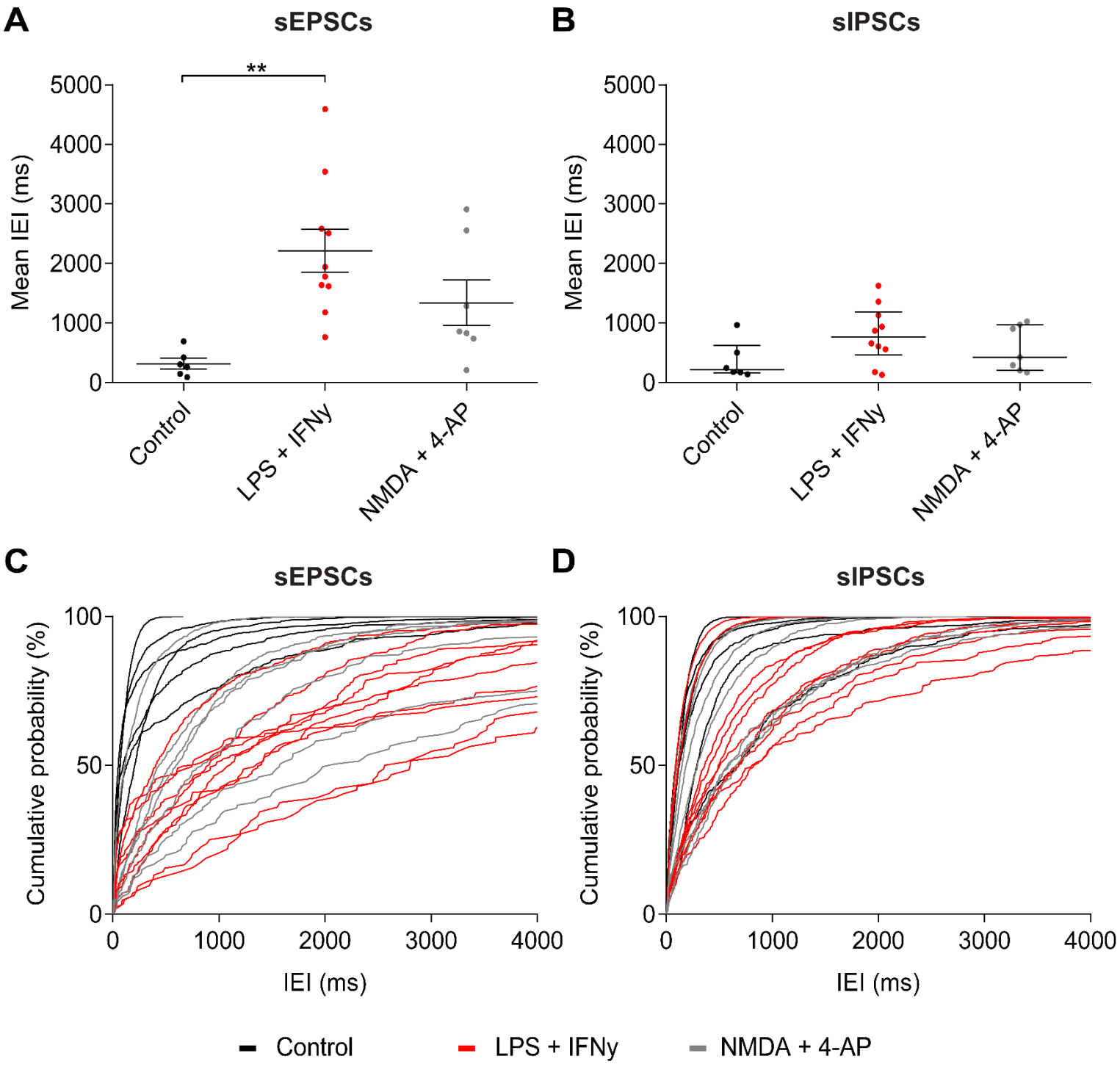

Figure 3.2.3. Immune activation via LPS+IFNγ treatment for 24 hours causes an increase in sEPSC inter-event interval in cultured hippocampal CA3/CA1 pyramidal neurons. *Hippocampal OBSCs were treated with vehicle (culture media), LPS (10 µg/mL) + IFNγ (100 ng/mL) or NMDA (5 µM) + 4-AP (100 µM) in the culture medium for **24 hours**. Whole-cell patch-clamp recordings were made from cultured hippocampal CA3/CA1 pyramidal neurons using a cesium-based internal solution. Recordings were performed in voltage-clamp mode to record sPSCs. Neurons were held at -70 mV*

*to record sEPSCs and at +15 mV to record sIPSCs. Population data (with means ± SEM or median ± IQR) demonstrating inter-event interval of sEPSCs (A) and sIPSCs (B) in control (N=6), LPS+IFNγ (N=10) or NMDA+4-AP (N=7) treatment conditions. IEIs of sEPSCs (A) in neurons treated with LPS+IFNγ were significantly increased as compared to control sEPSCs. Cumulative frequency plots of inter-event intervals of sEPSCs (C) and sIPSCs (D) in each patched neuron indicate that red traces (representing LPS+IFNγ) are right-shifted compared to black (control), indicating larger inter-event intervals, and thus less frequent events. All groups were tested for Gaussian distributions using the Shapiro-Wilk normality test. If any group was found to not have a Gaussian distribution or was too small to test for normality, the data were compared using a Kruskal-Wallis ANOVA test with Dunn's multiple comparison post-hoc test. If all groups were found to have Gaussian distributions, a Brown-Forsythe and Welch ANOVA with Games-Howell's multiple comparison post-hoc test was performed. Values with mean ± SEM (parametric) and with median ±IQR (nonparametric); * $p \leq 0.05$; ** $p \leq 0.01$; *** $p \leq 0.001$. Each data point represents a neuron.*

The mean sEPSC IEIs for control, LPS+IFNγ and NMDA+4-AP treated groups were 320.7 ms (SEM ±88.25 ms, N=6), 2215 ms (SEM ±361.6 ms, N=10) and 1341 ms (SEM ±380.4 ms, N=7), respectively (Figure 3.2.3A). Only the LPS+IFNγ treated group ($p=0.0014$) and not the NMDA+4-AP treated group ($p>0.05$) had significantly longer IEIs than the control group (Brown-Forsythe and Welch ANOVA with Games-Howell's multiple comparison post-hoc test) and these groups' means did not differ significantly from one another ($p>0.05$, Brown-Forsythe and Welch ANOVA with Games-Howell's multiple comparison post-hoc test).

The median IEIs for inhibitory PSCs in control, LPS+IFNγ and NMDA+4-AP treated groups were 214.4 ms (IQR 163.5-621.9 ms, N=6), 767.3 ms (IQR 463.6-1188 ms, N=10) and 426.1 ms (IQR 205.6-973.1 ms, N=7), respectively and none of these groups differed significantly from one another ($p>0.05$, Kruskal-Wallis ANOVA with Dunn's multiple comparison post-hoc test) despite the trend for the LPS+IFNγ and NMDA+4-AP treated groups to have longer IEIs (and thus less frequent events) than controls (Figure3.2.3B).

These data are represented in the example traces shown in Figure 3.2.2B (sEPSCs) and 3.2.2C (sIPSCs) as well as by the cumulative frequency plots of IEIs of sEPSCs in Figure 3.2.3C and of sIPSCs in Figure 3.2.3D where red traces (representing LPS+IFNγ) are right-shifted compared to black (control) traces, indicating larger IEIs, and thus less frequent events.

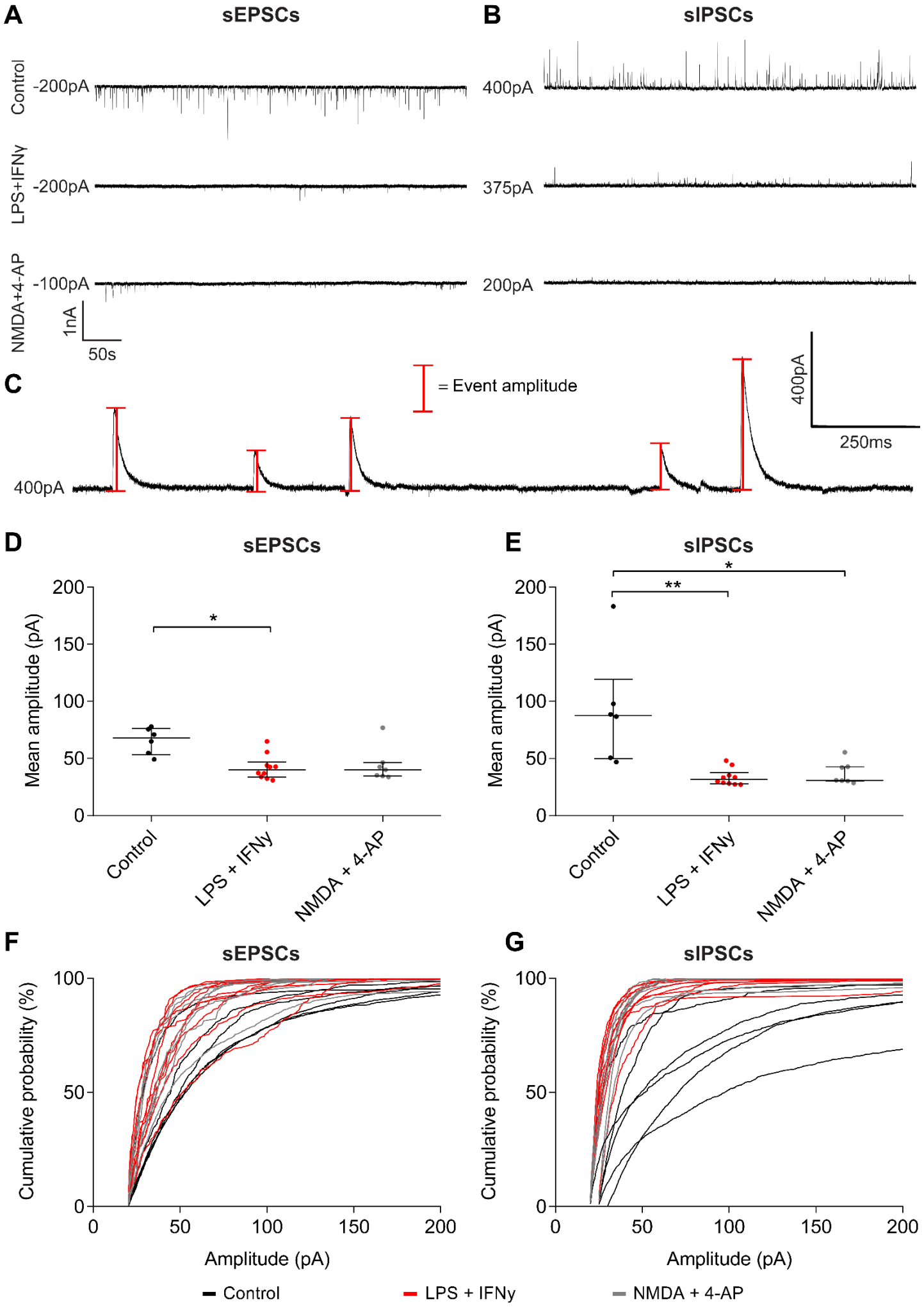
A
sEPSCs
Control
-200pA
LPS+IFNγ
-200pA
NMDA+4-AP
-100pA
1nA
50s
B
sIPSCs
400pA
375pA
200pA
C
= Event amplitude
400pA
400pA
250ms
D
sEPSCs
Mean amplitude (pA)
200
150
100
50
0
*
Control
LPS + IFNγ
NMDA + 4-AP
E
sIPSCs
Mean amplitude (pA)
200
150
100
50
0
**
*
Control
LPS + IFNγ
NMDA + 4-AP
F
sEPSCs
Cumulative probability (%)
100
50
0
0
50
100
150
200
Amplitude (pA)
G
sIPSCs
Cumulative probability (%)
100
50
0
0
50
100
150
200
Amplitude (pA)
Control
LPS + IFNγ
NMDA + 4-AP

Figure 3.2.4. Immune activation via combined LPS+IFNγ treatment for 24 hours reduces the amplitude of both sEPSCs and sIPSCs in cultured hippocampal CA3/CA1 pyramidal neurons. *Hippocampal OBSCs were treated with vehicle, LPS (10 µg/mL) + IFNγ (100 ng/mL) or NMDA (5 µM) + 4-AP (100 µM) in the culture medium for* ***24 hours****. Whole-cell patch-clamp recordings were made from cultured hippocampal CA3/CA1 pyramidal neurons using a cesium-based internal solution. Recordings were performed in voltage-clamp mode to record sPSCs. Neurons were held at -70 mV to record sEPSCs and at +15 mV to record sIPSCs. Example sEPSC (A) and sIPSC (B) traces from each treatment group. (C) Example sIPSC trace showing detection of event amplitude. Population data (with median ± IQR or mean ± SEM) demonstrating mean amplitude of sEPSCs (D) and sIPSCs (E) in control (N=6), LPS+IFNγ (N=10) or NMDA+4-AP (N=7) treatment conditions. The mean amplitude of sEPSCs and sIPSCs in neurons treated with LPS+IFNγ is significantly smaller than control neurons. sIPSC amplitudes in neurons treated with the positive excitotoxic control NMDA+4-AP are decreased compared to controls. Cumulative frequency plots of mean event amplitudes of sEPSCs (F) and sIPSCs (G) in each patched cell show that red (LPS+IFNγ) and grey (NMDA+4-AP) are left-shifted compared to black (control) traces, indicating smaller mean amplitudes. All groups were tested for Gaussian distributions using the Shapiro-Wilk normality test. If any group was found to not have a Gaussian distribution or was too small to test for normality, the data were compared using a Kruskal-Wallis ANOVA test with Dunn's multiple comparison post-hoc test. If all groups were found to have Gaussian distributions, a Brown-Forsythe and Welch ANOVA with Games-Howell's multiple comparison post-hoc test was performed. Values with median ± IQR (nonparametric) or mean ± SEM (parametric); * $p \leq 0.05$; ** $p \leq 0.01$; *** $p \leq 0.001$. Each data point represents a neuron.*

The median sEPSC amplitudes of control, LPS+IFNγ and NMDA+4-AP treated groups were 67.88 pA (IQR 53.37-76.18 pA, N=6), 39.85 pA (IQR 33.54-46.91 pA, N=10) and 40.03 pA (IQR 34.62-46.41 pA, N=7), respectively (Figure 3.2.4D). Only the median sEPSC amplitude of LPS+IFNγ ($p=0.0195$) and not NMDA+4-AP ($p>0.05$) treated cells was significantly smaller than that of controls (Kruskal-Wallis ANOVA with Dunn's multiple comparison post-hoc test), but these two groups' medians were not significantly different from one another ($p>0.05$, Kruskal-Wallis ANOVA with Dunn's multiple comparison post-hoc test).

The median sIPSC amplitude was 87.68 pA (IQR 49.69-119.2 pA, N=6) in control neurons, 31.53 pA (IQR 27.89-37.54 pA, N=10) for LPS+IFNγ treated neurons and 31 pA (IQR 30.31-42.76 pA, N=7) for NMDA+4-AP treated neurons (Figure 3.2.4E). Both the LPS+IFNγ and NMDA+4-AP treated groups had median sIPSC amplitudes that were significantly smaller than that of the control group ($p=0.0023$ and $p=0.0374$ respectively, Kruskal-Wallis ANOVA with Dunn's multiple comparison post-hoc test), but these two groups were not significantly different from each other ($p>0.05$, Kruskal-Wallis ANOVA with Dunn's multiple comparison post-hoc test).

These data are apparent in the example traces of Figure 3.2.4A&B, as well as in the cumulative frequency plots of sEPSC (Figure 3.2.4F) and sIPSC (Figure 3.2.4G) amplitude, where red (LPS+IFNγ) and grey (NMDA+4-AP) are left-shifted compared to black (control) traces indicating smaller amplitudes than controls.

3.3. Immune activation by LPS+IFNγ over short time scales does not affect basic membrane properties.

At this point I had established that immune activation has profound effects on network function from 24 hours until at least 72 hours. Pascual *et al*. (2012) previously showed that washing LPS over an organotypic slice while recording from individual neurons causes a transient rise in spontaneous EPSC frequency at AMPAergic synapses on very short timescales. As such, I wanted to determine if washing-in LPS+IFNγ during an electrophysiological recording would change the basic membrane properties of cultured hippocampal CA3/CA1 neurons on short time scales (~1 hour). To do this, I made whole-cell voltage- and current-clamp recordings from CA3/CA1 pyramidal neurons in hippocampal OBSCs. After patching a cell, I established a baseline recording for 15 minutes and then, whilst recording the electrical activity from neurons, I washed LPS (10 μg/mL) + IFNγ (100 ng/mL) over the slice in circulating aCSF (Figure 3.3.1A) for 45 minutes. Every five minutes for 60 minutes, I applied voltage- and current-steps to the cell, as well as recorded voltage output from the cell whilst in current clamp mode.

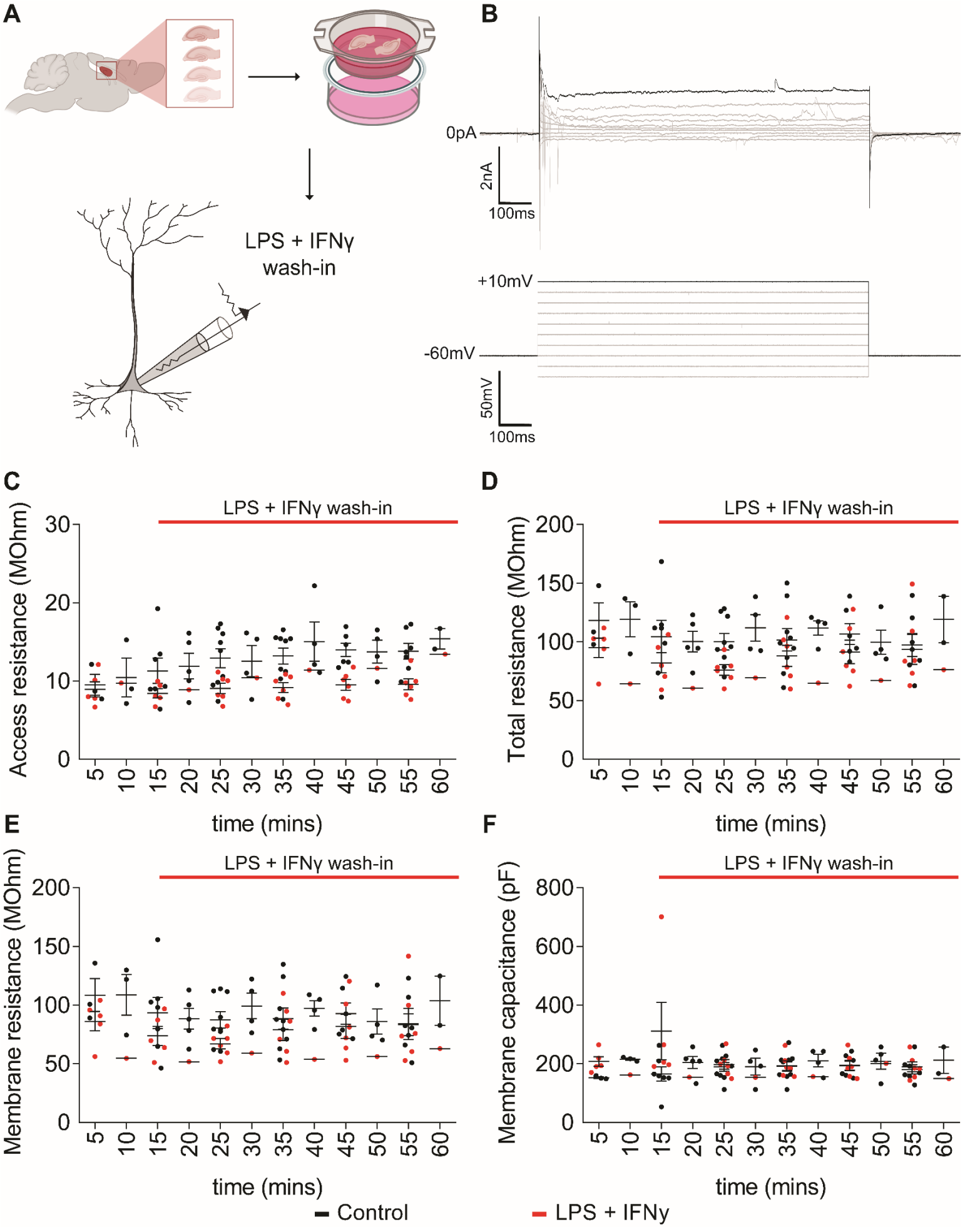
A
LPS + IFNγ
wash-in
B
0pA
2nA
100ms
+10mV
-60mV
50mV
100ms
C
LPS + IFNγ wash-in
Access resistance (MOhm)
time (mins)
D
LPS + IFNγ wash-in
Total resistance (MOhm)
time (mins)
E
LPS + IFNγ wash-in
Membrane resistance (MOhm)
time (mins)
F
LPS + IFNγ wash-in
Membrane capacitance (pF)
time (mins)
Control
LPS + IFNγ

Figure 3.3.1. Immune activation over short time scales via wash-in of LPS+IFNγ does not cause changes to basic membrane properties of cultured hippocampal CA3/CA1 pyramidal neurons. *(A) Schematic diagram of experimental set-up. Whole-cell voltage- and current-clamp recordings were made from CA3/CA1 pyramidal neurons in hippocampal OBSCs. Whilst recording the electrical activity from neurons, LPS (10 µg/mL) + IFNγ (100 ng/mL) were washed over the slice in circulating aCSF. Every five minutes, voltage-steps and current-steps were applied to the cell, as well as recording voltage output from the cell whilst in current-clamp mode. (B) Example trace showing voltage steps applied to a pyramidal neuron (lower panel) and the current output (upper panel) as a result of these applied voltage steps. Population data (with means ± SEM or median ± IQR) showing no change in access resistance (C), total resistance (D) membrane resistance (E) or membrane capacitance (F) from baseline when LPS+IFNγ is washed over the slice for 45 minutes. To compare population data, a baseline data set was calculated by grouping population data readings from 0-15 minutes for each cell in control and LPS+IFNγ groups respectively. Then, a wash-in response data set was compiled by grouping population data readings from 30-60 minutes (allowing time for LPS+IFNγ to arrive at the slice) for each cell. These baseline and wash-in averages were tested for Gaussian distributions using the Shapiro-Wilk normality test. If any group was found to not have a Gaussian distribution or was too small to test for normality (nonparametric), the data were compared using an unpaired Mann Whitney-U test. If all groups were found to have Gaussian distributions (parametric), an unpaired t-test with Welch's correction was performed. Values with mean ± SEM (parametric) or median ± IQR (nonparametric); * $p \leq 0.05$; ** $p \leq 0.01$; *** $p \leq 0.001$. Each data point represents a single patched neuron.*

As before, R_a was measured to assess the quality of each patch and therefore of the data that was collected (Figure 3.3.1C) and cells with R_a above 30 MΩ were excluded. I grouped the mean R_a at each time point for the control and LPS+IFNγ groups. Thus, the grouped mean R_a for control neurons was 12.90 MΩ (SEM ±0.6111 MΩ) and that of LPS+IFNγ treated neurons was 10.22 MΩ (SEM ±0.4810 MΩ). These groups were significantly different from one another (p=0.0031), Unpaired t-test with Welch's correction). This introduces some issues for further comparisons, but since both groups had R_a below 30 MΩ for the duration of the experiment, the results were considered reliable.

To compare data from groups in these experiments I first grouped values of each recorded parameter at each of the first three time points (0-15 minutes) for each treatment group, hence, a baseline data set consisted of three values, representing readings taken during the first 15 minutes of recording. I now had a baseline data set for the control and the LPS+IFNγ wash-in group, though the latter group had not yet been exposed to LPS+IFNγ and hence could be used as a baseline to which I could compare data collected during the period which LPS+IFNγ were washed-in. I then allowed 15 minutes for LPS+IFNγ (or vehicle in the case of controls) to reach the slice through the pump system (15-30 minutes). I grouped data values

collected between 30 and 60 minutes to make a 'wash-in' data set, consisting of seven values, for each treatment group. I then compared each treatment group's 'wash-in' data set to its relevant baseline data set, using statistical tests relevant to the non/parametric status of the data sets.

The basic properties of a neuron are the fundamental modulators of neuronal signaling. To calculate these data, I performed a series of voltage steps which increased the holding voltage of the neuron while recording the current response from the cell (Figure 3.3.1B). Analysis of this current output provides the necessary/reported data. The mean baseline total resistance (R_T) value for control cells was 113.9 MΩ (SEM ±4.710 MΩ) and the mean wash-in R_T was 106.9 MΩ (SEM ±2.969 MΩ) (Figure 3.3.1D). These data sets were not significantly different from one another (Unpaired t-test with Welch's correction, $p>0.05$). The mean R_T's for the baseline and wash-in of the LPS+IFNγ group were 80.50 MΩ (SEM ±8.924 MΩ) and 78.70 MΩ (SEM ±4.588 MΩ), respectively, and these were not significantly different from one another either (Unpaired t-test with Welch's correction, $p>0.05$) (Figure 3.3.1D). The median baseline and wash-in membrane resistances for the control groups were 108.5 MΩ (IQR 93.19-108.7 MΩ) and 92.78 MΩ (IQR 86.05-99.22 MΩ) respectively, and these were not significantly different from one another (Mann Whitney-U test, $p>0.05$) (Figure 3.3.1E). For the LPS+IFNγ groups, the mean baseline and wash-in values were 71.49 MΩ (SEM ±9.169) and 68.06 MΩ (SEM ±4.924) respectively, and these too, were not significantly different from one another (Unpaired t-test with Welch's correction, $p>0.05$) (Figure 3.3.1E).

Next I examined the membrane capacitance to see if acute LPS+IFNγ exposure caused any changes. The mean baseline and wash-in capacitances for the control groups were 177.9 pF (SEM ±19.28 pF) and 197.9 pF (SEM ±4.678 pF) respectively, and these were not significantly different from one another (Unpaired t-test with Welch's correction, $p>0.05$) (Figure 3.3.1F). In the LPS+IFNγ treated groups, the mean baseline and wash-in capacitances for the control groups were 227.1 pF (SEM ±44.12 pF) and 176.6 pF (SEM ±8.506 pF) respectively. There was no significant difference between the baseline and wash-in group (Unpaired t-test with Welch's correction, $p>0.05$) (Figure 3.3.1F).

Having found no change to basic membrane properties of pyramidal neurons during acute immune activation, I next investigated if there was any effect on the resting membrane potential, action potential threshold or current threshold density in neurons exposed to LPS+IFNγ acutely.

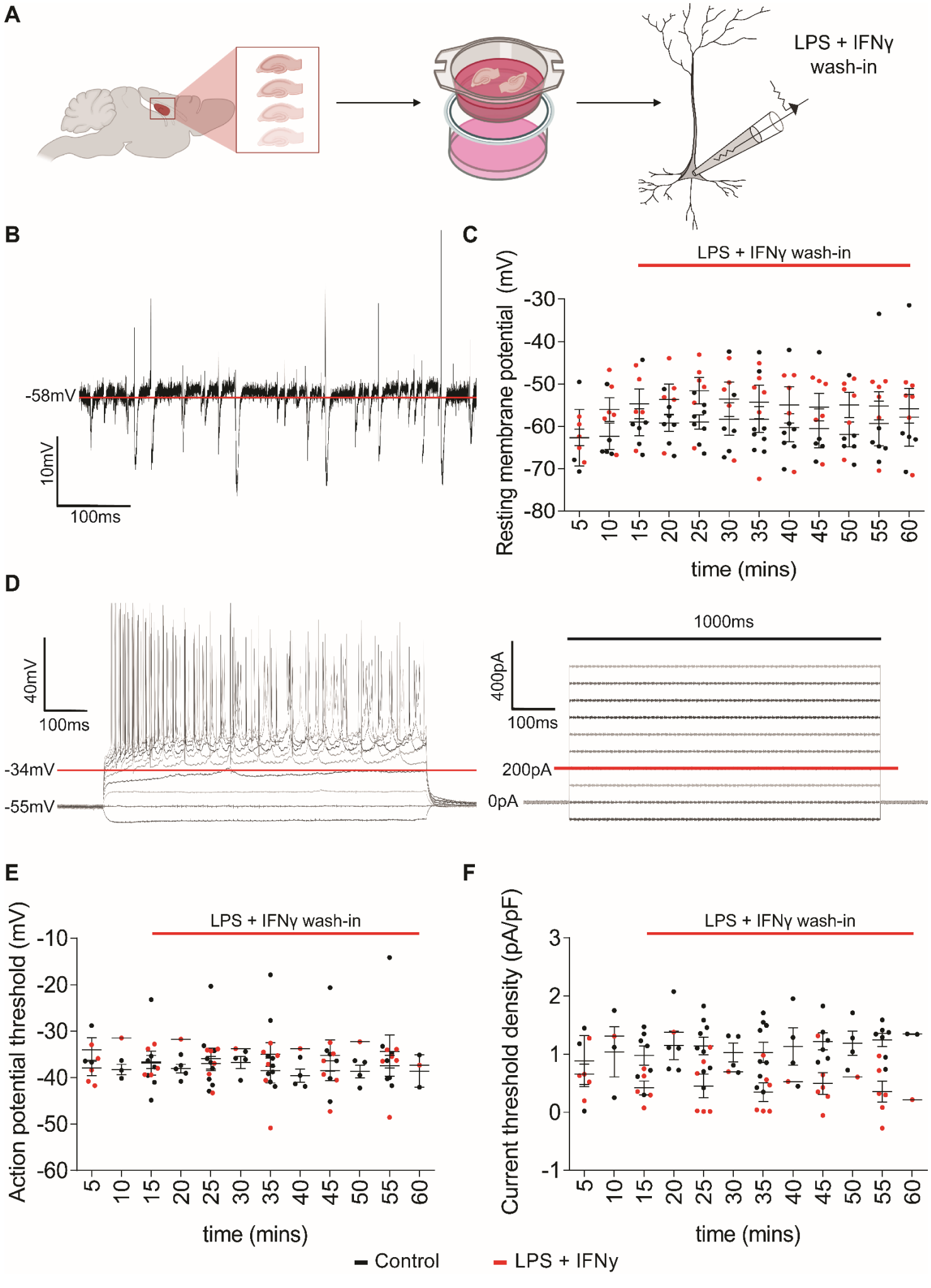
A
LPS + IFNγ
wash-in
B
-58mV
10mV
100ms
C
LPS + IFNγ wash-in
Resting membrane potential (mV)
-30
-40
-50
-60
-70
-80
5
10
15
20
25
30
35
40
45
50
55
60
time (mins)
D
40mV
100ms
-34mV
-55mV
1000ms
400pA
100ms
200pA
0pA
E
LPS + IFNγ wash-in
Action potential threshold (mV)
-10
-20
-30
-40
-50
-60
time (mins)
F
LPS + IFNγ wash-in
Current threshold density (pA/pF)
3
2
1
0
-1
time (mins)
Control
LPS + IFNγ

Figure 3.3.2. Immune activation over short time scales via wash-in of LPS+IFNγ does not cause changes to resting membrane potential, action potential threshold or current threshold density of cultured hippocampal CA3/CA1 pyramidal neurons. *(A) Schematic diagram of experimental set-up. Whole-cell voltage- and current-clamp recordings were made from CA3/CA1 pyramidal neurons in hippocampal OBSCs. Whilst recording the electrical activity from neurons, LPS (10 µg/mL) + IFNγ (100 ng/mL) were washed over the slice in circulating aCSF. Every five minutes, voltage-steps and current-steps were applied to the cell, as well as recording voltage output from the cell whilst in current-clamp mode. (B) Example trace showing calculation of the resting membrane potential of a neuron. (C) Population data showing resting membrane potential of patched cells which had regular aCSF (control) or aCSF supplemented with LPS+IFNγ washed over the slice for 45 minutes during recordings. (D) Example current clamp recording showing increasing current steps (right panel) applied to a patched cell until the cell produced an AP (left panel, first action potential indicated by red bar). (E) Population data showing AP threshold of patched cells which had regular aCSF (control) or aCSF supplemented with LPS+IFNγ washed over the slice for 45 minutes during recordings. (F) Population data showing current threshold density of recorded neurons. To compare population data, a baseline data set was calculated by grouping population data readings from 0-15 minutes for each cell in control and LPS+IFNγ groups respectively. Then, a wash-in response data set was compiled by grouping population data readings from 30-60 minutes (allowing time for LPS+IFNγ to arrive at the slice) for each cell. These baseline and wash-in averages were tested for Gaussian distributions using the Shapiro-Wilk normality test. If any group was found to not have a Gaussian distribution or was too small to test for normality (nonparametric), the data were compared using an unpaired Mann Whitney-U test. If all groups were found to have Gaussian distributions (parametric), an unpaired t-test with Welch's correction was performed. Values with mean ± SEM (parametric) or median ± IQR (nonparametric); * $p \leq 0.05$; ** $p \leq 0.01$; *** $p \leq 0.001$. Each data point represents a single patched neuron.*

The resting membrane potential (V_m) of a neuron is a measurement of the voltage potential across the membrane. When this basic property is altered, the excitability of the neuron could change. For example, if V_m becomes more positive, the cell is closer to its threshold potential, making it more likely to fire (*i.e.* more excitable). The mean V_m's for the baseline and wash-in control groups were -61.36 mV (SEM ±1.165 mV) and -59.53 mV (SEM ±0.5531 mV) respectively, and these did not differ significantly (Unpaired t-test with Welch's correction, p=0.2512) (Figure 3.3.2B). The baseline and wash-in V_m's for the LPS+IFNγ group were -57.80 mV (SEM ±2.457 mV) and -54.90 mV (SEM ±0.2841 mV) respectively. These means were not significantly different from one another in an unpaired t-test with Welch's correction (p>0.05) (Figure 3.3.2C).

The AP threshold is the voltage at which a neuron will 'spike' or 'fire' and action potential. This is one of a number of measures of the intrinsic excitability of a neuron. To calculate the spike threshold I performed a series of current injection steps; these increased the membrane potential until an AP was produced. The AP threshold was calculated as the

voltage at which the first AP was generated (Figure 3.3.2D). The mean AP thresholds for the control baseline and wash-in groups were -36.38 mV (SEM ±1.275 mV) and -35.58 mV (SEM ±0.8493 mV) respectively, and these did not differ significantly from each other (Unpaired t-test with Welch's correction, p=0.6315) (Figure 3.3.2E). The mean baseline and wash-in AP thresholds for the LPS+IFNγ exposed group were -35.37 mV (SEM ±1.973 mV) and -36.04 mV (SEM ±1.004 mV), respectively. These, too, did not differ significantly from each other (Unpaired t-test with Welch's correction, p>0.05) (Figure 3.3.2E).

Current threshold density (CTD) is the amount of current that a cell requires to fire its first AP normalized by the capacitance of the cell. Thus, this measure accounts for the size of the neuron and is a more refined way to measure excitability. The mean CTDs for the control baseline and wash-in groups were 0.9663 pA/pF (SEM ±0.04594 pA/pF) and 1.171 pA/pF (SEM ±0.04333 pA/pF) respectively, and these were significantly different from one another, with the wash-in group having a higher measured CTD (Unpaired t-test with Welch's correction, p=0.0194, not shown on figure) (Figure 3.3.2F) suggesting a change in the CTD of control neurons over the duration of the experiment. The mean CTDs for the LPS+IFNγ baseline and wash-in groups were 0.7947 pA/pF (SEM ±0.2656 pA/pF) and 0.4639 pA/pF (SEM ±0.06318 pA/pF) respectively, but these were not significantly different from each another (Unpaired t-test with Welch's correction, p>0.05) (Figure 3.3.2F).

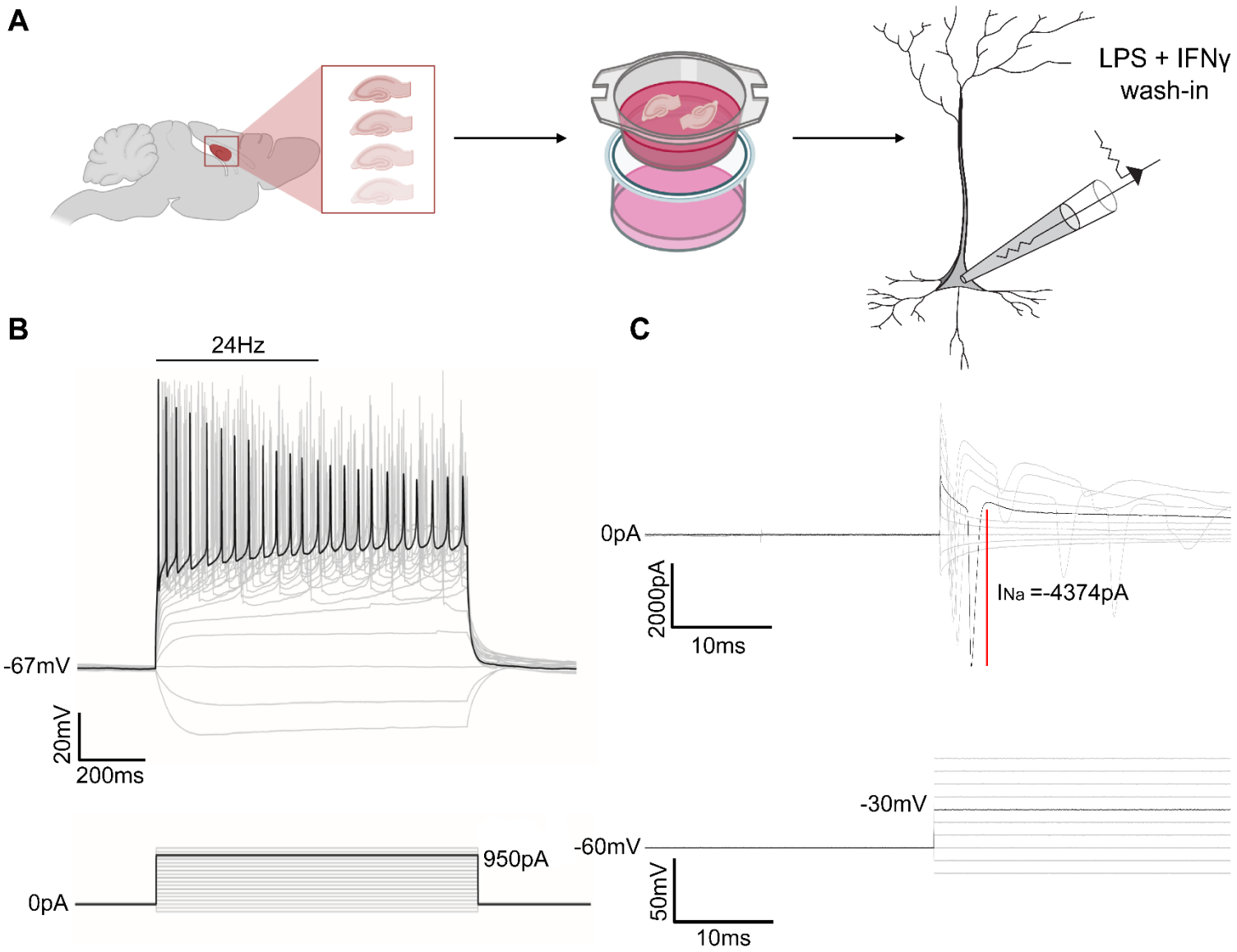
A
LPS + IFNγ
wash-in
B
24Hz
-67mV
20mV
200ms
0pA
950pA
C
0pA
2000pA
10ms
INa =-4374pA
-30mV
-60mV
50mV
10ms
D
LPS + IFNγ wash-in
Absolute max spike rate (Hz)
300
200
100
0
5
10
15
20
25
30
35
40
45
50
55
60
time (mins)
E
LPS + IFNγ wash-in
Maximum sodium current (pA)
0
-5000
-10000
5
10
15
20
25
30
35
40
45
50
55
60
time (mins)
Control
LPS + IFNγ

Figure 3.3.3. Immune activation over short time scales via wash-in of LPS+IFNγ does not cause changes to absolute maximum spike rate or maximum sodium current of cultured hippocampal CA3/CA1 pyramidal neurons. *(A) Schematic diagram of experimental set-up. Whole-cell voltage- and current-clamp recordings were made from CA3/CA1 pyramidal neurons in hippocampal OBSCs. Whilst recording the electrical activity from neurons, LPS (10 µg/mL) + IFNγ (100 ng/mL) were washed over the slice in circulating aCSF. Every five minutes, voltage-steps and current-steps were applied to the cell, as well as recording voltage output from the cell whilst in current-clamp mode. (B) Example current-clamp recording output (upper panel) after voltage steps (lower panel) are applied to a pyramidal neuron to achieve the fastest possible spiking rate from the recorded neuron (Traces provided by Dr Hayley Tomes). (C) Example trace showing calculation of maximum sodium current (upper panel) through the membrane after applied voltage pulses (lower panel). Population data (with means ± SEM or median ± IQR) showing no change in absolute maximum spiking rate (D) or maximum sodium current (E) when LPS+IFNγ is washed over the slice for 45 minutes. To compare population data, a baseline data set was calculated by grouping population data readings from 0-15 minutes for each cell in control and LPS+IFNγ groups respectively. Then, a wash-in response data set was compiled by grouping population data readings from 30-60 minutes (allowing time for LPS+IFNγ to arrive at the slice) for each cell. These baseline and wash-in averages were tested for Gaussian distributions using the Shapiro-Wilk normality test. If any group was found to not have a Gaussian distribution or was too small to test for normality (nonparametric), the data were compared using an unpaired Mann Whitney-U test. If all groups were found to have Gaussian distributions (parametric), an unpaired t-test with Welch's correction was performed. Values with mean ± SEM (parametric) or median ± IQR (nonparametric); * p ≤ 0.05; ** p ≤ 0.01; *** p ≤ 0.001. Each data point represents a single patched neuron.*

Finally, I wanted to examine more measures of intrinsic neuronal excitability, namely absolute maximum spiking rate (ABS Max SR) and maximum sodium current. The absolute maximum spike rate was calculated as the smallest time interval between two spikes. This is a theoretical measure of how fast a neuron can send signals, since this spike rate is unsustainable physiologically. The mean ABS Max SR's for the control baseline and wash-in groups were 96.26 Hz (SEM ±5.777 Hz) (though this baseline group did contain a large outlier which may have skewed downstream analyses) and 65.77 Hz (SEM ±2.159 Hz) respectively, and these were significantly different from one another (Unpaired t-test with Welch's correction, p=0.0224, not shown in figure) (Figure 3.3.3D) suggesting a natural degradation in the cells' ability to produce APs over time. In the LPS+IFNγ exposed group, the mean ABS Max SR's for the baseline and wash-in groups were 71.39Hz (SEM ±8.007Hz) and 58.09Hz (SEM ±6.680Hz) respectively, and despite this large decrease from baseline to wash-in, these groups were not significantly different from one another (Unpaired t-test with Welch's correction, p>0.05) (Figure 3.3.3D).

Changes in a neuron's membrane voltage are governed by ion flow across its membrane. Na^+ flux through voltage-gated Na^+ channels is the main driver of membrane depolarization, and this in turn is what constitutes an AP in the neuron. Figure 3.3.3C shows an example trace recorded in voltage-clamp mode which demonstrates the Na^+ current generated when voltage-gated Na^+ channels are opened following a voltage step to a more positive membrane potential. The mean absolute maximum voltage-gated Na^+ currents for the control baseline and wash-in groups were -8397 pA (SEM ±576.1 pA) and -5981 pA (SEM ±137.7 pA) respectively, the latter being larger (or less negative) than the former(Unpaired t-test with Welch's correction, p=0.0457, not shown in figure) (Figure 3.3.3E). The mean absolute maximum voltage-gated Na^+ currents for the LPS+IFNγ baseline and wash-in groups were -9920 pA (SEM ±165.2 pA) and -8915 pA (SEM ±258.8 pA), the latter being larger (or less negative) than the former (Unpaired t-test with Welch's correction, p=0.0114), indicating that acute immune activation is affecting the absolute maximum voltage-gated Na^+ currents in a relatively mild way; thus it could, under more drastic conditions, affect membrane depolarization (Figure 3.3.3E). These results, combined with those describing absolute maximum spiking rate (Figure 3.3.3D), tentatively suggest that the control neurons were losing the ability to produce APs over time, but that the LPS+IFNγ wash-in treated neurons maintained this ability.

Brought together, these results showed how an acute (minutes to one hour) inflammatory stimulus in the form of LPS+IFNγ wash-in causes only minor, insignificant alterations to the intrinsic excitability of neurons.

3.4. Immune activation for 24 or 72 hours causes major dysfunction in neuronal networks

Through this body of work I have shown that treatment with LPS alone or with combined LPS+IFNγ induces a strong pro-inflammatory cytokine response (Figures 3.1.1&3.1.7). On short time scales of immune activation by LPS+IFNγ there is no discernable alteration to the basic membrane properties or excitability of pyramidal neurons (Figures 3.3.1-3.3.3). After 24 hours of exposure to LPS+IFNγ, the properties of cultured hippocampal networks are affected, with functionality on the whole becoming dampened (Figure 3.2.1-3.2.4). A very

similar effect is seen at 72 hours of immune activation (Figures 3.1.2-3.1.5); however this network effect is not echoed in a change in apoptotic or necrotic cell death in organotypic slices (Figure 3.1.6).

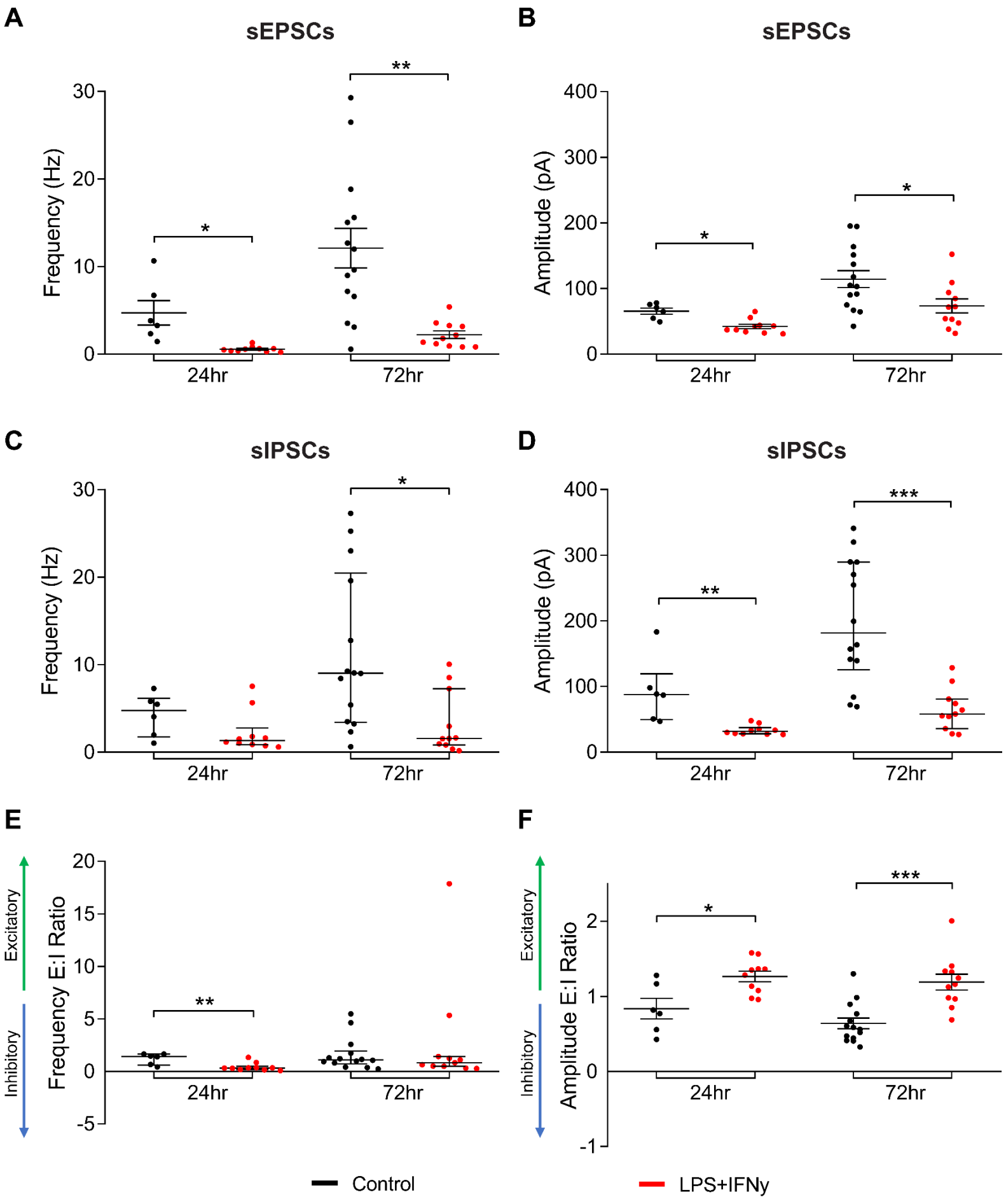
A
sEPSCs
Frequency (Hz)
30
20
10
0
*
**
24hr
72hr
B
sEPSCs
Amplitude (pA)
400
300
200
100
0
*
*
24hr
72hr
C
sIPSCs
Frequency (Hz)
30
20
10
0
*
24hr
72hr
D
sIPSCs
Amplitude (pA)
400
300
200
100
0
**
***
24hr
72hr
E
Excitatory
Inhibitory
Frequency E:I Ratio
20
15
10
5
0
-5
**
24hr
72hr
F
Excitatory
Inhibitory
Amplitude E:I Ratio
2
1
0
-1
*
***
24hr
72hr
Control
LPS+IFNy

Figure 3.4.1. Immune activation via combination treatment of LPS+IFNγ for 24 or 72 hours causes major disruptions to the frequency and amplitude of sEPSCs and sIPSCs in cultured hippocampal CA3/CA1 pyramidal neurons. *Population data (with means ± SEM or median ± IQR) showing sEPSC (A) and sIPSC (C) frequency after 24- and 72-hour inflammatory treatments. sEPSC (B) and sIPSC (D) amplitude after 24- and 72-hour inflammatory treatments. (E) Ratio of excitatory:inhibitory event* ***frequency*** *after 24- and 72-hour treatments. (F) Ratio of excitatory:inhibitory event* ***amplitude*** *after 24- and 72-hour treatments. All groups were tested for Gaussian distributions using the Shapiro-Wilk normality test. If any group was found to not have a Gaussian distribution or was too small to test for normality (nonparametric), the data were compared using an unpaired Mann Whitney-U test. If all groups were found to have Gaussian distributions (parametric), an unpaired t-test with Welch's correction was performed. Values with mean ± SEM (parametric data) or median ± IQR (nonparametric data); * p ≤ 0.05; ** p ≤ 0.01; *** p ≤ 0.001. Each data point represents a neuron.*

In Figure 3.4.1 I show that the effects of immune activation at 24 hours and 72 hours are indeed quite similar. As I have mentioned previously, the frequency of sPSCs provides information about the number of functional synapses in the network. Figure 3.4.1A shows the frequencies of sEPSCs for control and LPS+IFNγ treated groups after 24 and 72 hours. In the 24 hour treated group, the mean sEPSC frequencies of control and LPS+IFNγ groups were significantly different from one another, with the LPS+IFNγ treated group having a smaller mean sEPSC frequency than the control group. Further, the mean sEPSC frequencies in the 72 hour treated LPS+IFNγ group was also significantly smaller than that of the control group. In Figure 3.4.1C I show the sIPSC frequencies for control and LPS+IFNγ groups at 24 and 72 hours. After 24 hours of treatment, the sIPSC frequency of LPS+IFNγ treated neurons was not significantly different from that of controls. In contrast, LPS+IFNγ treated group had a significantly lower sIPSC frequency than that of the control group at 72 hours.

Figure 3.4.1E shows the ratio of excitatory to inhibitory (E:I) event frequencies. An increase or decrease in this ratio is a proxy for a shift to a more or less excitable network, respectively. The median ratio of E:I frequencies in the 24 hour treated control and LPS+IFNγ groups were 1.435 (IQR 0.6014-1.655) and 0.3326 (IQR 0.1661-0.4926) respectively, and these groups were significantly different from one another (Mann Whitney-U test, p=0.0030) (Figure 3.4.1E), with the ratio of E:I frequencies of the LPS+IFNγ treated group being significantly lower than that of the control group. In the 72 hour treated group, the median ratio of E:I frequencies in the control and LPS+IFNγ groups were 1.1111 (IQR 0.7186-1.946) and 0.8320 (IQR 0.4945-1.416) respectively, but these groups were not significantly different

from one another (Mann Whitney-U test, $p>0.05$) (Figure 3.4.1E). It seems that based on the E:I frequency ratios, the effect of LPS+IFNγ is more prominent after just 24 hours of exposure and this seems to wane at 72 hours of immune activation.

Examining the amplitude of excitatory sPSCs in Figure 3.4.1B, I found that, at 24 hours, the amplitudes in LPS+IFNγ treated neurons were significantly smaller than those of controls. Similarly, at 72 hours, the control and LPS+IFNγ treated groups had mean sEPSC amplitudes that were significantly different from each other, with the LPS+IFNγ sEPSC amplitudes being smaller than controls. Figure 3.4.1D shows the sIPSC event amplitudes for the control and LPS+IFNγ treated neurons at 24 and 72 hours. The median sIPSC event amplitudes at 24 hours in the LPS+IFNγ treated group were significantly smaller than those of controls. I found a similar result at 72 hours of treatment, where the sIPSC amplitudes of LPS+IFNγ treated neurons were significantly smaller than those of controls.

Finally, in Figure 3.4.1F I show the ratio of E:I event amplitudes for the control and LPS+IFNγ treated neurons at 24 and 72 hours. At 24 hours, there is a significant difference between the E:I amplitude ratio of the control and LPS+IFNγ treated groups (Unpaired t-test with Welch's correction, $p=0.0243$) where the mean E:I amplitude ratios of the control and LPS+IFNγ groups were 0.8367 (SEM ±0.1365) and 1.266 (SEM ±0.07033) respectively. Pivoting to the 72 hour treatment, I found that the control and LPS+IFNγ treated groups were also significantly different after this extended immune activation (Unpaired t-test with Welch's correction, $p=0.0004$). Here, the mean E:I amplitude ratios of the control and LPS+IFNγ groups were 0.6394 (SEM ±0.07155) and 1.190 (SEM ±0.1054), respectively. At both time points the mean E:I amplitude ratio of the LPS+IFNγ treated group was larger than that of the control group.

It should be noted that the frequency and amplitude of both sEPSCs and sIPSCs trend upwards from 24 hours to 72 hours of immune activation in both control and immune activated groups; demonstrating the importance of control groups at both time points. This is likely a result of the enhanced synaptic connectivity that occurs in OBSCs, which are cultured for extended periods.

Chapter 4

Discussion, conclusions and recommendations

4.1 Neuroinflammation and epilepsy have a complex relationship

Since the first descriptions of Rasmussen's encephalitis (a chronic inflammatory disorder of the CNS, of which seizures are a common symptom) in the late 1950's (Varadkar *et al*., 2014), the immune system has been implicated in at least some forms of epilepsy. Later developments showing the drastic effects of inflammatory molecules and cytokines on seizure threshold and development in multiple epilepsy models have served to confirm the pathological role of aberrant immune activation. Numerous links between inflammation and excitotoxicity have been proposed, some of which include:

1. the up- and down-regulation of neuronal ion channels and receptors (specifically $GABA_AR$, NMDAR and AMPAR), usually via cytokine action (Terrone *et al*., 2019; Vezzani *et al*., 2019),
2. blockage of neurotransmitter re-uptake (Rana & Musto, 2018; Vezzani *et al*., 2019),
3. changes to the transcriptional activation of genes involved in plasticity (Iori *et al*., 2013; Vezzani *et al*., 2013)
4. aberrant (re)growth of new neurons (Terrone *et al*., 2019)
5. BBB dysfunction (van Vliet *et al*., 2015)
6. nitric oxide-induced changes in glutamate management (Bal-Price & Brown, 2001; Chao *et al*., 1992; Papageorgiou *et al*., 2016), and
7. astrocytic glutamate release via microglial activation (Rana & Musto, 2018), amongst others.

Despite these descriptions, a uniform picture of the inflammatory etiologies of seizures and epilepsy is still lacking. Multiple immune signaling pathways have been implicated in the precipitation of, or fallout from, seizures. This includes the TLR-4 pathway, which is activated by LPS (as described in section 1.8 of the introduction). IFNγ has been suggested as a bolstering cytokine in LPS models of neuroinflammation, since the pathways of these

molecules seem to function synergistically to produce stronger inflammatory effects (as described in section 1.8 of the introduction) than either in their individual capacities. Previous work using these molecules in hippocampal OBSCs has shown that priming with IFNγ can slow neuronal gamma oscillations (effectively dampening network function), which require precise communication between the excitatory and inhibitory arms of a network (Papageorgiou *et al*., 2016), thus functioning as a sensitive proxy for normal network integrity (Ta *et al*., 2019). Other work has shown that acute application of LPS alone was sufficient to cause a rapid and transient rise in the frequency of sEPSCs (Pascual *et al*., 2012), a readout of the overall excitatory function of a network (Duan *et al*., 2018), suggesting that LPS can alter the excitatory:inhibitory balance in a network, possibly predisposing it to seizure-like events. In contrast, Hellstrom *et al*. (2005) showed that chronic exposure of OBSCs to LPS decreases membrane resistance, increases action potential threshold, reduces frequency of action potentials and increases IL-1β-dependent GABAergic tone in CA1 pyramidal neurons; overall suggesting that chronic immune activation tips neuronal networks to a more inhibited, quietened state. Furthermore, a study investigating the effects of co-application of LPS and IFNγ in hippocampal OBSCs, such as has been used in this thesis, showed that such bolstered immune activation results in severe neuronal dysfunction and death via a nitric oxide-mediated mechanism (Papageorgiou *et al*., 2016). They go on to show that LPS+IFNγ treatment abolishes neuronal gamma oscillations, indicating a profound effect of these molecules in combination. As such, there is a lack of consensus around the electrophysiological effects of LPS and IFNγ induced neuroinflammation.

4.2 Neuroinflammation disrupts neuronal networks but does not cause cell death in OBSC

Based on these previous findings, this project sought to explore the question; 'How does bolstered immune activation affect cytokine release, cell survival, neuronal network function and the basic membrane properties of neurons on different time scales?'. This study comprised of the following aims to answer this question:

Aim 1: Characterize the production of cytokines following immune activation over multiple days.

Aim 2: Explore and characterize cell death outcomes of hippocampal organotypic brain slice cultures following chronic immune activation.

Aim 3: Explore the effect of chronic immune activation on network synaptic function.

Aim 4: Investigate the effect of medium-term immune activation on network synaptic function.

Aim 5: Explore the effect of acute immune activation on the basic membrane properties of pyramidal neurons.

In fulfillment of aim 1 I characterized the release of cytokines from slices exposed to normal (LPS only) and bolstered (LPS+IFNγ) immune activation at 24, 48 and 72 hours, showing that my model reflected previous work and was reliably inducing inflammation. For aim 2 I developed an assay to determine cell death via apoptosis and necrosis in hippocampal OBSCs. I then used this assay to quantify cell death after 72 hours of both normal and bolstered immune activation via LPS and LPS+IFNγ treatment, respectively. Unlike previous work (Papageorgiou *et al*., 2016), I did not find any evidence of cell death following these treatments. In fulfillment of aims 3 and 4, I used whole-cell patch-clamping to record excitatory and inhibitory sPSCs from neurons that had been exposed to normal or bolstered immune activation in the form of LPS or LPS+IFNγ treatment respectively, for 72 (aim 3) or 24 (aim 4) hours. I found that, at both time points there were significant decreases in the frequency and amplitude of both excitatory and inhibitory sPSCs (Figures 3.1.2-3.1.5 and Figures 3.2.1-3.2.4), suggesting a general dampening of function of the network (fewer spontaneous currents), with a particularly strong decrease in the conductance (amplitude) of inhibitory postsynaptic receptors (Figure 3.4.1). Like others (Papageorgiou *et al*., 2016), I found that application of LPS alone was not able to modulate network activity in the same way as combined LPS and IFNγ treatment. Finally, for aim 5 I investigated the acute effects of LPS+IFNγ administration on the basic membrane properties of pyramidal neurons in hippocampal OBSCs, and found no drastic effects. I discuss below some possible reasons for my contradictory findings as well as what future experiments could elucidate the mechanisms by which bolstered immune activation affects network function and cell survival in hippocampal OBSCs.

4.2.1 LPS+IFNγ treatment reliably induces pro-inflammatory cytokine release

The major findings of this thesis agree with previous work. I observed pro-inflammatory (IL-6 and TNF-α) cytokine release (Figures 3.1.1 and 3.1.7), a hallmark of neuroinflammation, in levels similar to that observed in other studies (Häusler *et al*., 2002; Hellstrom *et al*., 2005; Papageorgiou *et al*., 2016; Zhang *et al*., 2020) following immune stimulation with both LPS and LPS+IFNγ. There was, however, a slight contradiction in my results – in the ELISA performed on culture media collected from OBSCs used for patch-clamping (plated 2 per well), I found that a combination of LPS+IFNγ evoked a stronger TNF-α release than LPS alone (Figure 3.1.1). In contrast, in the ELISA performed on culture media collected from OBSCs used for cell death staining experiments (plated 6 per well) (Figure 3.1.7), it was LPS that seemed to evoke a stronger TNF-α response. While true that the latter slices (6 per well) released a greater concentration of cytokine than the former (2 per well), one would still expect these data sets to mirror one another. It is not completely surprising however, since a similar result was found by Papageorgiou *et al*. (2016). On closer examination, both the data sets' highest and lowest data points do indeed overlap. It is likely then that natural biological variation has caused this would-be anomaly.

It should also be addressed that neither IL-10 nor IL-1β were detectable in my assays, whereas they have been detected by others (Hellstrom *et al*., 2005; Papageorgiou *et al*., 2016; Sun *et al*., 2019). It is likely that the cytokine assays I used were not sensitive enough to detect possibly low but biologically significant quantities of these cytokines, since others in our group have not been able to detect these in various pro-inflammatory studies, either (data not shown). It cannot however be ruled out that there was indeed no or very little release of these cytokines, especially since IL-10 is in fact an anti-inflammatory cytokine, though it is released as a counter to runaway inflammation (Gordon & Martinez, 2010). Despite this, Papageorgiou *et al*. (2016) report in their supplementary material that there was no significant difference in IL-10 release between control OBSCs or those exposed to LPS, LPS+IFNγ or IFNγ. In future, it would be advisable to use more sensitive ELISA reagents in order to detect more subtle changes in cytokine expression, or at least to confirm detection with a positive control.

4.2.2 LPS+IFNγ treatment disrupts hippocampal OBSC neuronal networks after 24 and 72 hour exposures

sPSCs are small electric currents generated by combined AP-dependent and -independent (quantal or single vesicle) release of neurotransmitter at synapses. As such, sPSCs provide a combination of the information gleaned from mPSCs and from actual, spontaneous AP-evoked signals in the network. Measuring sPSCs as a proxy for network function also allows for greater nuance in the understanding of alterations network function than other methods such as recordings of gamma oscillations. In general, changes to sPSC frequency are attributed to presynaptic effects, given that amplitude is unchanged in the same experiment (Beamer *et al*., 2017). Others have noted that the frequency of mPSCs provides insight into the overall function of the network and the number of functional synapses in the network (Duan *et al*., 2018). Since sPSCs include mPSCs and spontaneous AP-evoked currents, we expect that, if events are happening often, then many spontaneous APs are being generated by presynaptic neurons, constituting a busy, functional, and perhaps over-excited network. Likewise, others have also stated that changes to the frequency of events is a reflection of changes to presynaptic inputs (Heshmati *et al*., 2020) and can represent the release probability of individual synapses (Duan *et al*., 2018; Ke *et al*., 2010), though these characteristics are mainly attributable to mPSCs. In addition, the amplitude of the events tells us about the strength of individual synapses and the conductance of post-synaptic receptors.

However, assigning pre- and postsynaptic effects based on frequency and amplitude should be done with caution, especially since in my experiments I found changes to both frequency and amplitude, suggesting a combined pre- and postsynaptic effect or exclusive postsynaptic effect. For example, if synapses are very small, their current amplitudes are too small to be detected, which could lead to a decrease in the measured frequency and a wrongful attribution to presynaptic effects. In another exceptional case, when “silent” synapses which previously lacked AMPAR are unsilenced (by changes in AMPAR expression), one could record increased event frequency and attribute this to a presynaptic change, rather than the rightful postsynaptic change in receptor expression (Queenan *et al*., 2012).

The generalized dampening of network function (reduction in frequency, increase in IEIs and decrease in amplitude of both sEPSCs and sIPSCs) after both 24 and 72 hours of LPS+IFNγ application, but not LPS application, (72 hrs: Figures 3.1.2-3.1.5 and 24 hrs: Figures 3.2.1-3.2.4) that I have observed resembles the reduction in gamma oscillations (Papageorgiou *et al*., 2016; Ta *et al*., 2019) and reduction in AP frequency (Hellstrom et al., 2005) observed by others, though my findings did not resemble the severity reported by Papageorgiou *et al*. (2016). Since there were no changes to the basic membrane properties of neurons between treatment conditions at either 72 or 24 hours of immune stimulation (Figure 3.1.2 and Figure 3.2.1), it is likely that the changes seen in frequency and amplitude of sPSCs were mediated either by 1) a reduction in the generation of spontaneous APs in the OBSCs networks, 2) by changes in the function of synapses, or 3) changes to receptor expression at individual synapses. This latter hypothesis would not be surprising given what is known about the upregulation of AMPA and NMDA receptors and the endocytosis of $GABA_A$ receptors after inflammation (Papageorgiou *et al*., 2016; Stellwagen *et al*., 2005).

The frequency of both excitatory and inhibitory sPSCs at both 24 and 72 hours had decreased in my experiments (reflected in the corresponding increase in IEIs), which suggested to me that there were, overall, fewer functional synapses in the network producing spontaneous APs (and/or that the release probabilities of single vesicles at individual synapses were decreased). Both the frequency and amplitude were altered by immune stimulation in my experiments, signifying the possibility that, in addition to possible presynaptic changes, there was a postsynaptic effect (Beamer *et al*., 2017). Since one of the major functions of microglia is the pruning of synapses when neurons are damaged (Bar & Barak, 2019), it is not unlikely that neurons damaged by increased cytokine release in response to the applied LPS+IFNγ are being pruned by activated microglia and thus reducing the overall number of functional synapses in the network (though studies of synaptic pruning specifically by microglia are necessary to confirm this). Indeed, other work has shown that microglia are often the culprit behind neurodegeneration by phagocytosis after inflammation, specifically via a nitric oxide mechanism (Bal-Price & Brown, 2001; Chao *et al*., 1992), suggesting that microglia could be phagocytosing damaged/dying neurons, removing them

from the network, and thus reducing the overall spontaneous AP-generating capacity and number of functional synaptic connections in the network.

By comparing the ratio of the frequency of excitatory:inhibitory sPSCs, I showed that there is a greater overall reduction in excitatory events at 24 hours of immune activation (Figure 3.4.1) (this same trend is suggested for neurons exposed to immune activation for 72 hours) than inhibitory events. This suggests that, on the whole, excitatory presynaptic neurons are possibly not quite as functional as inhibitory neurons after immune activation, and are being dampened to a greater degree than their inhibitory counterparts. Excitatory neurons are possibly generating fewer spontaneous APs and could be experiencing a reduction in the number of glutamate-packed vesicles being released at each synapse, though more extensive kinetics analysis of the data presented here and future recordings of mPSCs are necessary to confirm this.

Alternatively, it is possible that presynaptic GABAergic interneurons are relatively more active than their glutamatergic counterparts following immune activation. This would imply that the inhibitory tone of the network has increased, such as was observed after chronic LPS stimulation by Hellstrom *et al*. (2005); though the drastic reduction in frequency and amplitude of sIPSCs I observed in LPS+IFNγ treated neurons casts doubt on this hypothesis. Indeed, when examining the amplitude of sPSCs, I found that inhibitory events were reduced in size to a greater degree than excitatory ones, resulting in an increased excitatory:inhibitory ratio (Figure 3.4.1). This suggests that the conductance of inhibitory postsynaptic receptors was affected more strongly than that of excitatory postsynaptic receptors. A possible cause might be changes in AMPA and $GABA_A$ receptor expression following exposure to the TNF-α released from activated microglia – when this happens, Ca^{2+}-permeable AMPA receptor expression is upregulated (Papageorgiou *et al*., 2016), and simultaneously, inhibitory $GABA_A$ receptors are endocytosed (Stellwagen *et al*., 2005), resulting in neurons that respond more strongly to excitatory stimuli, and less strongly to inhibitory stimuli. Otherwise, it is also possible that GABAergic interneurons are actually less active in the network following immune activation. Future experiments could attempt to unite previous work showing changes to receptor expression and work such as my own which shows the electrical

implications of inflammation. Future work could also examine whether the intrinsic properties of either glutamatergic or GABAergic neurons are altered by immune stimulation at both 24 and 72 hours, which could explain the disparity seen between effects on excitatory event frequency and inhibitory event amplitude.

Finally, it should be noted that the positive control for excitotoxicity, NMDA+4-AP, only contained two data points in the 72 hour patch clamping experiments due to difficulty in collecting data from cells that were quite heavily damaged by this treatment. This factor severely limits the legitimacy of this control group in these experiments.

4.2.3 LPS+IFNγ treatment does not cause apoptotic or necrotic cell death in hippocampal OBSC

In my cell death studies, I did not observe either apoptotic or necrotic cell death (Figure 3.1.6) as was reported in mixed neuronal cultures (Lehnardt *et al*., 2003) and rat hippocampal OBSCs (Papageorgiou *et al*., 2016). It is possible that the degree of neurodegeneration exhibited in my model was limited to synaptic pruning by microglia, rather than full-blown neuronal death and microglial phagocytosis, which could explain why I could still record sPSC data from neurons exposed to LPS+IFNγ for multiple days and why the network function was dampened but not lost altogether. I exposed OBSCs to immune stimulation at DIV05, whereas Papageorgiou *et al*. (2016) exposed their slices to LPS+IFNγ at DIV07-DIV10, although unlikely, it is possible that this could explain the difference in cell death results between their work and mine, especially given that (Czapiga & Colton, 1999) have demonstrated the differing activation states of microglia at early and later stages of brain slice culture.

Another explanation is that Papageorgiou *et al*. (2016) employed LDH assays as a method of cell death detection. This assay functions by detecting lactate dehydrogenase (LDH) released from lysed cells in the cell culture medium. LDH assays were attempted, without success, by others in our laboratory (data not shown), which prompted the development of the assay used in this thesis. I also attempted Alamar Blue cell viability assays, which detect living and growing cells, without success (data not shown). Furthermore, Papageorgiou *et al*. (2016) employed rat OBSCs, and I used mouse. It is possible that very slight differences

in the immune function of these rodents caused the difference in results, though it is unlikely. Performing more quality control experiments on a variety of cell death assays would serve to clarify my contradictory results.

4.2.4 LPS+IFNγ treatment does not change the basic membrane properties of cultured hippocampal CA3/CA1 pyramidal neurons on short time scales

Finally, when I examined the acute effects of bolstered immune activation on the basic membrane properties of pyramidal neurons (Figures 3.3.1-3.3.4), I found no changes between control and LPS+IFNγ-exposed neurons, similar to the basic membrane property results found after 24 (Figure 3.2.1) and 72 hours (Figure 3.1.2) of immune stimulation. This suggests that the network level changes I observed were attributable mainly to spontaneous AP generation or changes in postsynaptic receptor expression. Indeed, previous work by Pascual *et al*. (2012) showed that acute application of LPS alone to acute brain slices was sufficient to cause a rapid and transient rise in the frequency of sEPSCs which was mediated specifically by changes in AMPAergic transmission. Taken together, this suggests that changes to receptor expression following stimulation of microglia is possibly the main culprit of network-function modulation in inflammatory contexts, as I have hypothesized for the changes observed in network function at 24 and 72 hours of immune stimulation. Studies investigating the changes to AMPAR expression paired with microglial depletion (using the microglial inhibiting drug minocycline) in this bolstered immune stimulation model could clarify the true cause of network disruption.

It should be noted that the CTD, ABS Max SR and max Na^+ current of 'wash-in' control neurons were significantly different from their baseline counterparts. This is concerning, since it suggests that these properties evolve over time during a single recording, casting potential doubt over the LPS+IFNγ experimental results. It is possible that, due to the extended duration of patch-clamping in these experiments, cell health and/or patch-quality decreased during the course of recordings. Future experiments should be designed such that long recording times are avoided.

4.3 Limitations

There are limitations to this study which must be addressed. I used an *in situ* model of neuroinflammation, which cannot fully model inflammatory processes as they would occur *in vivo.* Furthermore, the study was performed using mice, which although having similar immune systems to humans, cannot model human disease in totality, hence the work presented here can only serve as a precursor to studies which must be confirmed in human tissue. Given the disparity between my cell death results and those of previous studies, a more nuanced investigation of different assays of cell death should be performed to optimize detection of neurodegeneration after inflammatory insult. In addition, my work failed to account for the varying activation states of microglia at different DIV of OBSCs (as demonstrated by Czapiga & Colton (1999)), possibly skewing results and not fully modelling a normal response to inflammation. Future work should address the stated limitations by performing these experiments on OBSCs at different DIV to determine the effect of variously activated microglia. These should be paired with studies of microglial activation state via microglial staining with the activation markers Iba1 or NFIL-6. My studies of spontaneous postsynaptic currents, while offering a more nuanced understanding of network changes after inflammation than gamma oscillation recordings, are not paired with recordings of mPSCs and do not include a full analysis of the kinetics (rise time, decay time, event half width, etc.); thus I do not present a full picture of what is happening at individual synapses after immune activation. This can, however, be rectified with more extensive analysis of data already collected and future experiments where TTX is washed in after sPSC recordings to record mPSCs. In addition, it could be argued that 72 hours does not constitute chronic immune activation, especially when compared to the time course of auto-immune disorders, where patients can experience immune overstimulation for multiple years. Thus, future studies should try to model more chronic immune stimulation such as was performed by Hellstrom *et al*. (2005) (7 days of immune stimulation in OBSCs).

Importantly, this thesis sought to investigate the effect of neuroinflammation on network function and basic membrane properties because of the established links between inflammation and seizure generation/epilepsy. My work has not shown pro-convulsant effects

of inflammation. Although I demonstrated a broad reduction in synaptic activity occurring in response to inflammation, a consistent excitatory or inhibitory shift in synaptic ratios was not demonstrated. In addition, my experiments did not directly investigate changes to seizure susceptibility following inflammation. To rectify this, 0 Mg^{2+} challenges could be performed on immune activated slices to determine their seizure susceptibility and would provide crucial insight linking the inflammatory process to seizure generation. Perhaps a more nuanced model would also survey the likelihood of developing seizures after immune stimulation *in vivo,* using intraperitoneal LPS+IFNγ injections (such as has been performed by others (Kovács *et al*., 2011)). Despite these limitations, this body of work takes important first-steps in linking inflammatory mechanisms to electrophysiological outcomes through the sPSC experiments, as well as highlighting flaws in cell death detection and thus cultivating healthy skepticism of other studies.

4.4 Additional recommendations for future work

Attempting to block the effects I have observed in this body of work using AEDs or anti-inflammatory drugs would provide helpful insight into the functionality of these drugs as well as confirm the mechanisms causing the observed damage. Indeed, others in our group have shown that the products released by *Tania crassiceps* larvae, a tape worm that infects the brain and causes neurocysticercosis (NCC) can be anti-inflammatory. Testing whether the products of these larvae could block the network alterations I have observed could provide further insight into the disease processes of NCC as well as those operating in inflammatory epilepsy.

Given the profound neurotoxic effects of nitric oxide that others have found (Bal-Price & Brown, 2001; Chao *et al*., 1992; Papageorgiou *et al*., 2016), it would also be useful to explore the role NO may or may not be playing in the hippocampal OBSCs model used here. Such work could inform therapies that block NO release, providing an alternative for AED-refractory patients.

Finally, I strongly recommend that future studies explore changes to synaptic function after immune activation, since I believe that this is a promising avenue in understanding the link

between inflammation and seizure development. For example, drugs that limit the trafficking, endocytosis or change in AMPA and or $GABA_A$ receptor expression could be investigated. Hopefully, such work could inform the development of new types of therapies for inflammatory or immune-mediated seizures and epilepsy.

4.5 Conclusion

Taken together, this body of work suggests that bolstered immune activation via co-application of LPS+IFNγ in a hippocampal OBSC model for either 24 or 72 hours causes significant network disruption, possibly via extensive synaptic pruning, changes in presynaptic AP generation and/or presynaptic vesicle release probabilities or changes to postsynaptic receptor expression, which is not observed with LPS application alone. My sPSC data suggests changes to both the excitatory and inhibitory arms of the network, with each being affected in subtle ways that would require more analysis and experimentation to fully elucidate. This work serves to fill gaps in the collective knowledge of the time course of immune stimulation, as well as providing more nuance to our understanding of the electrophysiological damage induced by bolstered immune activation in hippocampal OBSCs. My data will inform future research which could one day lead to novel drug development in the context of infections of the nervous system or in the emerging context of anti-inflammatory drugs as alternatives to classic AEDs in refractory epilepsy patients. Such advances are especially necessary in sub-Saharan Africa, where very high levels of brain infection contribute to high rates of seizures and epilepsy in the population.

Chapter 5

References

Ackermann, R. F., & Moshé, S. L. (2010). Excitation/Inhibition Interactions and Seizures: The Brain's Lifelong Balancing Act. In C. P. Panayiotopoulos (Ed.), *Atlas of Epilepsies* (pp. 177–184). Springer London. https://doi.org/10.1007/978-1-84882-128-6_24

Ajmone-Cat, M. A., Mancini, M., De Simone, R., Cilli, P., & Minghetti, L. (2013). Microglial polarization and plasticity: Evidence from organotypic hippocampal slice cultures. *Glia*, *61*(10), 1698–1711. https://doi.org/10.1002/glia.22550

Alyu, F., & Dikmen, M. (2017). Inflammatory aspects of epileptogenesis: Contribution of molecular inflammatory mechanisms. *Acta Neuropsychiatrica*, *29*(1), 1–16. https://doi.org/10.1017/neu.2016.47

Ang, C. W., Carlson, G. C., & Coulter, D. A. (2006). Massive and Specific Dysregulation of Direct Cortical Input to the Hippocampus in Temporal Lobe Epilepsy. *Journal of Neuroscience*, *26*(46), 11850–11856. https://doi.org/10.1523/JNEUROSCI.2354-06.2006

Baalman, K., Marin, M. A., Ho, T. S.-Y., Godoy, M., Cherian, L., Robertson, C., & Rasband, M. N. (2015). Axon initial segment-associated microglia. *The Journal of Neuroscience: The Official Journal of the Society for Neuroscience*, *35*(5), 2283–2292. https://doi.org/10.1523/JNEUROSCI.3751-14.2015

Balosso, S., Ravizza, T., Perego, C., Peschon, J., Campbell, I. L., De Simoni, M. G., & Vezzani, A. (2005). Tumor necrosis factor-alpha inhibits seizures in mice via p75 receptors. *Annals of Neurology*, *57*(6), 804–812. https://doi.org/10.1002/ana.20480

Bal-Price, A., & Brown, G. C. (2001). Inflammatory Neurodegeneration Mediated by Nitric Oxide from Activated Glia-Inhibiting Neuronal Respiration, Causing Glutamate Release and Excitotoxicity. *The Journal of Neuroscience*, *21*(17), 6480–6491. https://doi.org/10.1523/JNEUROSCI.21-17-06480.2001

Bar, E., & Barak, B. (2019). Microglia roles in synaptic plasticity and myelination in homeostatic conditions and neurodevelopmental disorders. *Glia*, *67*(11), 2125–2141. https://doi.org/10.1002/glia.23637

Bazhanova, E. D., Kozlov, A. A., & Litovchenko, A. V. (2021). Mechanisms of Drug Resistance in the Pathogenesis of Epilepsy: Role of Neuroinflammation. A Literature Review. *Brain Sciences*, *11*(5), 663. https://doi.org/10.3390/brainsci11050663

Beamer, E., Kovács, G., & Sperlágh, B. (2017). ATP released from astrocytes modulates action potential threshold and spontaneous excitatory postsynaptic currents in the neonatal rat prefrontal cortex. *Brain Research Bulletin*, *135*, 129–142. https://doi.org/10.1016/j.brainresbull.2017.10.006

Bedner, P., Dupper, A., Hüttmann, K., Müller, J., Herde, M. K., Dublin, P., Deshpande, T., Schramm, J., Häussler, U., Haas, C. A., Henneberger, C., Theis, M., & Steinhäuser, C. (2015). Astrocyte uncoupling as a cause of human temporal lobe epilepsy. *Brain*, *138*(5), 1208–1222. https://doi.org/10.1093/brain/awv067

Bhatia, A., Moza, S., & Bhalla, U. S. (2019). Precise excitation-inhibition balance controls gain and timing in the hippocampus. *ELife*, *8*, 29. https://doi.org/10.7554/eLife.43415

Bianchi, M. E., & Manfredi, A. A. (2009). Immunology. Dangers in and out. *Science (New York, N.Y.)*, *323*(5922), 1683–1684. https://doi.org/10.1126/science.1172794

Biber, K., Owens, T., & Boddeke, E. (2014). What is microglia neurotoxicity (Not)? *Glia*, *62*(6), 841–854. https://doi.org/10.1002/glia.22654

Bonhoeffer, T., & Yuste, R. (2002). Spine motility. Phenomenology, mechanisms, and function. *Neuron*, *35*(6), 1019–1027. https://doi.org/10.1016/s0896-6273(02)00906-6

Borges, K., Gearing, M., McDermott, D. L., Smith, A. B., Almonte, A. G., Wainer, B. H., & Dingledine, R. (2003). Neuronal and glial pathological changes during epileptogenesis in the mouse pilocarpine model. *Experimental Neurology*, *182*(1), 21–34. https://doi.org/10.1016/S0014-4886(03)00086-4

Bosetti, F. (2007). Arachidonic acid metabolism in brain physiology and pathology: Lessons from genetically altered mouse models. *Journal of Neurochemistry*, *102*(3), 577–586. https://doi.org/10.1111/j.1471-4159.2007.04558.x

Bowman, C. C., Rasley, A., Tranguch, S. L., & Marriott, I. (2003). Cultured astrocytes express toll-like receptors for bacterial products. *Glia*, *43*(3), 281–291. https://doi.org/10.1002/glia.10256

Carpentier, P. A., Begolka, W. S., Olson, J. K., Elhofy, A., Karpus, W. J., & Miller, S. D. (2005). Differential activation of astrocytes by innate and adaptive immune stimuli. *Glia*, *49*(3), 360–374. https://doi.org/10.1002/glia.20117

Caspase-3 Activation: An Indicator of Apoptosis in Image-Based Assays. (2012). 4.

Catterall, W. A. (2012). Sodium Channel Mutations and Epilepsy. In J. L. Noebels, M. Avoli, M. A. Rogawski, R. W. Olsen, & A. V. Delgado-Escueta (Eds.), *Jasper's Basic Mechanisms of the Epilepsies* (4th ed.). National Center for Biotechnology Information (US). http://www.ncbi.nlm.nih.gov/books/NBK98185/

Chacon, E., Acosta, D., & Lemasters, J. J. (1997). 9—Primary Cultures of Cardiac Myocytes as In Vitro Models for Pharmacological and Toxicological Assessments. In J. V. Castell & M. J. Gómez-Lechón (Eds.), *In Vitro Methods in Pharmaceutical Research* (pp. 209–223). Academic Press. https://doi.org/10.1016/B978-012163390-5.50010-7

Chao, C. C., Hu, S., Molitor, T. W., Shaskan, E. G., & Peterson, P. K. (1992). Activated microglia mediate neuronal cell injury via a nitric oxide mechanism. *Journal of Immunology (Baltimore, Md.: 1950)*, *149*(8), 2736–2741.

Coleman, L. G., Zou, J., & Crews, F. T. (2020). Microglial depletion and repopulation in brain slice culture normalizes sensitized proinflammatory signaling. *Journal of Neuroinflammation*, *17*(1), 27. https://doi.org/10.1186/s12974-019-1678-y

Combrinck, M. I., Perry, V. H., & Cunningham, C. (2002). Peripheral infection evokes exaggerated sickness behaviour in pre-clinical murine prion disease. *Neuroscience*, *112*(1), 7–11. https://doi.org/10.1016/s0306-4522(02)00030-1

Coulter, D. A., & Eid, T. (2012). Astrocytic regulation of glutamate homeostasis in epilepsy. *Glia*, *60*(8), 1215–1226. https://doi.org/10.1002/glia.22341

Cunningham, C., Campion, S., Lunnon, K., Murray, C. L., Woods, J. F. C., Deacon, R. M. J., Rawlins, J. N. P., & Perry, V. H. (2009). Systemic inflammation induces acute behavioral and cognitive changes and accelerates neurodegenerative disease. *Biological Psychiatry*, *65*(4), 304–312. https://doi.org/10.1016/j.biopsych.2008.07.024

Cunningham, C., Wilcockson, D. C., Campion, S., Lunnon, K., & Perry, V. H. (2005). Central and systemic endotoxin challenges exacerbate the local inflammatory response and increase neuronal death during chronic neurodegeneration. *The Journal of Neuroscience: The Official Journal of the Society for Neuroscience*, *25*(40), 9275–9284. https://doi.org/10.1523/JNEUROSCI.2614-05.2005

Czapiga, M., & Colton, C. A. (1999). Function of microglia in organotypic slice cultures. *Journal of Neuroscience Research*, *56*(6), 644–651. https://doi.org/10.1002/(SICI)1097-4547(19990615)56:6%3C644::AID-JNR10%3E3.0.CO;2-9

Daria, A., Colombo, A., Llovera, G., Hampel, H., Willem, M., Liesz, A., Haass, C., & Tahirovic, S. (2017). Young microglia restore amyloid plaque clearance of aged microglia. *The EMBO Journal*, *36*(5), 583–603. https://doi.org/10.15252/embj.201694591

Davalos, D., Grutzendler, J., Yang, G., Kim, J. V., Zuo, Y., Jung, S., Littman, D. R., Dustin, M. L., & Gan, W.-B. (2005). ATP mediates rapid microglial response to local brain injury in vivo. *Nature Neuroscience*, *8*(6), 752–758. https://doi.org/10.1038/nn1472

De Sarro, G., Russo, E., Ferreri, G., Giuseppe, B., Flocco, M. A., Di Paola, E. D., & De Sarro, A. (2004). Seizure susceptibility to various convulsant stimuli of knockout interleukin-6 mice. *Pharmacology, Biochemistry, and Behavior*, *77*(4), 761–766. https://doi.org/10.1016/j.pbb.2004.01.012

De Simoni, A., & MY Yu, L. (2006). Preparation of organotypic hippocampal slice cultures: Interface method. *Nature Protocols*, *1*(3), 1439–1445. https://doi.org/10.1038/nprot.2006.228

De Simoni, M. G., Perego, C., Ravizza, T., Moneta, D., Conti, M., Marchesi, F., De Luigi, A., Garattini, S., & Vezzani, A. (2000). Inflammatory cytokines and related genes are induced in the rat hippocampus by limbic status epilepticus. *The European Journal of Neuroscience*, *12*(7), 2623–2633. https://doi.org/10.1046/j.1460-9568.2000.00140.x

Diaz Verdugo, C., Myren-Svelstad, S., Aydin, E., Van Hoeymissen, E., Deneubourg, C., Vanderhaeghe, S., Vancraeynest, J., Pelgrims, R., Cosacak, M. I., Muto, A., Kizil, C., Kawakami, K., Jurisch-Yaksi, N., & Yaksi, E. (2019). Glia-neuron interactions underlie state transitions to generalized seizures. *Nature Communications*, *10*(1), 3830. https://doi.org/10.1038/s41467-019-11739-z

Duan, L., Zhang, X.-D., Miao, W.-Y., Sun, Y.-J., Xiong, G., Wu, Q., Li, G., Yang, P., Yu, H., Li, H., Wang, Y., Zhang, M., Hu, L.-Y., Tong, X., Zhou, W.-H., & Yu, X. (2018). PDGFRβ Cells Rapidly Relay Inflammatory Signal from the Circulatory System to Neurons via Chemokine CCL2. *Neuron*, *100*(1), 183-200.e8. https://doi.org/10.1016/j.neuron.2018.08.030

Dupuis, N., Curatolo, N., Benoist, J.-F., & Auvin, S. (2015). Ketogenic diet exhibits anti-inflammatory properties. *Epilepsia*, *56*(7), e95–e98. https://doi.org/10.1111/epi.13038

EB Bromfield, JE Cavazos, & JI Sirven. (2006). Chapter 2, Clinical Epilepsy. In *Clinical Epilepsy—An Introduction to Epilepsy—NCBI Bookshelf*. American Epilepsy Society. https://www.ncbi.nlm.nih.gov/books/NBK2511/

Erta, M., Quintana, A., & Hidalgo, J. (2012). Interleukin-6, a major cytokine in the central nervous system. *International Journal of Biological Sciences*, *8*(9), 1254–1266. https://doi.org/10.7150/ijbs.4679

Eyo, U. B., Murugan, M., & Wu, L.-J. (2017). Microglia-Neuron Communication in Epilepsy: Microglia in Epilepsy. *Glia*, *65*(1), 5–18. https://doi.org/10.1002/glia.23006

Facci, L., Barbierato, M., Marinelli, C., Argentini, C., Skaper, S. D., & Giusti, P. (2015). Toll-Like Receptors 2, -3 and -4 Prime Microglia but not Astrocytes Across Central Nervous System Regions for ATP-Dependent Interleukin-1β Release. *Scientific Reports*, *4*(1), 6824. https://doi.org/10.1038/srep06824

Field, R., Campion, S., Warren, C., Murray, C., & Cunningham, C. (2010). Systemic challenge with the TLR3 agonist poly I:C induces amplified IFNalpha/beta and IL-1beta responses in the diseased brain and exacerbates chronic neurodegeneration. *Brain, Behavior, and Immunity*, *24*(6), 996–1007. https://doi.org/10.1016/j.bbi.2010.04.004

Fiest, K. M., Sauro, K. M., Wiebe, S., & Patten, S. B. (2016). *Prevalence and incidence of epilepsy*. 8.

Gordon, S., & Martinez, F. O. (2010). Alternative activation of macrophages: Mechanism and functions. *Immunity*, *32*(5), 593–604. https://doi.org/10.1016/j.immuni.2010.05.007

Hanisch, U.-K., & Kettenmann, H. (2007). Microglia: Active sensor and versatile effector cells in the normal and pathologic brain. *Nature Neuroscience*, *10*(11), 1387–1394. https://doi.org/10.1038/nn1997

Hasegawa, S., Sakuragi, S., Tominaga-Yoshino, K., & Ogura, A. (2015). Dendritic spine dynamics leading to spine elimination after repeated inductions of LTD. *Scientific Reports*, *5*(1), 7707. https://doi.org/10.1038/srep07707

Häusler, K. G., Prinz, M., Nolte, C., Weber, J. R., Schumann, R. R., Kettenmann, H., & Hanisch, U.-K. (2002). Interferon-γ differentially modulates the release of cytokines and chemokines in lipopolysaccharide- and pneumococcal cell wall-stimulated mouse microglia and macrophages: IFNg modulation of microglial release activity. *European Journal of Neuroscience*, *16*(11), 2113–2122. https://doi.org/10.1046/j.1460-9568.2002.02287.x

Hellstrom, I. C., Danik, M., Luheshi, G. N., & Williams, S. (2005). Chronic LPS exposure produces changes in intrinsic membrane properties and a sustained IL-β-dependent increase in GABAergic inhibition in hippocampal CA1 pyramidal neurons. *Hippocampus*, *15*(5), 656–664. https://doi.org/10.1002/hipo.20086

Heshmati, M., Christoffel, D. J., LeClair, K., Cathomas, F., Golden, S. A., Aleyasin, H., Turecki, G., Friedman, A. K., Han, M.-H., Menard, C., & Russo, S. J. (2020). Depression and Social Defeat Stress Are Associated with Inhibitory Synaptic Changes in the Nucleus Accumbens. *The Journal of Neuroscience*, *40*(32), 6228–6233. https://doi.org/10.1523/JNEUROSCI.2568-19.2020

Hezel, M., Ebrahimi, F., Koch, M., & Dehghani, F. (2012). Propidium iodide staining: A new application in fluorescence microscopy for analysis of cytoarchitecture in adult and developing rodent brain. *Micron*, *43*(10), 1031–1038. https://doi.org/10.1016/j.micron.2012.04.006

Hoshiko, M., Arnoux, I., Avignone, E., Yamamoto, N., & Audinat, E. (2012). Deficiency of the microglial receptor CX3CR1 impairs postnatal functional development of thalamocortical synapses in the barrel cortex. *The Journal of Neuroscience: The Official Journal of the Society for Neuroscience*, *32*(43), 15106–15111. https://doi.org/10.1523/JNEUROSCI.1167-12.2012

Hubbard, J. A., & Binder, D. K. (2016). *Astrocytes and epilepsy*. Elsevier/AP, Academic Press is an imprint of Elsevier.

Ichiyama, T., Nishikawa, M., & Furukawa, S. (1998). Tumor necrosis factor-a, interleukin-lp, and interleukin-6 in cerebrospinal fluid from children with prolonged febrile seizures. *Neurology*, *50*, 407–411. https://doi.org/10.1212/WNL.50.2.407

Ichiyama, T., Okada, K., Lipton, J. M., Matsubara, T., Hayashi, T., & Furukawa, S. (2000). Sodium valproate inhibits production of TNF-alpha and IL-6 and activation of NF-kappaB. *Brain Research*, *857*(1–2), 246–251. https://doi.org/10.1016/s0006-8993(99)02439-7

Iori, V., Maroso, M., Rizzi, M., Iyer, A. M., Vertemara, R., Carli, M., Agresti, A., Antonelli, A., Bianchi, M. E., Aronica, E., Ravizza, T., & Vezzani, A. (2013). Receptor for Advanced Glycation Endproducts is upregulated in temporal lobe epilepsy and contributes to experimental seizures. *Neurobiology of Disease*, *58*, 102–114. https://doi.org/10.1016/j.nbd.2013.03.006

Ji, K., Akgul, G., Wollmuth, L. P., & Tsirka, S. E. (2013). Microglia actively regulate the number of functional synapses. *PloS One*, *8*(2), e56293. https://doi.org/10.1371/journal.pone.0056293

Kalueff, A. V., Lehtimaki, K. A., Ylinen, A., Honkaniemi, J., & Peltola, J. (2004). Intranasal administration of human IL-6 increases the severity of chemically induced seizures in rats. *Neuroscience Letters*, *365*(2), 106–110. https://doi.org/10.1016/j.neulet.2004.04.061

Kandel, E. (2000). *Principles of Neural Science* (4th ed.). McGraw-Hill.

Kann, O., Huchzermeyer, C., Kovács, R., Wirtz, S., & Schuelke, M. (2011). Gamma oscillations in the hippocampus require high complex I gene expression and strong functional performance of mitochondria. *Brain: A Journal of Neurology*, *134*(Pt 2), 345–358. https://doi.org/10.1093/brain/awq333

Ke, J.-B., Chen, W., Yang, X.-L., & Wang, Z. (2010). Characterization of spontaneous inhibitory postsynaptic currents in cultured rat retinal amacrine cells. *Neuroscience*, *165*(2), 395–407. https://doi.org/10.1016/j.neuroscience.2009.10.010

Kopczynska, M., Zelek, W. M., Vespa, S., Touchard, S., Wardle, M., Loveless, S., Thomas, R. H., Hamandi, K., & Morgan, B. P. (2018). Complement system biomarkers in epilepsy. *Seizure*, *60*, 1–7. https://doi.org/10.1016/j.seizure.2018.05.016

Kossoff, E. H., & Dorward, J. L. (2008). The Modified Atkins Diet. *Epilepsia*, *49*(s8), 37–41. https://doi.org/10.1111/j.1528-1167.2008.01831.x

Kovács, Z., Czurkó, A., Kékesi, K. A., & Juhász, G. (2011). Intracerebroventricularly administered lipopolysaccharide enhances spike–wave discharges in freely moving WAG/Rij rats. *Brain Research Bulletin*, *85*(6), 410–416. https://doi.org/10.1016/j.brainresbull.2011.05.003

Kwon, M.-S., Seo, Y.-J., Choi, S.-M., Won, M.-H., Lee, J.-K., Park, S.-H., Jung, J.-S., Sim, Y.-B., & Suh, H.-W. (2010). The time-dependent effect of lipopolysaccharide on kainic acid-induced neuronal death in hippocampal CA3 region: Possible involvement of cytokines via glucocorticoid. *Neuroscience*, *165*(4), 1333–1344. https://doi.org/10.1016/j.neuroscience.2009.11.060

Laxer, K. D., Trinka, E., Hirsch, L. J., Cendes, F., Langfitt, J., Delanty, N., Resnick, T., & Benbadis, S. R. (2014). The consequences of refractory epilepsy and its treatment. *Epilepsy & Behavior*, *37*, 59–70. https://doi.org/10.1016/j.yebeh.2014.05.031

Lehnardt, S., Massillon, L., Follett, P., Jensen, F. E., Ratan, R., Rosenberg, P. A., Volpe, J. J., & Vartanian, T. (2003). Activation of innate immunity in the CNS triggers neurodegeneration through a Toll-like receptor 4-dependent pathway. *Proceedings of the National Academy of Sciences*, *100*(14), 8514–8519. https://doi.org/10.1073/pnas.1432609100

Levin, S. G., & Godukhin, O. V. (2017). Modulating Effect of Cytokines on Mechanisms of Synaptic Plasticity in the Brain. *Biochemistry. Biokhimiia*, *82*(3), 264–274. https://doi.org/10.1134/S000629791703004X

Li, G., Bauer, S., Nowak, M., Norwood, B., Tackenberg, B., Rosenow, F., Knake, S., Oertel, W. H., & Hamer, H. M. (2011). Cytokines and epilepsy. *Seizure*, *20*(3), 249–256. https://doi.org/10.1016/j.seizure.2010.12.005

Li, Y., Du, X.-F., Liu, C.-S., Wen, Z.-L., & Du, J.-L. (2012). Reciprocal regulation between resting microglial dynamics and neuronal activity in vivo. *Developmental Cell*, *23*(6), 1189–1202. https://doi.org/10.1016/j.devcel.2012.10.027

Liu, T., Zhang, L., Joo, D., & Sun, S.-C. (2017). NF-κB signaling in inflammation. *Signal Transduction and Targeted Therapy*, *2*, 17023. https://doi.org/10.1038/sigtrans.2017.23

Liu, Z., Zhou, T., Ziegler, A. C., Dimitrion, P., & Zuo, L. (2017). Oxidative Stress in Neurodegenerative Diseases: From Molecular Mechanisms to Clinical Applications. *Oxidative Medicine and Cellular Longevity*, *2017*, 2525967–2525967. PubMed. https://doi.org/10.1155/2017/2525967

Llinás, R., & Jahnsen, H. (1982). Electrophysiology of mammalian thalamic neurones in vitro. *Nature*, *297*(5865), 406–408. https://doi.org/10.1038/297406a0

Lobo-Silva, D., Carriche, G. M., Castro, A. G., Roque, S., & Saraiva, M. (2016). Balancing the immune response in the brain: IL-10 and its regulation. *Journal of Neuroinflammation*, *13*(1), 297. https://doi.org/10.1186/s12974-016-0763-8

Luca, G. D., Giorgio, R. M. D., Macaione, S., Calpona, P. R., Costantino, S., Paola, E. D. D., Sarro, A. D., Ciliberto, G., & Sarro, G. D. (2004). Susceptibility to audiogenic seizure and neurotransmitter amino acid levels in different brain areas of IL-6-deficient mice. *Pharmacology, Biochemistry and Behavior*, *78*(1), 75–81. https://doi.org/10.1016/j.pbb.2004.02.004

MacFadden, D. K., Edelson, J. D., Hyland, R. H., Rodriguez, C. H., Inouye, T., & Rebuck, A. S. (1987). Corticosteroids as adjunctive therapy in treatment of Pneumocystis carinii pneumonia in patients with acquired immunodeficiency syndrome. *Lancet (London, England)*, *1*(8548), 1477–1479. https://doi.org/10.1016/s0140-6736(87)92219-7

Malkin, S. L., Kim, K. Kh., Tikhonov, D. B., & Zaitsev, A. V. (2014). Properties of spontaneous and miniature excitatory postsynaptic currents in neurons of the rat prefrontal cortex. *Journal of Evolutionary Biochemistry and Physiology*, *50*(6), 506–514. https://doi.org/10.1134/S0022093014060052

Marchi, N., Angelov, L., Masaryk, T., Fazio, V., Granata, T., Hernandez, N., Hallene, K., Diglaw, T., Franic, L., Najm, I., & Janigro, D. (2007). Seizure-promoting effect of blood-brain barrier disruption. *Epilepsia*, *48*(4), 732–742. https://doi.org/10.1111/j.1528-1167.2007.00988.x

Marchi, N., Teng, Q., Ghosh, C., Fan, Q., Nguyen, M. T., Desai, N. K., Bawa, H., Rasmussen, P., Masaryk, T. K., & Janigro, D. (2010). Blood-brain barrier damage, but not parenchymal white blood cells, is a hallmark of seizure activity. *Brain Research*, *1353*, 176–186. https://doi.org/10.1016/j.brainres.2010.06.051

Mark F. Bear, Barry W. Connors, & Michael A. Paradiso. (2007). *Neuroscience: Exploring the Brain* (3rd ed.). Lippincott Williams & Wilkins.

Maroso, M., Balosso, S., Ravizza, T., Liu, J., Aronica, E., Iyer, A. M., Rossetti, C., Molteni, M., Casalgrandi, M., Manfredi, A. A., Bianchi, M. E., & Vezzani, A. (2010). Toll-like receptor 4 and high-mobility group box-1 are involved in ictogenesis and can be targeted to reduce seizures. *Nature Medicine*, *16*(4), 413–419. https://doi.org/10.1038/nm.2127

Masuch, A., van der Pijl, R., Füner, L., Wolf, Y., Eggen, B., Boddeke, E., & Biber, K. (2016). Microglia replenished OHSC: A culture system to study in vivo like adult microglia. *Glia*, *64*(8), 1285–1297. https://doi.org/10.1002/glia.23002

Matoth, I., Pinto, F., Sicsic, C., & Brenner, T. (2000). Inhibitory effect of carbamazepine on inflammatory mediators produced by stimulated glial cells. *Neuroscience Research*, *38*(2), 209–212. https://doi.org/10.1016/s0168-0102(00)00127-9

Mizuno, T., Zhang, G., Takeuchi, H., Kawanokuchi, J., Wang, J., Sonobe, Y., Jin, S., Takada, N., Komatsu, Y., & Suzumura, A. (2008). Interferon-gamma directly induces neurotoxicity through a neuron specific, calcium-permeable complex of IFN-gamma receptor and AMPA GluR1 receptor. *FASEB Journal: Official Publication of the Federation of American Societies for Experimental Biology*, *22*(6), 1797–1806. https://doi.org/10.1096/fj.07-099499

Monteiro, S., Ferreira, F. M., Pinto, V., Roque, S., Morais, M., de Sá-Calçada, D., Mota, C., Correia-Neves, M., & Cerqueira, J. J. (2016). Absence of IFNγ promotes hippocampal plasticity and enhances cognitive performance. *Translational Psychiatry*, *6*, e707. https://doi.org/10.1038/tp.2015.194

Montero, M., González, B., & Zimmer, J. (2009). Immunotoxic depletion of microglia in mouse hippocampal slice cultures enhances ischemia-like neurodegeneration. *Brain Research*, *1291*, 140–152. https://doi.org/10.1016/j.brainres.2009.06.097

Musto, A. E., Gjorstrup, P., & Bazan, N. G. (2011). The omega-3 fatty acid-derived neuroprotectin D1 limits hippocampal hyperexcitability and seizure susceptibility in kindling epileptogenesis. *Epilepsia*, *52*(9), 1601–1608. https://doi.org/10.1111/j.1528-1167.2011.03081.x

Musto, A. E., Rosencrans, R. F., Walker, C. P., Bhattacharjee, S., Raulji, C. M., Belayev, L., Fang, Z., Gordon, W. C., & Bazan, N. G. (2016). Dysfunctional epileptic neuronal circuits and dysmorphic dendritic spines are mitigated by platelet-activating factor receptor antagonism. *Scientific Reports*, *6*(1), 30298. https://doi.org/10.1038/srep30298

Nagelhus, E. A., Amiry-Moghaddam, M., Bergersen, L. H., Bjaalie, J. G., Eriksson, J., Gundersen, V., Leergaard, T. B., Morth, J. P., Storm-Mathisen, J., Torp, R., Walhovd, K. B., & Tønjum, T. (2013). The glia doctrine: Addressing the role of glial cells in healthy brain ageing. *Mechanisms of Ageing and Development*, *134*(10), 449–459. https://doi.org/10.1016/j.mad.2013.10.001

Nägerl, U. V., Willig, K. I., Hein, B., Hell, S. W., & Bonhoeffer, T. (2008). Live-cell imaging of dendritic spines by STED microscopy. *Proceedings of the National Academy of Sciences*, *105*(48), 18982–18987. https://doi.org/10.1073/pnas.0810028105

Nimmerjahn, A., Kirchhoff, F., & Helmchen, F. (2005). Resting microglial cells are highly dynamic surveillants of brain parenchyma in vivo. *Science (New York, N.Y.)*, *308*(5726), 1314–1318. https://doi.org/10.1126/science.1110647

Olmos, G., & Lladó, J. (2014). Tumor Necrosis Factor Alpha: A Link between Neuroinflammation and Excitotoxicity. *Mediators of Inflammation*, *2014*, 1–12. https://doi.org/10.1155/2014/861231

Owolabi, L. F., Adamu, B., Jibo, A. M., Owolabi, S. D., Isa, A. I., Alhaji, I. D., & Enwere, O. O. (2020). Prevalence of active epilepsy, lifetime epilepsy prevalence, and burden of epilepsy in Sub-Saharan Africa from meta-analysis of door-to-door population-based surveys. *Epilepsy & Behavior*, *103*. https://doi.org/10.1016/j.yebeh.2019.106846

Paolicelli, R. C., Bolasco, G., Pagani, F., Maggi, L., Scianni, M., Panzanelli, P., Giustetto, M., Ferreira, T. A., Guiducci, E., Dumas, L., Ragozzino, D., & Gross, C. T. (2011). Synaptic pruning by microglia is necessary for normal brain development. *Science (New York, N.Y.)*, *333*(6048), 1456–1458. https://doi.org/10.1126/science.1202529

Paolicelli, R. C., & Gross, C. T. (2011). Microglia in development: Linking brain wiring to brain environment. *Neuron Glia Biology*, *7*(1), 77–83. https://doi.org/10.1017/S1740925X12000105

Papageorgiou, I. E., Lewen, A., Galow, L. V., Cesetti, T., Scheffel, J., Regen, T., Hanisch, U.-K., & Kann, O. (2016). TLR4-activated microglia require IFN-γ to induce severe neuronal dysfunction and death in situ. *Proceedings of the National Academy of Sciences*, *113*(1), 212–217. https://doi.org/10.1073/pnas.1513853113

Pascual, O., Ben Achour, S., Rostaing, P., Triller, A., & Bessis, A. (2012). Microglia activation triggers astrocyte-mediated modulation of excitatory neurotransmission. *Proceedings of the National Academy of Sciences*, *109*(4), E197–E205. https://doi.org/10.1073/pnas.1111098109

Penkowa, M., Molinero, A., Carrasco, J., & Hidalgo, J. (2001). Interleukin-6 deficiency reduces the brain inflammatory response and increases oxidative stress and neurodegeneration after kainic acid-induced seizures. *Neuroscience*, *102*(4), 805–818. https://doi.org/10.1016/s0306-4522(00)00515-7

Pinheiro, P. S., & Mulle, C. (2008). Presynaptic glutamate receptors: Physiological functions and mechanisms of action. *Nature Reviews Neuroscience*, *9*(6), 423–436. https://doi.org/10.1038/nrn2379

Preux, P.-M., & Druet-Cabanac, M. (2005). Epidemiology and aetiology of epilepsy in sub-Saharan Africa. *The Lancet Neurology*, *4*(1), 21–31. https://doi.org/10.1016/S1474-4422(04)00963-9

Queenan, B. N., Lee, K. J., & Pak, D. T. S. (2012). Wherefore Art Thou, Homeo(stasis)? Functional Diversity in Homeostatic Synaptic Plasticity. *Neural Plasticity*, *2012*, 1–12. https://doi.org/10.1155/2012/718203

Rana, A., & Musto, A. E. (2018). The role of inflammation in the development of epilepsy. *Journal of Neuroinflammation*, *15*(1), 144. https://doi.org/10.1186/s12974-018-1192-7

Ransohoff, R. M., & Perry, V. H. (2009). Microglial physiology: Unique stimuli, specialized responses. *Annual Review of Immunology*, *27*, 119–145. https://doi.org/10.1146/annurev.immunol.021908.132528

Ravizza, T., Balosso, S., & Vezzani, A. (2011). Inflammation and prevention of epileptogenesis. *Neuroscience Letters*, *497*(3), 223–230. https://doi.org/10.1016/j.neulet.2011.02.040

Ravizza, T., & Vezzani, A. (2006). Status epilepticus induces time-dependent neuronal and astrocytic expression of interleukin-1 receptor type I in the rat limbic system. *Neuroscience*, *137*(1), 301–308. https://doi.org/10.1016/j.neuroscience.2005.07.063

Rojas, A., Jiang, J., Ganesh, T., Yang, M.-S., Lelutiu, N., Gueorguieva, P., & Dingledine, R. (2014). Cyclooxygenase-2 in epilepsy. *Epilepsia*, *55*(1), 17–25. https://doi.org/10.1111/epi.12461

Rumbaugh, J. A., & Nath, A. (2009). Neuronal Cell Death and Inflammation. In M. D. Binder, N. Hirokawa, & U. Windhorst (Eds.), *Encyclopedia of Neuroscience* (pp. 2772–2776). Springer Berlin Heidelberg. https://doi.org/10.1007/978-3-540-29678-2_3910

Samland, H., Huitron-Resendiz, S., Masliah, E., Criado, J., Henriksen, S. J., & Campbell, I. L. (2003). Profound increase in sensitivity to glutamatergic- but not cholinergic agonist-induced seizures in transgenic mice with astrocyte production of IL-6. *Journal of Neuroscience Research*, *73*(2), 176–187. https://doi.org/10.1002/jnr.10635

Sayyah, M., Javad-Pour, M., & Ghazi-Khansari, M. (2003). The bacterial endotoxin lipopolysaccharide enhances seizure susceptibility in mice: Involvement of proinflammatory factors: nitric oxide and prostaglandins. *Neuroscience*, *122*(4), 1073–1080. https://doi.org/10.1016/j.neuroscience.2003.08.043

Scemes, E., & Spray, D. C. (2003). The astrocytic syncytium. In *Advances in Molecular and Cell Biology* (Vol. 31, pp. 165–179). Elsevier. https://doi.org/10.1016/S1569-2558(03)31007-0

Schröder, W., Hinterkeuser, S., Seifert, G., Schramm, J., Jabs, R., Wilkin, G. P., & Steinhäuser, C. (2000). Functional and Molecular Properties of Human Astrocytes in Acute Hippocampal Slices Obtained from Patients with Temporal Lobe Epilepsy. *Epilepsia*, *41*(s6), S181–S184. https://doi.org/10.1111/j.1528-1157.2000.tb01578.x

Seiffert, E., Dreier, J. P., Ivens, S., Bechmann, I., Tomkins, O., Heinemann, U., & Friedman, A. (2004). Lasting blood-brain barrier disruption induces epileptic focus in the rat somatosensory cortex. *The Journal of Neuroscience: The Official Journal of the Society for Neuroscience*, *24*(36), 7829–7836. https://doi.org/10.1523/JNEUROSCI.1751-04.2004

Sheppard, O., Coleman, M. P., & Durrant, C. S. (2019). Lipopolysaccharide-induced neuroinflammation induces presynaptic disruption through a direct action on brain tissue involving microglia-derived interleukin 1 beta. *Journal of Neuroinflammation*, *16*(1), 106. https://doi.org/10.1186/s12974-019-1490-8

Soares, F. L. P., de Oliveira Matoso, R., Teixeira, L. G., Menezes, Z., Pereira, S. S., Alves, A. C., Batista, N. V., de Faria, A. M. C., Cara, D. C., Ferreira, A. V. M., & Alvarez-Leite, J. I. (2013). Gluten-free diet reduces adiposity, inflammation and insulin resistance associated with the induction of PPAR-alpha and PPAR-gamma expression. *The Journal of Nutritional Biochemistry*, *24*(6), 1105–1111. https://doi.org/10.1016/j.jnutbio.2012.08.009

Stellwagen, D., Beattie, E. C., Seo, J. Y., & Malenka, R. C. (2005). Differential regulation of AMPA receptor and GABA receptor trafficking by tumor necrosis factor-alpha. *The Journal of Neuroscience: The Official Journal of the Society for Neuroscience*, *25*(12), 3219–3228. https://doi.org/10.1523/JNEUROSCI.4486-04.2005

Stellwagen, D., & Malenka, R. C. (2006). Synaptic scaling mediated by glial TNF-alpha. *Nature*, *440*(7087), 1054–1059. https://doi.org/10.1038/nature04671

Stoppini, L., Buchs, P.-A., & Muller, D. (1991). A simple method for organotypic cultures of nervous tissue. *Journal of Neuroscience Methods*, *37*(2), 173–182. https://doi.org/10.1016/0165-0270(91)90128-M

Sun, Y., Ma, J., Li, D., Li, P., Zhou, X., Li, Y., He, Z., Qin, L., Liang, L., & Luo, X. (2019). Interleukin-10 inhibits interleukin-1β production and inflammasome activation of microglia in epileptic seizures. *Journal of Neuroinflammation*, *16*(1), 66. https://doi.org/10.1186/s12974-019-1452-1

Ta, T.-T., Dikmen, H. O., Schilling, S., Chausse, B., Lewen, A., Hollnagel, J.-O., & Kann, O. (2019). Priming of microglia with IFN-γ slows neuronal gamma oscillations in situ. *Proceedings of the National Academy of Sciences*, *116*(10), 4637–4642. https://doi.org/10.1073/pnas.1813562116

Taylor, D. L., Jones, F., Kubota, E. S. F. C. S., & Pocock, J. M. (2005). Stimulation of microglial metabotropic glutamate receptor mGlu2 triggers tumor necrosis factor alpha-induced neurotoxicity in concert with microglial-derived Fas ligand. *The Journal of Neuroscience: The Official Journal of the Society for Neuroscience*, *25*(11), 2952–2964. https://doi.org/10.1523/JNEUROSCI.4456-04.2005

Terrone, G., Frigerio, F., Balosso, S., Ravizza, T., & Vezzani, A. (2019). Inflammation and reactive oxygen species in status epilepticus: Biomarkers and implications for therapy. *Epilepsy & Behavior*, *101*, 106275. https://doi.org/10.1016/j.yebeh.2019.04.028

Tremblay, M.-È., Lowery, R. L., & Majewska, A. K. (2010). Microglial interactions with synapses are modulated by visual experience. *PLoS Biology*, *8*(11), e1000527. https://doi.org/10.1371/journal.pbio.1000527

van Vliet, E. A., Aronica, E., & Gorter, J. A. (2015). Blood–brain barrier dysfunction, seizures and epilepsy. *Seminars in Cell & Developmental Biology*, *38*, 26–34. https://doi.org/10.1016/j.semcdb.2014.10.003

van Vliet, E. A., da Costa Araújo, S., Redeker, S., van Schaik, R., Aronica, E., & Gorter, J. A. (2007). Blood-brain barrier leakage may lead to progression of temporal lobe epilepsy. *Brain: A Journal of Neurology*, *130*(Pt 2), 521–534. https://doi.org/10.1093/brain/awl318

Varadkar, S., Bien, C. G., Kruse, C. A., Jensen, F. E., Bauer, J., Pardo, C. A., Vincent, A., Mathern, G. W., & Cross, J. H. (2014). Rasmussen's encephalitis: Clinical features, pathobiology, and treatment advances. *The Lancet Neurology*, *13*(2), 195–205. https://doi.org/10.1016/S1474-4422(13)70260-6

Varvel, N. H., Neher, J. J., Bosch, A., Wang, W., Ransohoff, R. M., Miller, R. J., & Dingledine, R. (2016). Infiltrating monocytes promote brain inflammation and exacerbate neuronal damage after status epilepticus. *Proceedings of the National Academy of Sciences*, *113*(38), E5665–E5674. https://doi.org/10.1073/pnas.1604263113

Verkuyl, J. M., & Matus, A. (2006). Time-lapse imaging of dendritic spines in vitro. *Nature Protocols*, *1*(5), 2399–2405. https://doi.org/10.1038/nprot.2006.357

Verrotti, A., Iapadre, G., Di Francesco, L., Zagaroli, L., & Farello, G. (2020). Diet in the Treatment of Epilepsy: What We Know So Far. *Nutrients*, *12*(9). https://doi.org/10.3390/nu12092645

Vezzani, A. (2014). Epilepsy and Inflammation in the Brain: Overview and Pathophysiology: Epilepsy and Inflammation in the Brain. *Epilepsy Currents*, *14*(2_suppl), 3–7. https://doi.org/10.5698/1535-7511-14.s2.3

Vezzani, A., Balosso, S., & Ravizza, T. (2019). Neuroinflammatory pathways as treatment targets and biomarkers in epilepsy. *Nature Reviews Neurology*, *15*(8), 459–472. https://doi.org/10.1038/s41582-019-0217-x

Vezzani, A., Dingledine, R., & Rossetti, A. O. (2015). Immunity and inflammation in status epilepticus and its sequelae: Possibilities for therapeutic application. *Expert Review of Neurotherapeutics*, *15*(9), 1081–1092. https://doi.org/10.1586/14737175.2015.1079130

Vezzani, A., French, J., Bartfai, T., & Baram, T. Z. (2011). The role of inflammation in epilepsy. *Nature Reviews Neurology*, *7*(1), 31–40. https://doi.org/10.1038/nrneurol.2010.178

Vezzani, A., Friedman, A., & Dingledine, R. J. (2013). The role of inflammation in epileptogenesis. *Neuropharmacology*, *69*, 16–24. https://doi.org/10.1016/j.neuropharm.2012.04.004

Vezzani, A., & Granata, T. (2005). Brain Inflammation in Epilepsy: Experimental and Clinical Evidence. *Epilepsia*, *46*(11), 1724–1743. https://doi.org/10.1111/j.1528-1167.2005.00298.x

Vinet, J., van Weering, H. R., Heinrich, A., Kälin, R. E., Wegner, A., Brouwer, N., Heppner, F. L., van Rooijen, N., Boddeke, H. W., & Biber, K. (2012). Neuroprotective function for ramified microglia in hippocampal excitotoxicity. *Journal of Neuroinflammation*, *9*(1), 27. https://doi.org/10.1186/1742-2094-9-27

Vogl, T., Tenbrock, K., Ludwig, S., Leukert, N., Ehrhardt, C., van Zoelen, M. A. D., Nacken, W., Foell, D., van der Poll, T., Sorg, C., & Roth, J. (2007). Mrp8 and Mrp14 are endogenous activators of Toll-like receptor 4, promoting lethal, endotoxin-induced shock. *Nature Medicine*, *13*(9), 1042–1049. https://doi.org/10.1038/nm1638

Volman, V., Bazhenov, M., & Sejnowski, T. J. (2012). Computational models of neuron-astrocyte interaction in epilepsy. *Frontiers in Computational Neuroscience*, *6*. https://doi.org/10.3389/fncom.2012.00058

von Bartheld, C. S., Bahney, J., & Herculano-Houzel, S. (2016). The Search for True Numbers of Neurons and Glial Cells in the Human Brain: A Review of 150 Years of Cell Counting. *The Journal of Comparative Neurology*, *524*(18), 3865–3895. https://doi.org/10.1002/cne.24040

Wake, H., Moorhouse, A. J., Jinno, S., Kohsaka, S., & Nabekura, J. (2009). Resting microglia directly monitor the functional state of synapses in vivo and determine the fate of ischemic terminals. *The Journal of*

Neuroscience: The Official Journal of the Society for Neuroscience, *29*(13), 3974–3980. https://doi.org/10.1523/JNEUROSCI.4363-08.2009

Wallraff, A. (2006). The Impact of Astrocytic Gap Junctional Coupling on Potassium Buffering in the Hippocampus. *Journal of Neuroscience*, *26*(20), 5438–5447. https://doi.org/10.1523/JNEUROSCI.0037-06.2006

Wang, H., Dharmalingam, P., Vasquez, V., Mitra, J., Boldogh, I., Rao, K. S., Kent, T. A., Mitra, S., & Hegde, M. L. (2017). Chronic oxidative damage together with genome repair deficiency in the neurons is a double whammy for neurodegeneration: Is damage response signaling a potential therapeutic target? *Mechanisms of Ageing and Development*, *161*(Pt A), 163–176. PubMed. https://doi.org/10.1016/j.mad.2016.09.005

Weinhard, L., di Bartolomei, G., Bolasco, G., Machado, P., Schieber, N. L., Neniskyte, U., Exiga, M., Vadisiute, A., Raggioli, A., Schertel, A., Schwab, Y., & Gross, C. T. (2018). Microglia remodel synapses by presynaptic trogocytosis and spine head filopodia induction. *Nature Communications*, *9*(1), 1228. https://doi.org/10.1038/s41467-018-03566-5

Wells, J., Swaminathan, A., Paseka, J., & Hanson, C. (2020). Efficacy and Safety of a Ketogenic Diet in Children and Adolescents with Refractory Epilepsy—A Review. *Nutrients*, *12*(6), 1809. https://doi.org/10.3390/nu12061809

Welsch, J., Lionnet, C., Terzian, C., Horvat, B., Gerlier, D., & Mathieu, C. (2017). Organotypic Brain Cultures: A Framework for Studying CNS Infection by Neurotropic Viruses and Screening Antiviral Drugs. *BIO-PROTOCOL*, *7*(22). https://doi.org/10.21769/BioProtoc.2605

Wu, Y., Dissing-Olesen, L., MacVicar, B. A., & Stevens, B. (2015). Microglia: Dynamic Mediators of Synapse Development and Plasticity. *Trends in Immunology*, *36*(10), 605–613. https://doi.org/10.1016/j.it.2015.08.008

Youn, Y. A., Kim, S. J., Sung, I. K., Chung, S. Y., Kim, Y. H., & Lee, I. G. (2012). Serial examination of serum IL-8, IL-10 and IL-1Ra levels is significant in neonatal seizures induced by hypoxic-ischaemic encephalopathy. *Scandinavian Journal of Immunology*, *76*(3), 286–293. https://doi.org/10.1111/j.1365-3083.2012.02710.x

Youn, Y., Sung, I. K., & Lee, I. G. (2013). The role of cytokines in seizures: Interleukin (IL)-1β, IL-1Ra, IL-8, and IL-10. *Korean Journal of Pediatrics*, *56*(7), 271–274. https://doi.org/10.3345/kjp.2013.56.7.271

Zhang, J., He, H., Qiao, Y., Zhou, T., He, H., Yi, S., Zhang, L., Mo, L., Li, Y., Jiang, W., & You, Z. (2020). Priming of microglia with IFN-γ impairs adult hippocampal neurogenesis and leads to depression-like behaviors and cognitive defects. *Glia*, *68*(12), 2674–2692. https://doi.org/10.1002/glia.23878

Zhang, J., Malik, A., Choi, H. B., Ko, R. W. Y., Dissing-Olesen, L., & MacVicar, B. A. (2014). Microglial CR3 activation triggers long-term synaptic depression in the hippocampus via NADPH oxidase. *Neuron*, *82*(1), 195–207. https://doi.org/10.1016/j.neuron.2014.01.043

Zhao, X., Liao, Y., Morgan, S., Mathur, R., Feustel, P., Mazurkiewicz, J., Qian, J., Chang, J., Mathern, G. W., Adamo, M. A., Ritaccio, A. L., Gruenthal, M., Zhu, X., & Huang, Y. (2018). Noninflammatory Changes of Microglia Are Sufficient to Cause Epilepsy. *Cell Reports*, *22*(8), 2080–2093. https://doi.org/10.1016/j.celrep.2018.02.004

Zhu, W., Zheng, H., Shao, X., Wang, W., Yao, Q., & Li, Z. (2010). Excitotoxicity of TNFα derived from KA activated microglia on hippocampal neurons in vitro and in vivo. *Journal of Neurochemistry*, *114*(2), 386–396. https://doi.org/10.1111/j.1471-4159.2010.06763.x